Influence of inland vessel stern shape aspects on propulsive performance
Derivation of insights and guidelines based on a computational study

Rotteveel, Erik

DOI
10.4233/uuid:8d8c14e3-cdfb-4e15-8314-35dc296fdbde

Publication date
2019

Document Version
Final published version

Citation (APA)
Rotteveel, E. (2019). *Influence of inland vessel stern shape aspects on propulsive performance: Derivation of insights and guidelines based on a computational study*. [Dissertation (TU Delft), Delft University of Technology]. Delft University of Technology. https://doi.org/10.4233/uuid:8d8c14e3-cdfb-4e15-8314-35dc296fdbde

Influence of inland vessel stern shape aspects on propulsive performance

Derivation of insights and guidelines based on a computational study

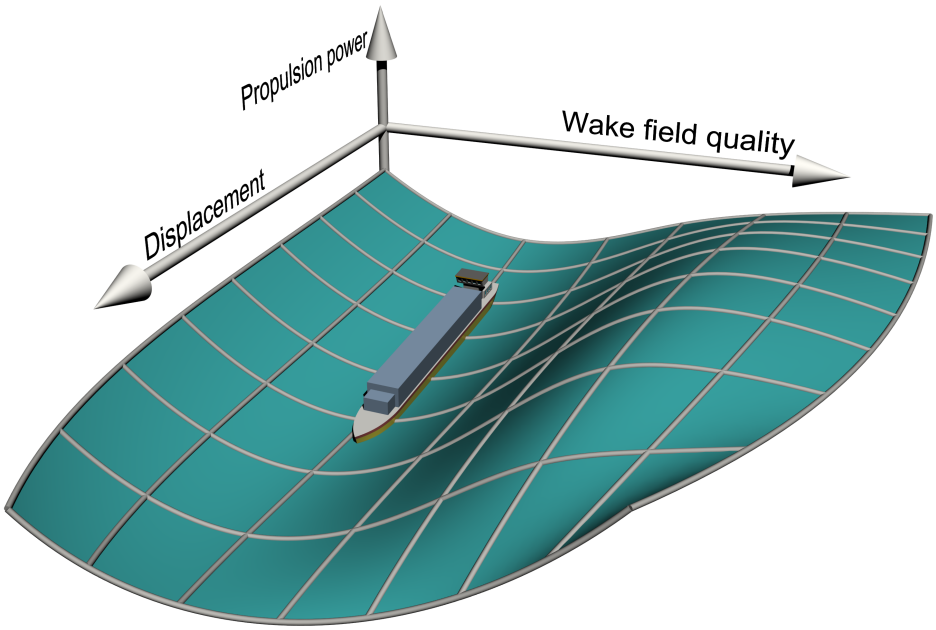

Erik Rotteveel

Influence of inland vessel stern shape aspects on propulsive performance

Derivation of insights and guidelines based on a computational study

Dissertation

for the purpose of obtaining the degree of doctor
at Delft University of Technology,
by the authority of the Rector Magnificus Prof.dr.ir. T.H.J.J. van der Hagen,
chair of the Board for Doctorates
to be defended publicly on
Monday 1 April 2019 at 12:30 o'clock

by

Erik ROTTEVEEL

Master of Science in Maritime Technology,
Delft University of Technology,
the Netherlands.
born in Leiden, the Netherlands.

This dissertation has been approved by the promotors.

Composition of the doctoral committee:

Rector Magnificus,	Chairperson
Prof. ir. J.J. Hopman	Delft University of Technology, promotor
Prof. dr. ir. T.J.C. van Terwisga	Delft University of Technology, promotor
Dr. ir. R.G. Hekkenberg	Delft University of Technology, copromotor

Independent members:

Prof. dr. B.O. el Moctar	Universität Duisburg-Essen, Germany
Prof. ir. J.S. Carlton	City University of London, United Kingdom
Prof. dr. ir. C. van Rhee	Delft University of Technology
Prof. dr. ir. J. van Westerweel	Delft University of Technology

The research presented in this thesis was part of a joint-industry project. The following companies and/or organizations were part of this project and contributed to this research: the Delft University of Technology, Maritime Research Institute Netherlands (MARIN), Conoship International B.V., SARC, Sip Marine, Groenendijk & Soetermeer, and Concordia Shipping.

Cover design and printed by: ProefschriftMaken || www.proefschriftmaken.nl
(Cover image provided by the author)

ISBN 978-94-6380-242-0

An electronic version of this dissertation is available at
http://repository.tudelft.nl/.

Summary

The hull form design of an inland ship affects, among others, the ship's performance, its emissions, the on-board comfort and the competitive position of the owner in the transport market. An optimized hull form design aids in reducing fuel consumption and thereby operational costs. However, optimizing an inland ship hull form requires a relatively large investment compared to the overall budget available for the design. This is partly due to the fact that multiple situations have to be considered during optimization, because an inland ship encounters multiple water depths and will be operating a varying draft. Because of the large investments required for optimization, inland ship designers fall back on design guidelines and empirical methods, both of which are scarcely available for inland ships.

This thesis focuses on gaining insights in effects of inland ship hull form parameters as well as to investigate how these parameters should be chosen in order to obtain an inland ship that performs well. These insights are presented as guidelines to ship designers, so that they now which hull form aspects are most important in order to obtain decent propulsion performance, while a direction for the optimization process is provide as well.

The thesis focuses specifically on the stern of an inland ship. This choice is made because of the complexity of the stern itself as well as that of the flow around it and the interaction between the propeller and the hull form. Additionally, three stern types are considered: a single-propeller tunnel stern, a twin-propeller tunnel stern and a twin-propeller pram-shaped stern. Finally, multiple water depths are considered, ranging from h/T (ratio between water depth and ship draft) values from 3.0 down to 1.5.

Goal and research questions

The goal of the research presented in this thesis is *to better understand the relation between stern shape aspects, water depth, and inland ship propulsion performance*. The understanding and gained insights are presented such that they serve as guidelines that 1) *show which stern shape aspects are most important to propulsion performance*, and 2) *describe the optimal shape of the stern for an inland ship depending on required displacement*. The guidelines therefore do not only describe a single ship design, but also describe how the ship design should be adapted if it is to meet a different displacement requirement.

To achieve this goal, multiple research questions are posed. The answers to these questions lead to the goal as described above:

1. What are typical inland ship stern shape aspects?
2. How can the influence of each aspect be tested?

3. Which of the aspects are most important to propulsion performance?
4. How do these aspects affect propulsion performance?
5. How can an optimal ship design be found depending on design constraints?
6. What is an optimal design for each of the aspects considered, given constraints?

Of which the first question is answered in chapter 3. The effect of each hull form aspect is tested using computational fluid dynamics (CFD), for which input is generated by a parametric model. This parametric model is discussed in chapter 3, while the set-up of and results from CFD are discussed in chapters 4 and 5 respectively. To find which are the most important aspects and how those aspects affect performance, surrogate modeling has been applied. This was discussed in chapter 6. Finally, the search for an optimal design is performed by optimization, which is discussed in chapter 7.

Approach

Firstly, chapter 2 discusses the state-of-the-art of inland ship design. Several design guidelines are available that can be used by designers to obtain a decent design for an inland ship stern. However, it is concluded that the available guidelines are rough and only present a single design solution. The guidelines do not provide information about the impact on performance when a designer must deviate from the presented guideline due to design requirements (for example, if more displacement is required).

To obtain guidelines that do provide such information, varying inland ship hull forms are required. Typical differences among inland ship hull forms are investigated in chapter 3. Variations of interest have been chosen based on visual inspection, discussion and literature study. Next, a parametric model has been developed that allows the generation of multiple hull forms so that the impact of variations on propulsive performance can be tested.

Computational fluid dynamics (CFD) has been used to test each of the hull forms generated by the parametric model. The RANS-equations solver PARNASSOS has been used to obtain the flow around the ship. In chapter 4, the required set-up of PARNASSOS is discussed. A multi-block structure has been applied in order to model shallow water. The chapter also discussed the size of the domain and the size of the grid cells. The output from PARNASSOS are the ship's resistance and the wake field. Chapter 5 then discussed how this data has been used to obtain estimates on propulsive performance, which is a combination of propeller shaft power and wake field quality. Chapters 4 and 5 together answer the second question.

The approach to determine the importance of hull form aspects and their impact on propulsive performance is derived in chapter 6. Surrogate modeling is applied for this. A surrogate model is a replacement for an expensive or time-consuming model such as CFD, and is able to predict the outcomes for cases that have not yet been tested. There are multiple types of surrogate models. For the present study,

a Kriging response surface is found to be suitable and produces the most accurate predictions. The Kriging model has been used to determine which hull form aspect is the most important one by means of parameter selection methods. The used method uses a genetic algorithm to determine which hull form aspects should be in the model in order to obtain accurate predictions.

In chapter 7 a method is described to obtain guidelines as well as how to present them. Derivation of design guidelines is done by using optimization. The optimization process focused on three objectives: displacement, propulsion power and wake field quality. For the latter, a fixed maximum value has been set as a constraint for the optimization process. The resulting two-objective (displacement and power) led to a Pareto front, in which each point represents a hull form that requires minimal power for the corresponding amount of displacement. By investigating how hull form aspects changed (or remained constant) along the Pareto front, hull form aspects that are important for the power/displacement trade-off have been identified. Additionally, the approach showed which hull form aspects should, regardless of displacement or water depth, always be designed in a certain way.

The results therefore present which hull form aspect has to be changed preferably if more displacement is required. As propulsion power for each point in the Pareto front has been determined as well, the impact of increasing displacement on propulsion power is also known. That allows ship designers to assess the trade-off between displacement and propulsion power.

Conclusions

For inland ships with a tunnel stern, it is found that the length of the stern, the athwartships propeller position and the propeller diameter are the most important parameters for propulsive performance. Based on optimization, it is concluded that the starting point of the tunnel should be smooth such that the bottom plane width is reduced *before* the tunnel skirt emerge from the hull. Additionally, optimization in shallow water resulted in different hull frames: whereas at $h/T = 3.0$, the tunnel top curve is made smooth and the tunnel entrance is lowered, optimization in shallower water ($h/T = 1.5$) resulted in a tunnel top curve with a more pronounce s-curve such that the propeller inflow is aligned with the ship's longitudinal axis. Finally, the bilge radius is advised to be large in order to prevent energy losses in the flow due to generated vortices.

Contents

1

Introduction

Inland ships are a common sight on rivers. In Europe, a significant portion of the total amount of transported cargo is taken care of by those ships, especially from large sea-ports into the hinterland. For example, 35 percent of the containers going from the port of Rotterdam into the hinterland are transported by inland vessels (voorlichting Binnenvaart [1]). For all types of cargo within the Netherlands, Germany and Belgium, inland ships take care of respectively 37, 10 and 21 percent of the transported amount, measured in tonkilometer (amount of cargo times distance traveled).

A main concern for the designers of inland ships is fuel consumption. The costs of fuel contribute by 10 to 30 percent to the yearly expenses (including capital cost, insurance) for inland ships (Beelen [2]). Reduction of fuel consumption, and thus fuel costs, improves the competitive position for an inland ship operator on the transport market. Moreover, reduction of fuel consumption reduces the production of greenhouse gases and other emissions such as NOx or particulate matter.

Fuel consumption (and the production of emissions) can be decreased by reducing the required amount of power for propulsion and auxiliary equipment. For example, more efficient propulsion engines or generator sets can be installed. Furthermore, the ship's propellers can be replaced by optimized ones or the hull form can be improved so that its resistance is reduced or to obtain a better flow towards the propellers.

This thesis addresses the hull form of an inland ship because it specifically involves a trade-off between cargo capacity (through displacement) and fuel consumption. Therefore, it influences the competitive position of a ship operator. More specifically, the focus is on the submerged part of the stern. Investigation of the bow form is omitted, since the flow around it is less complex compared to the flow around the stern and adjusting the bow only affects a relatively small portion of the total resistance of an inland ship. The design of the stern, however, does not only affect resistance but also has a significant influence on the propulsive performance of the ship.

Figure 1.1: Example of an inland ship propeller tunnel. The skirts on the sides are closing off the volume in front of the propeller, so that air is prevented from entering the propeller from upstream. When the propeller is active, its suction will eventually have the tunnel filled with water, so that the propeller can provide sufficient thrust, even when it is only partially submerged in still conditions.

The stern is a complex part of an inland ship. It has to lead the flow around the ship towards the aft end of the ship in such a way that resistance remains acceptably low. Meanwhile, it has to provide space for the propellers and rudders, while it also has to lead sufficient flow towards them. The flow should be such that the propellers work efficiently and the rudders can adequately maneuver the ship. However, since the main dimensions (length, width, draft and depth) of inland ships are subject to strict limitations imposed by locks, river dimensions and bridges, the hull form of an inland ship is full to provide maximum cargo capacity. This means that the stern part of the ship has to provide all of the above under tight constraints.

The full hull form of an inland ship leads to high ship resistance and heavily loaded propellers. To decrease propeller loading, the diameter is maximized and ducted propellers are applied. The former requires tunnels to be fitted to the ship in order to prevent propeller ventilation, which can occur if a propeller operates close to the water surface. Ducted propellers reduce propeller load since the duct also produces thrust. Examples of both a tunnel and a duct are presented in Figure 1.1. Despite these measures, the load on the propellers remains high. This requires attention for the propeller inflow: if the inflow contains strong variations, vibration nuisance and possibly damage to the ship and the propellers can be the result.

Furthermore, inland ships regularly - if not continuously - navigate in shallow water. The presence of the bottom in shallow water forces the flow to follow another trajectory around the stern and makes the flow towards the propellers more difficult. Impacts of shallow water on the flow around the stern are complex and not yet fully understood.

1.1. Challenges for inland ship stern design

To ease the design process of an inland ship stern and to cope with the complexities that come with it, a ship designer can use design guidelines, empirical tools to estimate the performance of the ship, model tests, or computational fluid dynamics (CFD).

The most complete set of design guidelines specifically aimed at self-propelled inland ships was published by Heuser and Müller [3]. These guidelines consist of drawings of what a ship should look like, along with limits to dimensions or ratios between different dimensions. If these limits are not exceeded, at least reasonable performance can be achieved.

However, available design guidelines do not provide sufficient detail to actually improve an inland ship. For example, the guidelines do not describe how performance changes if designers change their ships without exceeding the proposed limits, or if requirements force them to exceed the limits. To provide this information would have required the analysis of numerous hull forms in varying operational conditions; an exercise too costly if model testing is the only available option to perform this analysis, as was the case at the time the guidelines were developed. In addition, the guidelines are relatively coarse: a wide variety of ships fit within the limits defined by the guidelines, while the performance among ships may differ significantly. Meanwhile, these differences in performance can not be observed from the guidelines.

Empirical tools give an estimate of a ship's performance for a limited set of input parameters. Moreover, the input can be varied to assess the sensitivity of the performance to certain parameters. The method by Holtrop and Mennen [4] is widely used and requires input that can be determined from most hull forms. Similar methods have been proposed by Hollenbach [5] or Guldhammer & Harvald [6] and are used for inland ship performance analysis according to Pompée [7].

Drawbacks of empirical methods are that most of them were developed based on data from sea-going ships and that their purpose mainly has been to assess performance of those ships. Therefore, these methods include parameters that are relevant to sea-going ships but do not vary among most inland ships. Moreover, because their basis largely consists of sea-going ships, typical inland ship features, such as a tunnel and (extreme) shallow water effects are not included in these methods.

Testing a ship design at model scale or performing CFD calculations gives more insight into the flow around a ship and thereby overcomes the lack of detail of design guidelines or empirical methods. Both, but especially CFD, allow to pinpoint which aspect of a ship should be adapted to improve performance. Nowadays, with increasing computational power available, CFD is used more often and is becoming more accessible.

Despite the possibilities, model tests and CFD calculations are relatively expensive compared to the design budget for inland ships. While the cost of applying these techniques does not depend significantly on ship size, the design budget of an inland ship does. The budget is lower because it is smaller and its design is less complex than a sea going ship. Moreover, fuel consumption costs are lower

because of the smaller ship and thus less propulsion power, increasing payback time of the investment.

Apart from the cost per calculation or model test, multiple operational conditions have to be investigated since inland ships encounter varying speed, water depth and draft during their lifetime. Moreover, the complexities of the flow around an inland ship stern described above cause strong interactions between the hull form and propellers. This requires an approach that integrates hull form and propeller design, leading to expensive calculations. Altogether, a large investment is needed to obtain valuable results, for which the budget is usually not appropriate.

Because guidelines and empirical methods are not satisfactory, and CFD often is too expensive, designers have to fall back on their experience, which is based on previous designs or on what they have observed among existing ships. A designer of inland ships often resorts to adapting a previous design to meet the requirements for the new design. In some cases, an old design is simply copied. This is a fail-safe approach and can lead to fine ships, but it will not lead to performance improvements that are needed to reduce fuel consumption and to comply with increasingly strict regulations and demands regarding fuel consumption and reduction of emissions.

1.2. Design guidelines for requirements

As discussed in the previous section, design guidelines give initial limits for the design which, when not exceeded, should lead to a ship that performs well in terms of propulsion. These guidelines, however, do not show how performance is affected if designers do exceed the given limits. One example is the case where a designer aims for a larger displacement. Currently available guidelines do not show which aspects of a ship should be adapted in order to increase displacement and maintain good propulsive performance. The guidelines do not provide the impact of increasing displacement either, preventing designers to make a trade-off between displacement (and thus cargo capacity) and propulsion power.

If design guidelines also tell how the performance of a ship is affected if certain parameters related to the stern change, it becomes possible for designers to assess the impact of increasing displacement. They can then make the trade-off between displacement and propulsion power and, if required, they can increase displacement knowing the impact on fuel consumption. Moreover, it shows designers which parameters to adjust preferably when increasing displacement.

To develop such guidelines, the analysis of numerous hull forms in varying environmental conditions is required. Heuser developed his guidelines based on model test results (Heuser and Müller [3]). Investigating a multitude of (systematically varied) hull forms and environmental conditions is unfeasible using model tests. That, together with inland ships usually being designed based on experience from previous designs rather than applying detailed analysis (either to assess performance or improve the hull form), prevents gathering quantitative data that is required to identify trends with regard to propulsion performance.

Today, however, CFD has become a mature tool and more computational power is available, making it possible to analyze a large number of hull forms. This allows

for the development of guidelines that not only provide a single design point but also show how propulsion performance is affected if more displacement is required.

1.3. Research objectives

The goal of the research presented in this thesis is *to better understand the relation between stern shape aspects, water depth, and inland ship propulsion performance*. Using the obtained understanding, guidelines are developed that *1)* show which stern shape aspects are most important to propulsion performance, and *2)* describe the optimal shape of the stern for an inland ship with certain main dimensions (thus belonging to a specific CEMT-class), depending on required displacement. The guidelines therefore do not only describe a single ship design, but also describe how the ship design should be adapted if a different displacement requirement should be met.

1.4. Focus and limitations of the study

To develop the guidelines mentioned in section 1.3, multiple inland ship stern shapes have to be analyzed under varying operational conditions. It is not possible to include every possible stern design or operational condition. This section discusses the choices made regarding stern design aspects and operational conditions to limit the scope of the study. Readers unfamiliar with inland ships and inland waterway transport can refer to chapter 2 for more information on fairways, ship classes, and typical inland ship design aspects.

1.4.1. Ship types

This thesis mainly focuses on a self-propelled inland ship of the CEMT-class Va type. This is a ship measuring 110.00, 11.40 and 3.50 meters in length, width and draft respectively. However, to be able to apply the guidelines more widely, class IV and VIa ships are included as well. The main dimensions (length, width, and draft) of these are 86.00, 9.50, and 2.80 meters (class IV) and 135.00, 14.20 and 4.00 meters (class VIa). Ships in classes Va, IV and VIa are among the most frequently built ships in the Netherlands over the past decades; see Figure 1.2.

1.4.2. Inland ship stern aspects

Multiple general stern shapes can be distinguished among inland ships, but this thesis focuses on single- and double-propeller tunnel sterns and pram-shaped sterns. A single-propeller tunnel stern is presented in Figure 1.1, while a pram-shaped stern is shown in Figure 1.3.

An inland ship stern design, especially that of a tunnel stern, is complex. For example, Figure 1.3 shows the tunnel, skirts, rudders, and a ducted propeller. In some cases, flow extenders are fitted that extend the top of the tunnel behind the propellers to improve propeller outflow, or rudder headboxes are attached to the ship (see Figure 1.4). Moreover, each of the aspects and details are designed differently for every new ship design, making up a vast number of possibilities.

The present study focuses on the bare hull and the tunnel skirts only, so that

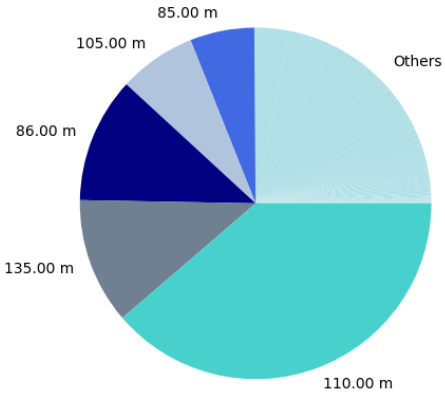

Figure 1.2: Distribution of ship lengths [m] among ships built between 1980 and 2018, own image based on data from www.debinnenvaart.nl

both the complexity of the hull form analysis and the number of hull forms to be investigated (more parameters would require more tests) is limited. This means that details such as headboxes, propeller ducts, rudders, rudder shafts, anchor holdings, and the propeller shaft are not included. Although omitting such details is a simplification of the ship geometry, it leads to cleaner trends with respect to hull form aspects. For example, using a specific rudder design would make a hull form for which that rudder design is suitable, appear better than hull forms that would actually require a different rudder design. Furthermore, taking only hull form aspects into account still allows for a large number of parameters to be investigated.

The impact of the simplification does not affect the trends significantly. In chapter 4, a comparison of trends for influential hull form aspects is presented, showing that inclusion of the duct geometry would not lead to significantly different trends. Furthermore, it is shown that effects of the duct on the flow around the ship are limited to the region near the duct. Because omitting the duct is the most significant simplification to the ship's geometry, it is assumed that trends are not significantly affected by other simplifications either.

While the previous paragraphs stated that only the bare hull form itself is taken into account, the position of the propeller is included. In this way, the propeller-hull interaction, which is important for the overall propulsive performance, can be investigated. The effect of the propeller on the flow is modeled by forces acting on the flow in the CFD calculation. This is known as the actuator disk. The propeller geometry itself is therefore not considered (in fact, there are already numerous parameters to be investigated for the propeller itself (Vesting *et al.* [8])).

Figure 1.3: Left: Example of a pram-shaped stern, including a skeg. Right: Stern of an inland ship, including a tunnel, rudders, a propeller duct and anchor vaults. (Photos by René Rapati, Groenendijk & Soetermeer)

1.4.3. Operational and environmental conditions

As discussed in section 1.1, inland ships encounter numerous operational conditions. For every route, or even along a specific route, changes to water depth, draft, and speed occur. Not all possible combinations can be included in the present study, and a selection was made. Which operational conditions were included is discussed below.

The water depths that were taken into account are those that are regularly encountered and affecting ship resistance and propulsion performance significantly. Figure 1.5 shows how frequent certain water depths are encountered along the main inland waterway transport route from Rotterdam to Germany (the Waal and Rhine rivers). For a class Va ship, which is allowed to navigate on that river, most water depths encountered correspond to a water depth to ship draft ratio (h/T) with values between 2.0 and 3.0. Another frequently used canal is the Amsterdam-Rhine canal that connects Amsterdam to the Waal. The guaranteed water depth in the Amsterdam-Rhine canal is 6.0 meters, whereas the maximum allowed draft is 4.0 meters (class VIa of the CEMT classes). This corresponds to an h/T ratio of 1.5. Therefore, water depths corresponding to h/T ratios of 1.5, 2.0 and 3.0 are taken into account in this thesis. These are encountered relatively often while the effect on propulsion power is still present.

Speed is kept constant in most of the calculations. The reason for this is that the major part of an inland ship's resistance, which is viscous resistance, generally scales with V_S^2. The part of the ship's resistance for which the relation with ship speed is less clear, wave resistance, only accounts for approximately 15 percent of total resistance (Larsson and Raven [9]), since the speed of an inland ship is in general low with Froude numbers between 0.10 and 0.15. Furthermore, this portion of resistance itself is mostly produced by the bow, which has not been taken into account in the study.

Lastly, draft changes are taken into account. However, the variation of draft is limited, so that the propeller remains sufficiently submerged. The CFD code applied in this study, PARNASSOS (Hoekstra [10], Van der Ploeg *et al.* [11], Raven *et al.*

Figure 1.4: Stern of an inland ship on a transport barge, showing propeller ducts and tunnel skirts. The ship in the foreground features an headbox as well. Headboxes, however, are not studied in this thesis. (Photo by René Rapati, Groenendijk & Soetermeer)

[12]), does not allow the propeller to emerge from the water surface. Furthermore, having the propeller very close to the water surface would cause problems in generating the grid for the CFD calculations. Hence, draft is varied so that the minimum distance between the propeller and the still water level is 0.5 meter, while the maximum draft equals that of the ship class considered.

1.5. Research questions and outline of this thesis

As implied in sections 1.3 and 1.4, the guidelines that are developed are based on data obtained from CFD calculations. Obtaining and using the data, obtaining insights on hull form aspects from it, as well as transforming these insights into design guidelines, requires additional steps. The path towards the goal is therefore divided into steps, each of which can be addressed by a key question. These questions are as follows:

1. What are typical inland ship stern shape aspects?
2. How can the influence on propulsive performance of each aspect be tested?
3. Which of the aspects are most important to propulsion performance?
4. How do these aspects affect propulsion performance?
5. How to find a series of optimal designs for a varying design constraint?
6. For a varying displacement constraint, what is the optimal choice for each of the aspects considered?

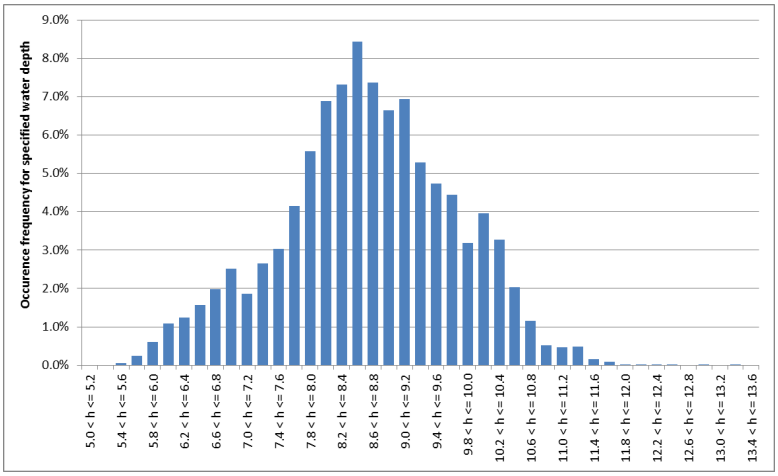

Figure 1.5: Waterdepth [m] occurence (in percent) on the Rhine on February 26th, 2016, measured from an inland ship. Own figure made with data from the CoVaDem project (MARIN, 2017)

The first question addresses typical inland ship design features, why they are used, and how they vary among existing inland ships. This question also settles part of the scope: which hull form aspects are included in the study? The question is answered by means of a literature study, described in chapter 2, and analysis of existing hull forms, described in chapter 3.

The second question aims at finding a method to determine the effect of variations observed while answering the first question. This involves three steps: parameterization of the hull form, choosing which hull forms to test (design of experiments) and obtaining an estimate of the performance of each hull form. The first and second steps are discussed in chapter 3. The third step requires an adequate set-up of CFD simulations (i.e. grid, boundary conditions, domain size), which is discussed in chapter 4. Finally, determination of the objectives that define the performance of a hull form is described in chapter 5.

Identifying the most important hull form aspects and filtering aspects of secondary importance is the topic addressed by the third question. The most important hull form aspects are the first a designer should focus on in order to improve a stern design. Furthermore, if design guidelines tell the designer to adjust a series of hull form aspects, the designer understands the impact of not following a guideline exactly, or which of the guidelines should not be ignored. Methods to determine the most important parameters are discussed in chapter 6.

The fourth question focuses on finding the trend between a certain hull form aspect and the propulsive performance of an inland ship. Methods to obtain these trends are discussed in chapter 6.

Next, the fifth question focuses on a method used for derivation of design guidelines from the trends obtained after answering the fourth question. This includes optimization of the stern shape, aiming at minimizing propulsion power while ensur-

ing that the ship accommodates a sufficient amount of displacement, for example. The question is answered in chapter 7.

Finally, the sixth question aims at finding optimal designs depending on water depth and displacement, while satisfying constraints imposed on the design. The result is a series of hull forms as well as information on which hull form aspects to change, depending on required displacement and the water depth that the ship is designed for. Part of the results are presented together with the approach to derive them in chapter 7. The remainder is presented in chapter 8.

After each of the questions stated above has been discussed and the design guidelines have been presented, the main findings are briefly summarized in chapter 9, where the conclusions of this study are presented, and the most important guidelines are summarized.

2

State-of-the-art of inland ship stern design

In the previous chapter, several aspects of the design of an inland ship stern and the flow around it are discussed. To understand the complexity of an inland ship stern, each of the aspects should be known, as well as their impact on the flow around the stern or whether and how they conflict with other aspects. With that information, available information in literature (i.e. design guidelines or methods to assess ship performance) can be investigated to determine whether and to which extent the design of these aspects is covered.

This chapter, therefore, aims to identify the gap in available methods and guidelines with respect to the design of an inland ship stern. It does so by first identifying the relevant design aspects (sections 2.1 and 2.2) and describing their effects on the flow around the ship and how they conflict with design requirements. Then, available literature on inland ship stern design is discussed (2.3). Finally, a summary of inland ship stern design and literature about it is given in section 2.4, together with a discussion on what is required to enhance available knowledge.

Figure 2.1: An inland ship sailing with small freeboard

2.1. Hull form of inland ships

The hull form of inland ships is different from that of sea-going ships. With respect to main dimensions (i.e. length, width and draft), inland ships have relatively high length-to-width and high length-to-draft ratios. Also, the depth is such that there is only a small amount of freeboard in case a ship is fully loaded as shown in Figure 2.1.

Inland ships have a very full hull form: block coefficients from 0.80 to 0.90 are common. These high block coefficients follow from limitations imposed on the main dimensions by locks, bridges and fairway dimensions. These limitations do not allow that the ship's main dimensions are enlarged in order to transport more cargo, and more cargo space can only be obtained by increasing the block coefficient. The bow and stern region of an inland ship are therefore relatively short, and the parallel midship extends over a large portion of the ship length (see Figure 2.2).

In Europe, inland ships have been divided in classes with regard to their main dimensions. This classification system is based on the dimensions of ship types that were common at the time the system was developed. Nowadays, the system serves as a guideline for the construction of locks, bridges and channels while also serving as an indication for captains showing if they can use a certain fairway or not (dr.ir J.U. Brolsma and ir. K. Roelse [13]). Table 2.1 shows the classes of self-propelled inland cargo vessels in Europe. Most of the recently built ships belong to the classes IV, Va and VIa (Hekkenberg [14]).

Figure 2.2: Inland ships width a length of 135.0 meters stacked on a pontoon. The long parallel midship, and the short bow and stern regions, are visible. (Photo by René Rapati, Groenendijk & Soetermeer)

Class	Length	Width	Draft	Tonnage
I	38.50	5.05	2.50	400
II	55.00	6.60	2.60	800
III	67.00	8.20	2.70	1250
IV	85.00	9.50	3.00	2000
Va	110.00	11.40	3.50	3300
VIa	135.00	17.00	4.00	4000

Table 2.1: Fairway classes as defined by the ECMT

2.2. Inland ship stern features

The stern of an inland ship has to provide inflow to the propellers and rudders. It also has to provide space for machinery related to propulsion, maneuvering and in some cases also for the generation of electricity. Furthermore, it provides room for the accommodation of the crew. Focusing on the submerged part of the stern, this section discusses propulsion and rudder configurations, the propeller tunnel and other features such as headboxes and flow cover plates. Examples of these features on inland ships are given in Figure 2.3.

2.2.1. Short stern with high curvature

The high block coefficients of inland ships lead to strong curvature of the hull form in the stern region. If the curvature is too strong, local pressure gradients - that follow from the curvature - can cause flow separation. This can then cause higher resistance, or strong variations in the propeller inflow. The latter can cause vibration hindrance, cavitation, and possibly damage to the propellers, as discussed in the previous paragraphs. However, the high block coefficients are chosen to increase loading capacity at the same length, width and draft of the ship as discussed in 2.1.

2.2.2. Propulsion configurations

Due to limitations of draft and in order to prevent the propeller from piercing the water surface in case of low draft (due to limited water depth or when in ballast

condition), the propeller diameter is usually small. This leads to heavily loaded propellers, which makes them prone to cavitation. To decrease the loading on the propellers, multi-propeller configurations are applied, or a propeller duct is installed.

A multi-propeller configuration, for example twin-propeller, provides a significant reduction of propeller loading while also adding redundancy: if one shaft drive fails, there is an additional propeller available so that the ship remains manoeuvrable and can safely reach a mooring location. A drawback of a multi-propeller system is that the propeller inflow becomes inclined, which leads to a loss of efficiency. Also, twin-propellers can not be fitted at the location where they would operate efficiently: at the ship center, where the wake of the ship is strongest (Wald [15], van Terwisga [16]).

A propeller duct is a ring around a propeller with a foil-shaped cross-section. The duct generates a lift force due to the pressure difference between the inside and outside of the duct, which is generated by the suction of the propeller. The lift force serves as additional thrust, which can be 30 % of the propeller's thrust (Oosterveld [17]). Additionally, the duct increases the efficiency of the propulsion system for heavily loaded propellers.

Apart from the advantage of decreasing propeller loading, a duct does make the flow around the stern more complex. Namely, the efficiency of a ducted propeller decreases in oblique inflow (Ghassemi *et al.* [18]), and even flow separation can occur at both the in- and outside of the duct. When a propeller blade passes through the flow separation on the inside of the duct, the angle of attack on the blade changes, which can cause vibrations.

2.2.3. Tunnels

The propellers of an inland ship is commonly fitted in a tunnel. This tunnel prevents propeller ventilation, which occurs if a propeller operates close to the water surface and starts taking in air and thereby loses thrust. Especially when the propeller is not supplied with a decent inflow of water (e.g. in bollard pull conditions or acceleration of the ship from low speed), ventilation can occur. The skirts of the tunnel (see the left photo in Figure 2.3) prevent this by increasing the effective distance between the propeller and the water surface. Namely, air would have to pass around the skirt first in order to reach the propeller. In most cases, the skirt are 'appended' to the hull, but they can be integrated as well, see Figure 2.4.

The tunnels do, however, increase the ship's resistance (van der Meij and Raven [19]) due to a portion the flow leaving the tunnel around the skirt before reaching the propeller, after initially moving into the tunnel. Adjustments to the tunnel design reduce this effect, but the optimal design of the skirt depends on water depth (Rotteveel and Hekkenberg [20]). The required size of the skirt needed in order to prevent ventilation is usually determined from guidelines (Rotteveel *et al.* [21]).

2.2.4. Shallow water design

One of the effects that shallow water has on the flow around a ship is that it makes the flow follow a trajectory parallel to the horizontal plane. The flow becomes two-dimensional and more flow enters the tunnel, and eventually the propeller,

from aside the ship rather than from underneath. That the design of the stern should be adapted to this changed flow pattern has been shown by Rotteveel *et al.* [20, 22]. A typical adaptation of the stern design to the two-dimensional flow is that for example, the tunnel skirt follows a horizontal line when viewed from aside. Similarly, von der Stein [23] showed that a ship with a tunnel skirt starting from the side of the parallel midbody performs better in shallow water while a pram-shaped stern (possibly with a tunnel starting from the bottom) performs better in deep water.

2.2.5. Rudder configurations

The rudder system for the ships in Figure 2.3 consists of multiple rudders. This is also a typical inland ship feature that distinguishes inland ships from sea-going ships (Liu *et al.* [24]). Multi-rudder configurations are installed because rudder size is limited due to draft, while a sufficient rudder area is required to provide the maneuvering forces needed to navigate through winding rivers and perform maneuvers in the limited space that inland waterways provide.

Since the forces produced by rudders depend on the flow speed around them, the propeller outflow speed should preferably be high. This, however, conflicts with - as stated above - locating the propeller in the area where the wake of the ship is the largest. Namely, velocities are lower in that area, meaning that the propeller outflow velocities, and thus the velocity around the rudder are lower. Putting the propellers (and rudders) in an area of higher velocity (and less energy losses due to the hull) yields large rudder forces but leads to a loss of propulsion efficiency.

An extensive study into the choice of rudder configurations and the corresponding rudder sections for inland ships has been performed by (Liu [25]).

2.2.6. Other features

Inland ships usually have a large transom, which will be submerged if the ship is loaded. Although the large transom results in additional resistance, making it smaller is usually difficult since the aft most end of the stern should provide space for machinery driving the rudders. Moreover, inland ships usually have an anchor holding at the transom as well (see Figure 2.3) . If the transom area is reduced, the anchor would be partially be submerged which may either lead to even more resistance, or damage the anchor.

Another feature sometimes used in inland ships is a flow extender (or cover plate) (Hekkenberg and Thill [26]). A flow extender is a plate above the rudders that forces the outflow of the propeller to become more parallel to the horizontal plane and increases the performance of rudders at high angles of attack. Also, it directs the propeller outflow horizontally, so as to lose less energy to vertical motions in the flow and increase the efficiency of the propulsion system. An example is shown in the right picture in Figure 2.3.

Concluding, shallow water, high block coefficients, small propeller diameter and even requirements imposed on manoeuvrability make that the design of an inland ship stern is complex, being subject to multiple trade-offs that sometimes conflict. Moreover, the above discussion only focused on the hydrodynamic part of

Figure 2.3: Two sterns of inland ships during repairs or maintenance (Photos by René Rapati, Groenendijk & Soetermeer)

Figure 2.4: Example of an inland ship stern with a tunnel, but integrated tunnel skirts (Photo by René Rapati, Groenendijk & Soetermeer)

the design, while requirements on the interior of the ship hull (machinery, steering equipment, housing, etc) also conflict with preferable conditions for the wetted part of the stern.

2.3. Inland ship stern design in literature

In literature, multiple design guidelines and empirical tools have been presented that can help the design of an inland ship. An overview of existing guidelines and tools has been presented by Rotteveel *et al.* [21]. The following sections are a summary of this work.

2.3.1. Design guidelines

Design guidelines can be used to design a stern that is feasible and provides reasonable performance while avoiding problems due to the complexities described in section 2.2. This section discusses the design guidelines that are available from literature.

The most extensive set of guidelines for self-propelled inland vessels has been published by Heuser and Müller [3]. These guidelines include favorable dimensions of the overall ship as well as specific dimensions for the bow and stern. The guidelines are relatively simple. The advised length of the stern is determined from equation 2.1 for a single-propeller ship, a double-propeller ship with converging propeller shafts and a double-propeller ship with parallel propeller shafts respectively:

$$\begin{aligned} L_{WL-H} &= 1.9 \cdot D + 1.85 \cdot B \\ L_{WL-H} &= 2.5 \cdot D + 1.65 \cdot B \\ L_{WL-H} &= 3.2 \cdot D + 1.45 \cdot B \end{aligned} \tag{2.1}$$

where D is the propeller diameter and L_{WL-H} stands for the water line length of the stern (H stands for *Hinterschiff*, which is the stern). In addition to the stern length, Heuser advised [3] that the distance between the propeller should be approximately $0.28 \cdot B$ and $0.45 \cdot B$ for the converging and parallel propeller shafts respectively.

To provide a more detailed guidelines, Heuser added sketches of specific frames. These are presented in Figure 2.5. One measure given is that of the tunnel dimensioning: according to Heuser, the radius of the tunnel above the propeller should equal the propeller's diameter.

Additional details are given by Heuser as well [3]. These include the minimum immersion of the tunnel skirts and the immersion of the tunnel at its end near the propeller. Also, Heuser added several notes which provide qualitative guidelines and allow for various interpretations.

Nowadays, some of Heusers advises have become rules-of-thumb for inland ship designers. One of these is the radius of the tunnel around the propeller, which also in existing ships is often equal to the propeller diameter.

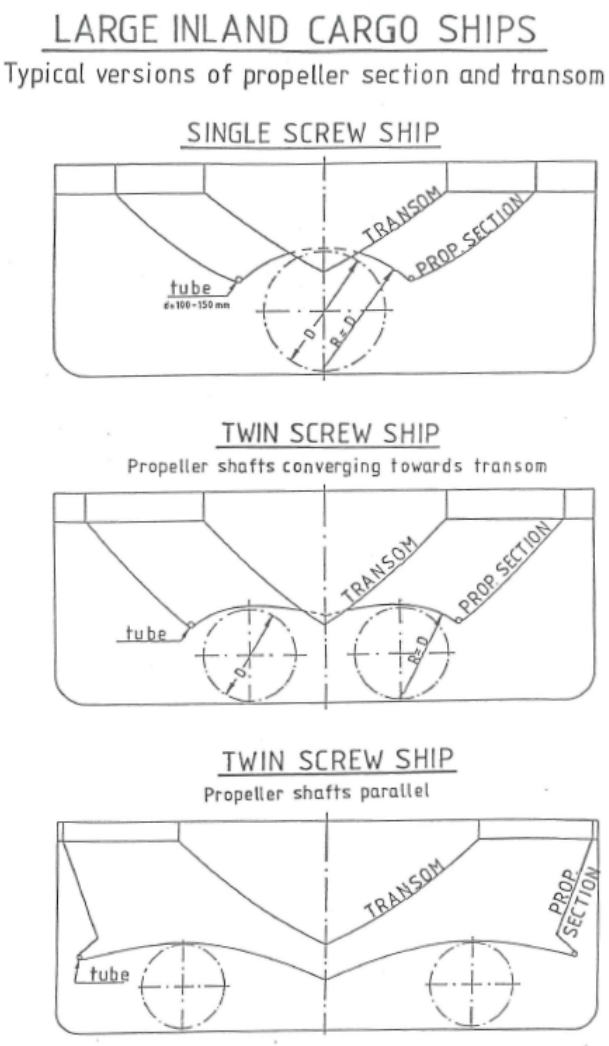

Figure 2.5: Overview of Heuser's guidelines relating to the propeller section frame of single-propeller and double-propeller inland cargo vessels

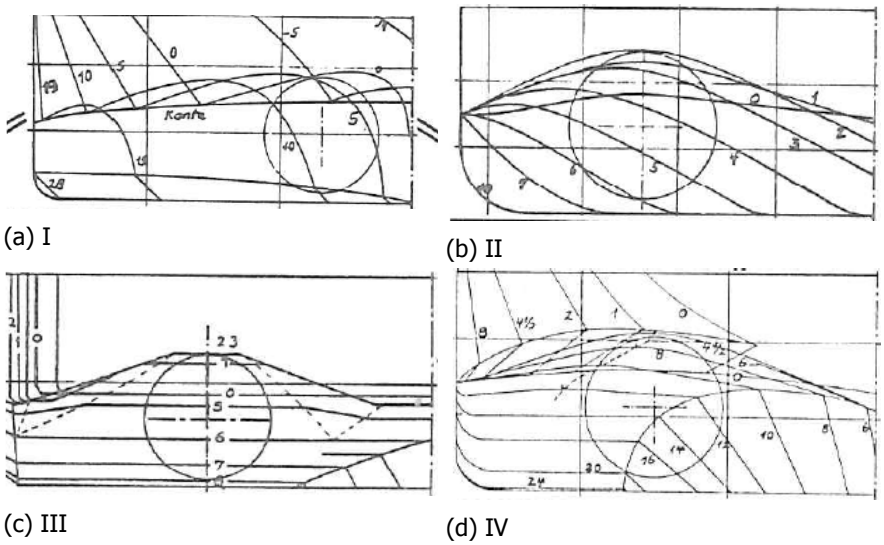

(a) I (b) II

(c) III (d) IV

Figure 2.6: Ship types defined by N. von der Stein. I is most suited for shallow water. II and IV are suited for intermediate water depth. III is best suited for deep water, and is mostly used with pushboats.

For pram-shaped sterns, several guidelines that are available in literature are discussed by van Terwisga [27]. Among them is the rounding off of waterlines and buttocks. Compared to sharp angles, a slightly rounded off edge already has a significant effect on the resistance of the barge. Also discussed is the effect of the run angle (i.e. the angle between the horizontal plane and the bottom of the stern, when viewing the ship from aside). The effect of the run angle, however, appears to depend on the B/T ratio of the barge.

Latorre and Ashcroft [28] discuss several options for rounding of the stern and choosing the run angle. Furthermore, they included multiple options for skegs, which may be required for course-keeping and berthing.

Choosing between either a pram-shaped stern or a classical tunnel stern depends on the water depth that the ship is design for, according to von der Stein [23]. The pram-shaped stern performs well in water depths corresponding to relatively high h/T ratios. The classical tunnel stern performs well in intermediate water depth and very shallow water. For the latter, a single propeller ship or a double propeller ship where the propellers are fitted close to the ship centerline are preferred. To clarify, he drew four basic ship forms, as shown in Figure 2.6.

2.3.2. Empirical performance evaluation

While design guidelines such as those discussed above show how a well performing ship should look like, empirical methods can show effects of changes to certain hull form aspects on the ship's performance. Empirical methods usually consist of several formulas that give estimates of ship resistance and possible propulsion

related performance parameters. They are developed based on the analysis of model tests, CFD calculations or real-world observations. A main advantage of these empirical methods is that they yield an indication of performance with limited input.

Performance in deep water

The empirical method published by Holtrop and Mennen [4, 29, 30] is widely used. It provides estimates of resistance and propulsion power. It has been developed from the analysis of a vast number of model tests and their correlation with full-scale performance. The method only requires relatively general parameters, including but not limited to the transom area (if submerged), water plane coefficient, block coefficient and certain properties of appendages.

A similar empirical method was developed by Guldhammer and Harvald [6] and Holtrop, van Terwisga and Mennen developed a method specifically aimed at pontoon-shaped barges [31]. The method by Guldhammer and Harvald yields comparable results to the widely used method by Holtrop and Mennen when applied to inland ships [7]. The method specifically aimed at pontoon-shaped vessels includes parameters for local ship aspects such as the radius of curvature at the point where the parallel midship ends and the stern region begins.

A drawback for the methods Holtrop and Mennen and by Guldhammer and Harvald regarding application to inland ships is that their basis consists of sea-going ships. This means that waterplane coefficients (C_p) and length-to-width ratios (L/B) of ships included in the basis differ from those regularly seen at inland ships, which usually have C_p values exceeding 0.9 and L/B ratios of 8.5 and higher.

Another drawback of these methods is that the parameters used for input do not differ much among inland ships (von der Stein [32]). For example, the block coefficient for most inland ships varies from 0.8 to 0.9 which is already at the boundaries of applicability of both methods. Also, the waterplane coefficient is mostly large and does not vary significantly. The differences between inland ships are limited to local regions on the ship hull.

The parameters of the method by Holtrop [31] that focuses on pontoon-shaped vessels fit better to inland ships. The method includes parameters for stern length and bow length, as well as parameters for the curvature at the point where the parallel midship ends and the stern region begins. Furthermore, the bow and stern region are treated separately which is possible for inland ships as well according to Heuser [33]. Therefore, despite that the L/B ratios included in the work by Holtrop [31] do not exceed 7.5, the method may be effective when applied to inland ships with a pram-shaped stern.

None of the aforementioned methods does include effects of tunnels and corresponding parameters. That tunnels can be a major contributor to inland ship resistance has been shown by van der Meij and Raven [19]. Also, the method by Holtrop [31] for use with pontoon-shaped barges does not include a pram-shaped stern that is s-shaped (i.e. the end of the run is nearly horizontal). Therefore, empirical methods are missing specific details to use them as a tool to compare different inland ships with each other.

Performance in shallow water

Since inland ships nearly always navigate in shallow water, their resistance and propulsion power are affected by it. The estimated performance obtained by, for example, one of the methods above should therefore be corrected so that a reasonable estimate of performance is obtained for daily operation.

There are multiple methods available to correct ship performance for shallow water effects. Some method provide a speed correction at given power, while others estimate the added resistance in shallow water at given speed.

The most widely used method (Raven [34]) is probably that by Lackenby [35]. Based on a limited set of ship parameters, the method estimates the speed loss at equal power. Lackenby's method is a modification of Schlichting's approach [36], who provided a diagram to assess shallow water effects and was the first to systematically look into these effects. Apart from the methods by Lackenby and Schlichting, alternative methods have been published by Karpov (discussed by Terwisga [27]), Jiang [37] and Millward [38]. More recently, a method was published by Raven [39] mainly for correction of speed trials in shallow water.

For all available methods, however, the input parameters only consist of main dimensions and in some cases a block coefficient. Similar to empirical methods for estimation of deep water performance, they do not offer the possibility to distinguish between ships. That differences between ships can change in shallow water compared to the performance in deep water, was shown by Von der Stein [40] and by Rotteveel et al. [22].

Most empirical methods to correct for shallow water effects focus on resistance. However, propulsion parameters such as thrust deduction and wake fraction change as well (Harvald [41], Raven [34], Raven [39], Rotteveel *et al.* [22]). To assess the change of wake fraction, a method was proposed by Kulczyk [42, 43]. Depending on the sectional area curve and the design of a transverse section near the propeller, the method estimates the velocity distribution in the propeller inflow. It was developed for pushers rather than for self-propelled vessels.

2.3.3. Recent investigations

Van der Meij [19] proposed several possibilities to improve the flow around inland ships, including the enlargement of bilge radius towards the stern in order to prevent strong vortices from being shed. Geerts *et al.* [44] discussed a series of possible improvements, including the use of a five bladed propeller, which in certain cases led to an increase of speed at the same fuel consumption. Radojčić [45] wrote an extensive report on a multitude of design options available that should lead to improved efficiency. One of the options is a tunnel of which the skirts can be retracted if the propeller immersion is such that there is no risk of ventilation.

Zöllner [46] discusses multiple possibilities to enhance the performance of inland ships as well. He advices to apply cover plates or flow extenders above the propeller outflow to make this flow smoother. Another innovation proposed is the foldable tunnel skirt. The tunnel skirts can, if not well aligned with the flow, account for a significant portion of the ship resistance (van der Meij and Raven [19]). By applying a foldable tunnel that is retracted or folded into the ship hull when the tunnel is not

needed (in case of sailing at sufficient draft), resistance is decreased.

Multiple options to improve the stern and the flow around it have been investigated during the EU-project MoVeIT! [26] Similar to the advice given by Zöllner, it was found that a flow extender or cover plate (presented in Figure 2.3) can make the propeller outflow smoother, so that less energy is lost in the flow aft of the ship. Futhermore, gondolas (used to place the engines in), should be well aligned with the flow and preferably be positioned such that in a twin-gondola configuration, they are converging towards each other (van der Meij [47]). Another method that was found to improve ship efficiency is a stator in front of the propeller duct.

2.4. Conclusions

This chapter discussed typical inland ship features and why they make the stern design of an inland ship complex, as well as design guidelines or empirical tools that aid in the design of inland ship sterns. The complexity of an inland ship stern is mostly due to the limited space available to provide the propellers with sufficient inflow and shallow water effects. Both impose complexities on the flow towards the propellers.

Design guidelines and empirical tools that could aid the designer with the development of an inland ship stern, do not include sufficient detail to determine why a certain stern design performs well or not. Design guidelines do provide an region or area bounded by dimensions and ratios between them to at least achieve a working design. However, they do not tell how performance is affected if a designer moves around in, or out of the region dictated by the design guidelines. As for empirical methods, there are no methods available that include typical inland ship design aspects. But also for main dimensions, inland ships do not always fit within the scope of empirical methods since those have been developed for use with sea-going ships.

Base on the above, the goal of this thesis is to develop new design guidelines, that also provide information on trends and answers questions such as: *How should the stern be changed if displacement is increased?* or *How does propulsion performance depend on certain hull form aspects?* Trend information may also be valuable if a designer has to deviate from the guidelines because cargo capacity, structural design or space for the housing on the stern force him to do so.

3

Generating inland ship hull forms

The previous chapter described typical complexities of inland ship sterns and identified what is required to better aid designers in the design of inland ship sterns. To develop the design guidelines that are required, a large number of hull forms that vary among each other with regard to relevant design aspects must be analyzed and therefore have to be generated. This requires a parametric model as well as a decent choice to choose the input parameters for that model.

The hull form aspects to be included in the model must be defined first. This is discussed in section 3.1. In the following step, a parametric model must be developed that is able to generate inland ship hull forms representing realistic ships. Multiple methods are available for this. These methods are briefly discussed in section 3.2, where the chosen parametric modeling approach is presented as well. Section 3.3 then gives multiple examples of ways to choose parameter values and the number of ships to be analyzed. Finally, the main findings are summarized in the conclusions, section 3.4.

3.1. Identification of hull form aspects

This section discusses the hull form aspects that are included in the parametric model. Three different inland ship stern types are investigated:

- A tunnel stern for single-propeller inland ships
- A tunnel stern for twin-propeller inland ships
- Pram-shaped stern for twin-propeller inland ships

For single- and twin-propeller ships with a tunnel stern, most of the aspects are equal and they are therefore described together in section 3.1.1. Stern shape aspects specific for pram-shaped sterns are discussed separately in section 3.1.2.

The identification of hull form aspects has been done by visual inspection of existing stern shapes as well as by investigation of literature. By visual inspection, mainly differences between stern shapes are identified. However, certain design aspects that do not necessarily differ among ships may still deserve to be investigated. Such aspects are also identified as stern shape aspects to be varied in the present study.

For both the tunnel stern and the pram-shaped stern, an overview of all aspects is given, followed by elaboration through figures, photos or literature, on some of the aspects considered.

3.1.1. Tunnel stern ships

Figures 3.1 and 3.2 present the included hull form variants for tunnel-shaped sterns. Major hull form aspects are the athwart ships propeller position and the length of the stern region. Furthermore, multiple aspects relate to the shape and curvature of the tunnel.

In Figure 3.1, variants are specifically presented for double-propeller ships. While most of the variants also apply to single-propeller ships, the athwartships position of the propeller is 0.0 by definition. For a single-propeller ship, similar to the propeller position relative to the tunnel for twin-propeller ships, the width of the tunnel can be adjusted, as presented in Figure 3.3.

Figures 3.4, 3.5, 3.6 show examples from existing inland ships. Among the pictures, differing tunnel skirt inclination angles, varying transom shapes, athwartships propeller positions and different tunnel designs can be observed. Figure 3.4 shows:

- Varying athwartships propellers positions in the top-left and top right photos
- Variation of tunnel width for a single-propeller ship in the bottom photos
- Tunnel skirts being aligned with the horizontal plane
- Varying bilge radius between the bottom photos
- An s-shaped bottom plane(bottom-left) and a v-shaped bottom plane (bottom-right)

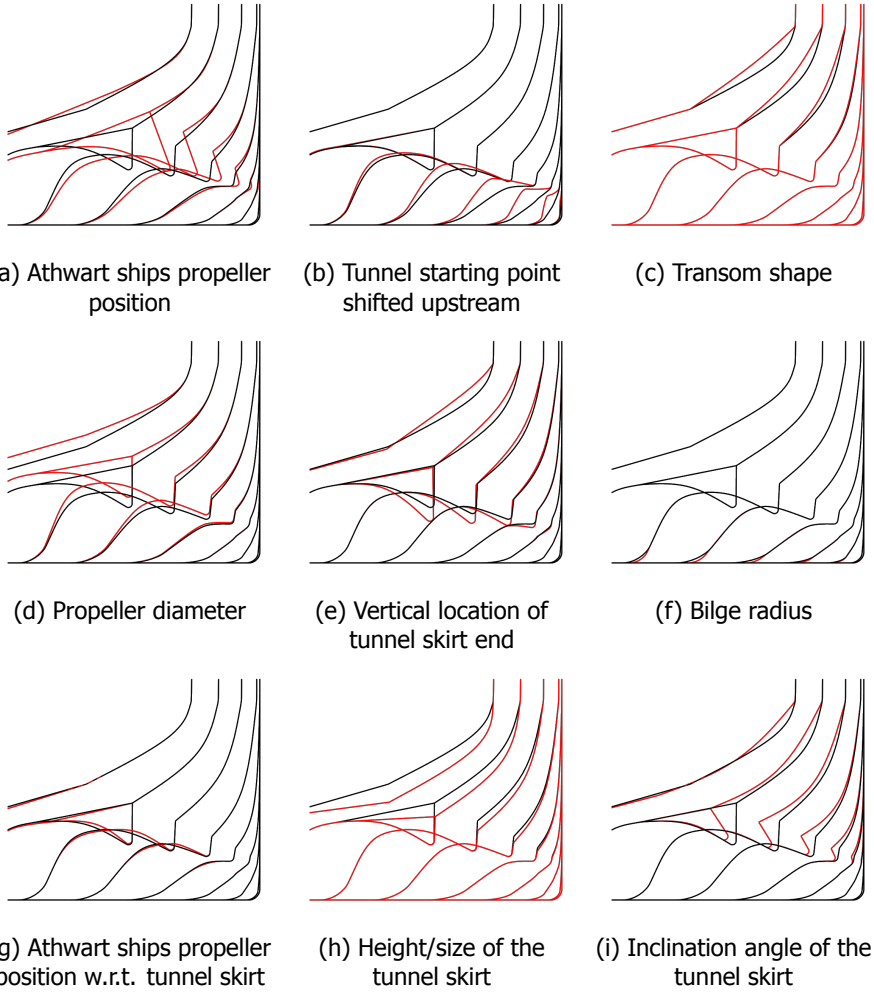

Figure 3.1: Overview of included hull form aspects. The black lines indicate a reference stern shape, while the red curves indicate a variant. More aspects can be found in Figure 3.2

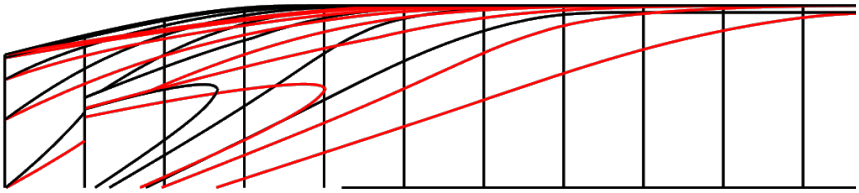

(a) Length of the stern region (i.e. distance between transom and parallel midbody)

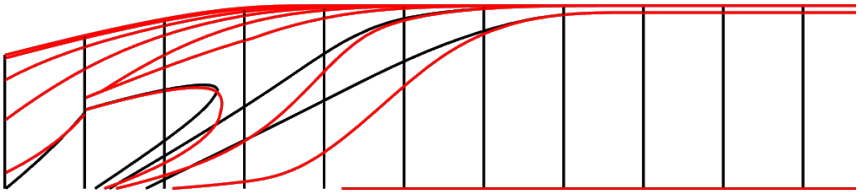

(b) Shape of the bottom plane (either S-shaped or V-shaped)

Figure 3.2: Variants that are more appropriately presented using water lines. Similar to Figure 3.1, black curves indicate the reference shape while red curves indicate a variant.

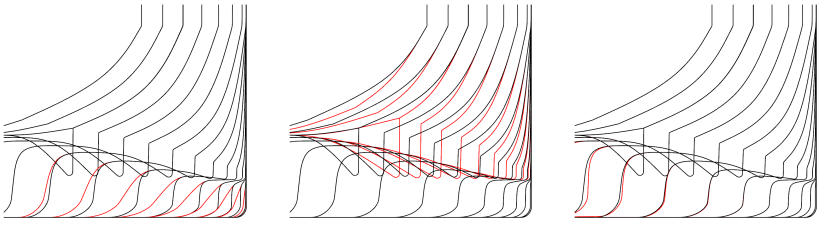

(a) Smoothening of the tunnel entrance

(b) Tunnel width

(c) Skeg / propeller bulb thickness

Figure 3.3: Overview of hull form aspects specific to single-propeller ships. The black lines indicate a reference stern shape, while the red curves indicate a variant.

- Inclined tunnel skirts (top photos) and vertical skirts (bottom photos)

The tunnel skirts being aligned with the horizontal plane shows that during the design process, the flow is assumed to follow horizontal trajectories (van der Meij and Raven [19]). However, the water also moves in vertical direction when passing from midship to the transom. Therefore, the vertical location of the skirt end point is varied so that the alignment between the tunnel skirt and the direction of the flow can be adjusted (see 3.1 (e)). Inclination of the tunnel skirt (compare top and bottom photos in Figure 3.4) can be done from a perspective of reducing area at the tunnel end in order to reduce resistance at a (limited) loss of displacement. On the other hand, the inclination can also be decreased in order to increase displacement if required.

The variation of the bottom plane as displayed in Figure 3.2 and observed from the bottom pictures in Figure 3.4 can depend on the athwart ships position of the propeller. In earlier guidelines proposed by von der Stein [23], two relevant stern designs have been presented: one with its propellers close to the ship's center, the other with the propellers further away from the center. Drawings of these designs are presented in Figure 3.7. The former is deemed more suitable for shallow water [23] and the bottom plane of that design is s-curved such as to prevent the flow entering the propellers with a large inclination (relative to the axial axis of the ship). The design with the propellers further away from the center line has a v-shaped bottom plane and is found to perform better at deeper water [23].

Figure 3.5 shows the tunnel top curve, which is the curve that follows the highest points in each tunnel frame. For the ship in Figure 3.5, the tunnel top curve ends at the propeller inclined relative to the longitudinal direction. The parameter in Figure 3.1 (b) affects how the tunnel top curve approaches the propeller plane.

Figure 3.6 shows two inland vessels between which the transom size differs. The size of the transom directly affects the volume of the hull part directly in front of it, and therefore affects displacement. The transom area is also incorporated as a separate parameter in empirical methods, in which a larger transom usually leads to an increase of resistance Holtrop and Mennen [4], [31].

The bilge radius in the stern region is also included in Figure 3.1. In general, a larger bilge radius leads to lower resistance (van der Meij and Raven [19]). For the length of the stern region, presented in Figure 3.2, guidelines have been given by Heuser and Müller [3]. These guidelines are, however, unclear on the impact that the stern length may have. This aspect involves a major trade-off between additional displacement (which can mean more cargo capacity) or less resistance and propulsion power, and is therefore added as a hull form aspect as well.

3.1.2. Pram-shaped sterns

The other stern type included in the scope of this study is the pram-shaped stern type. The main difference between a pram-shaped stern and a tunnel stern is the curve followed by the bilge line from the midship towards the transom. For a tunnel-stern, the bilge line is parallel to the horizontal plane, follows a path from the bilge at midship towards the ship center, to meet the bilge line of the other side of the ship at the skeg. For a pram-shaped stern, the bilge line does not remain parallel

Figure 3.4: Inland ships on pontoons during transport. One aspects to be observed between the sterns is that the distance between the propeller ducts differs among the ships (photos by René Rapati, Groenendijk & Soetermeer)

Figure 3.5: The tunnel of an double propeller inland ship under construction. The tunnel frames can be identified and by taking the highest point in each frame, one can draw the tunnel top curve and see that for this specific ship, the tunnel is such that the flow enters the duct and propeller under an angle. (photo by René Rapati, Groenendijk & Soetermeer)

(a) I (b) II

Figure 3.6: Two single-propeller inland ships with a different transom size. (photos by René Rapati, Groenendijk & Soetermeer)

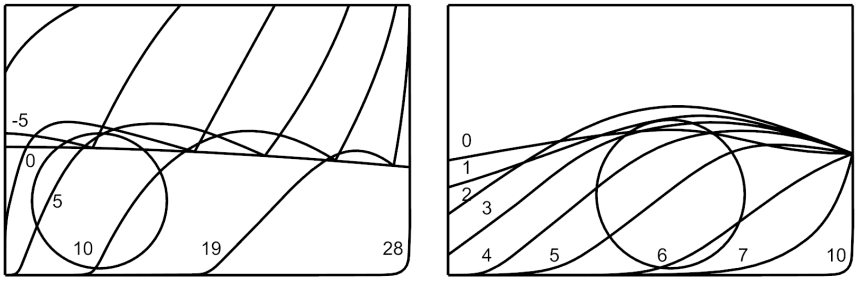

(a) type I (b) type II

Figure 3.7: Ship types defined by N. von der Stein. I has its propellers close to each other and therefore a s-curved bottom plane. II has its propellers farther away and therefore the bottom plane is v-shaped. (images recreated based on original images by von der Stein [23])

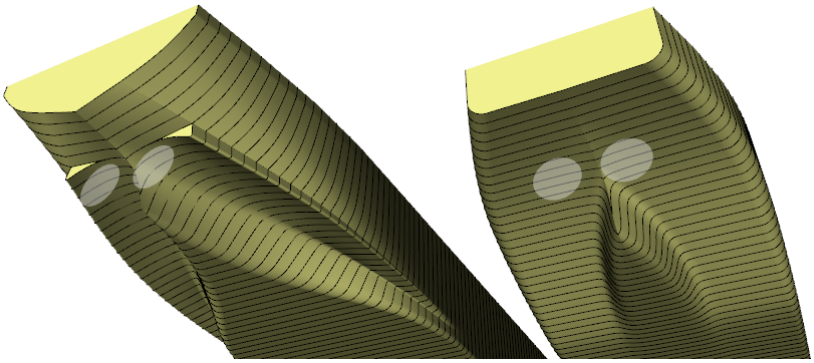

Figure 3.8: The tunnel stern and the pram-shaped stern. For the tunnel stern, the bilge remains in the horizontal bottom plane. For the pram-shaped stern, it travels upwards finally ending at the transom.

to the horizontal plane. Instead, it curves upward and ends at the transom. This is visualized in Figure 3.8.

The pram-shaped stern in this figure does not include a tunnel. The tunnel is excluded because one important reason to choose a pram-shaped stern is for its maneuvering capabilities, since a it allows for the installation of podded, azimuth propulsors. Appending a tunnel would limit the freedom of rotation for such pods. Moreover, a pram-shaped stern has been shown to be outperformed by a tunnel stern in shallow water (von der Stein [23]). Therefore, pram-shaped sterns with a tunnel are rarely used and thus not included in this thesis.

It is possible to add a tunnel to a pram-shaped stern, and the tunnel geometry is therefore not the main difference between the two stern types. However, a tunnel attached to a pram-shaped stern is not common, and it is therefore not considered in this study.

Similar to the discussion on classical stern shapes, an overview of variants included in the present study is given by a series of linesplans, which are presented in Figures 3.9 and 3.10. The overview of pram-shaped stern variants does not include the athwartships propeller position as it is for the classical stern shapes. For pram-shaped sterns, the this propeller position can vary freely as long as there is sufficient space for the propeller to fit between the keel line and the hull of the ship.

One aspect included is the skeg presence and shape. A skeg may be required for course-keeping stability (Holtrop [31]) or to house the main propulsion engines, but it also leads to an increase of ship resistance. The skeg is therefore part of an important trade-off, and is therefore added to the scope of the study. An aspect specific for the stern is its radius at the bottom plane of the ship. This is also added to the study. An example of a blunt pram-shaped stern is given in Figure 3.11. The ship in this Figure has a relatively short stern with strong curvature. Also, the skeg is thick and blunt.

Another aspect for pram-shaped sterns is shown in the second drawing in Figure 3.6. The aft most end of the stern is v-shaped. Depending on how the bottom is

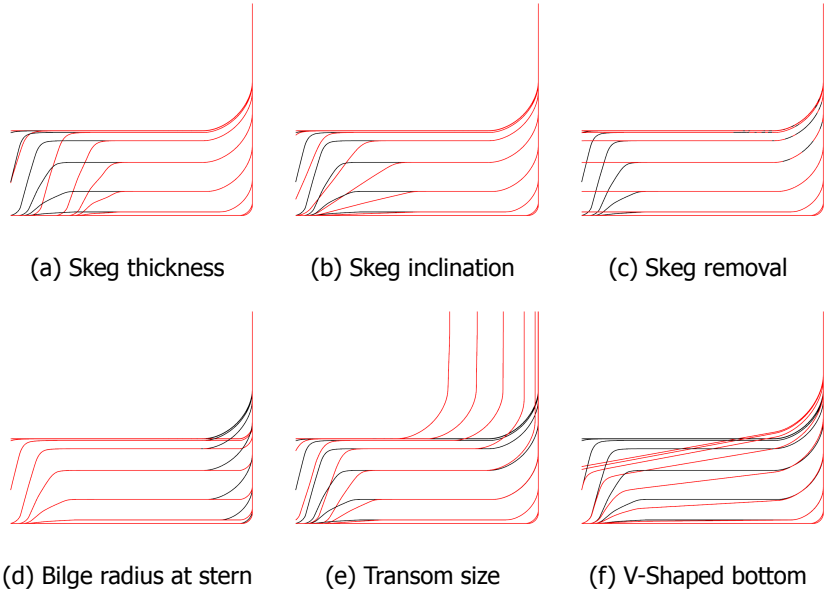

(a) Skeg thickness (b) Skeg inclination (c) Skeg removal

(d) Bilge radius at stern (e) Transom size (f) V-Shaped bottom

Figure 3.9: Overview of included hull form aspects for pram-shaped sterns. The black lines indicate a reference stern shape, while the red curves indicate a variant. More aspects can be found in Figure 3.10

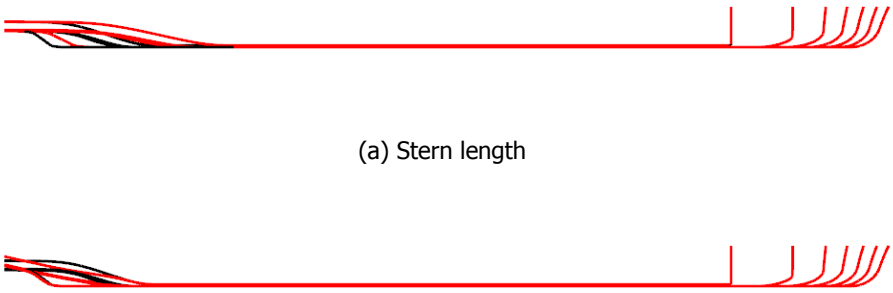

(a) Stern length

(b) Stern bottom curvature

Figure 3.10: Stern length and curvature variants for pram-shaped sterns. The black lines indicate a reference stern shape, while the red curves indicate a variant.

Figure 3.11: Example of a pram-shaped stern, including a skeg (photo by René Rapati, Groenendijk & Soetermeer).

made v-shaped, it reduces or increases displacement. Meanwhile, it also leads to less resistance since instead of having all the flow underneath the ship curving upward just past the midship, the flow at the sides is bend first before the flow closer to the ship center gradually follows along. Also, it may allow for the ship to be better suited for navigation in shallow water.

3.2. Parametrization of inland ship hull forms

The previous section discussed various hull form aspects that can be observed for inland ships. To generate hull forms that vary with respect to these aspects, a parametric model is set-up. This section describes this model. First, multiple approaches for the development of this model are discussed. Then, the working principle of the model is presented. Finally, examples of the outcomes of the model are presented.

3.2.1. Approach for parametric model development

Multiple methods can be used to vary a ship hull form. One example is Radial Basis Functions (RBF). With RBFs, control points are distributed across the hull form. Modifying the location of these control points then affects the hull surface, which will locally move along with the control point, depending on the distance from that point. Interior Radial Basis Functions (IRBF) are similar to conventional RBFs except that the radius within the hull surface moves along with a control point depends on the distance within the coordinate system that lies on the hull surface rather than a world-fixed coordinate system. Similar to using RBF is NURBS (Non Uniform Rational B-Splines). In NURBS, however, it is not the distance from a control point that determines whether the local hull shape moves along with the control point,

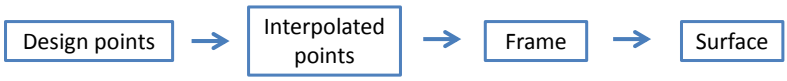

Figure 3.12: Schematic overview of the working principle of the parametric model

but rather the number of control points in a surface-aligned direction. An important drawback of RBF, IRBF and NURBS for the present study is that they generate smooth transformations. This is an advantage for conventional ships, but for inland ships such smooth transformations will distort the geometry of the tunnel skirt, for example.

An alternative method is to interpolate between known ship frames in order to achieve a hull form. In such an approach, multiple base frames are designed (at several x-positions along the ship length), and then a hull surface is drawn through these frames. A similar approach is used in the FRIENDSHIP-Modeler, developed at the Technical University of Berlin (Maisonneuve *et al.* [48]). The design of the frames themselves can be done through NURBS-curves, so that only a limited number of points is required to represent the ship hull form.

3.2.2. Parametric model set-up

The parametric model developed and used for this thesis generates a surface following the steps shown in Figure 3.12. Initial design points are chosen and then used to interpolate new points between them. Next, frames are drawn through these interpolated points. Using these frames, the hull surface is generated. The steps to generate the frames (which include the design and interpolated points) as well as the generation of the hull surface are discussed in more detail in the following sections.

Generating frames

A frame is generated from a polyline, which is defined by a series of design points. An example of the polyline that represents the frame at the propeller x-position is shown in Figure 3.13. These design points are chosen for multiple frames, which are shown in Figure 3.13 as well. The points shown in the figures are the only points that can be changed in the model, and not all of them are independent. For example, the points for three out of seven frames are determined by the width and height of the ship hull.

The frames shown in Figure 3.13 are not smooth. In order to generate smooth frames that allow for the generation of a realistic ship hull, a NURBS-curve can be drawn through the points that form the polyline. This, however, would lead to the tunnel skirt not being represented accurately. Therefore, additional points are interpolated between two consecutive points on the polyline, at locations such that

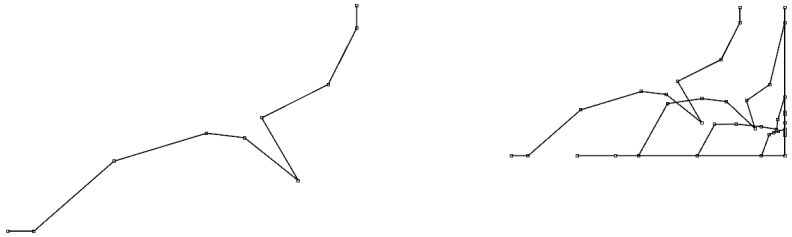

Figure 3.13: Left: Polyline representation of the frame at the propeller x-position. Right: Series of polylines representing the frames of an inland ship stern

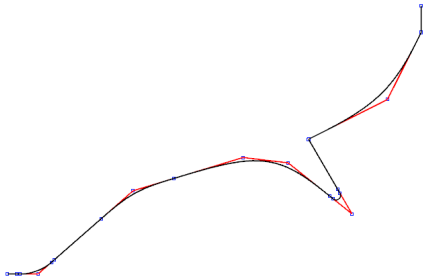

Figure 3.14: The polyline (red), interpolated points (blue) and the final curve of the frame (black) at the propeller's x-position

the the final frame represents a frame of a realistic inland ship. Figure 3.14 shows the frame at the propeller position, with the polyline based on design points and the points interpolated along this polyline to form the final frame geometry.

Generating a surface

From the frames, a surface is created. This is done by first interpolation additional frames between the frames described above, and then lofting a surface through these interpolated frames. The interpolated frames are required to preserve details of the hull form, especially for the skirt of the tunnel. An comparison of using frames described above directly and first adding interpolated frames is presented in Figure 3.15. Another advantage of first interpolating frames between the frames generated from design points is that the design points have a tighter control of the resulting surface.

Using the interpolated frames and a loft method, which uses the frames (including the interpolated frames) as curves pulling the surface towards them, smooth hull forms can be generated that still preserve details such as the tunnel skirt. An example is presented in Figure 3.16.

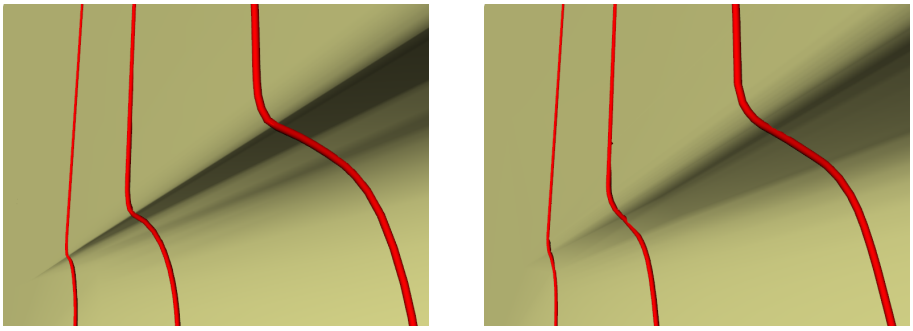

Figure 3.15: Effect of first generating additional frame by interpolation before drawing a surface through the frames: the tunnel skirt becomes smoother and the very sharp curvature is prevented.

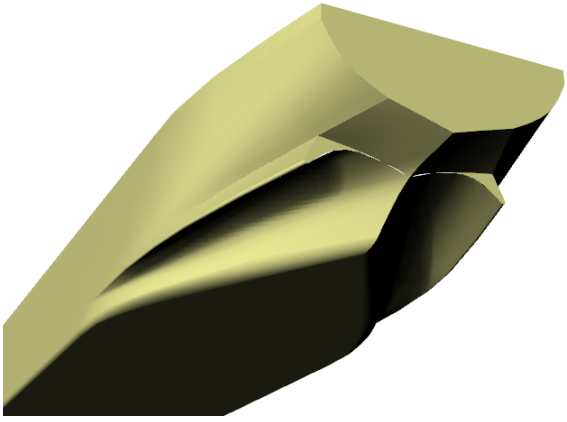

Figure 3.16: Result of a stern shape obtained with the parametric model

Bow and midship surfaces

Although the bow and midship are not included in the main focus of the present study, they must be generated as well to obtain a full representation of a ship. A CFD calculation can be conducted for the stern only, but the thickness of the boundary layer which varies in different water depth can affect the impact of certain stern shape parameters. As the boundary layer is already growing at the bow and mostly at the parallel midship, they are modeled as well. The shape of the bow and midship is kept simple: the midship is constructed from two frames only, while the bow is generated by a series of four frames, each consisting of only three design points (center line, bilge and at deck height). For adjustments to the main dimensions, the midship and bow are both scaled with B and T.

Hull form deformation

The main goal of the parametric model is to allow parameters to deform the shape of the hull form. This is achieved by designing multiple variants of the hull form and interpolating between each other.

Interpolation is performed based on the design points only. The restriction to the design of multiple variants is therefore that each of them consists of an equal number of design points, and that the base topology is the same as well. On the other hand, it allows for quick generation of new hull forms within the design space and since each of the variants is designed as a realistic ship, the outcome of the parametric model are - in most cases - realistic as well.

The interpolation is performed as follows: the difference in location between points of any variant compared to the default (or base) ship is computed by subtraction. Then, each parameter represents the factor (for each variant) by which the difference between a variant and the base ship is applied to the design points of the base ship.

In case, however, that multiple variants all apply a change of a specific design point in a similar direction, the differences add up which may lead to an unrealistic hull form anyway. To prevent the generation of unrealistic hull forms, basic restriction to point locations are implemented (i.e. the y-location of a certain point should not exceed that of another point). These basic restriction rule out most of the unrealistic hull forms. The remaining shapes may be deleted by hand by visual inspection of the ships in the design space.

3.2.3. Examples of model outcomes

Figure 3.17 shows four examples of parametric model outcomes. The most apparent changes that can be observed are the main dimensions (B and T), the length of the stern, the shape of the bottom and the bilge radius. Furthermore, the size of the transom changes between the ships.

3.3. Choosing parameter values

The previous section described the parametric model that generates the hull form of an inland ship. The purpose of using a parametric model is to be able to generate a large number of inland ships. These ships are then used in CFD simulations to obtain

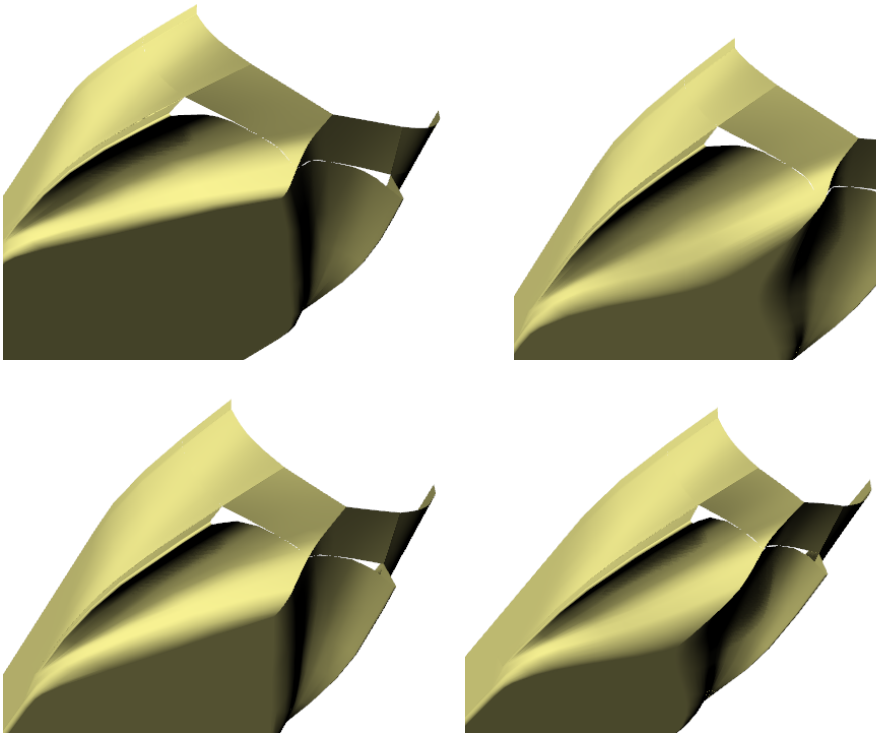

Figure 3.17: Examples of double-propeller ships being generated with the parametric model

trends on resistance, wake fraction, thrust deduction and eventually propulsion power.

The trends, and their accuracy, depend on the settings for the parametric models. If these input settings are not well-spread across the parameter ranges of interest (i.e. if the settings cluster around a certain value), the trends are less accurate outside of the clustered region. Hence, one can not randomly choose settings for the parametric model. It is possible to generate so many hull forms that the design point density across all parameter settings is sufficient. This is unfeasible since the time that a CFD calculation takes should be accounted for. The parameter settings much be chosen such that:

- the ships being tested in CFD differ significantly
- the variational range of all parameters is well-represented
- ships do not cluster in a certain region of the design space
- obtained trends are accurate throughout the design space
- a realistic number of calculations is to be conducted

The following discusses multiple options of choosing the parameter values, so-called experimental designs.

Design of experiments

Design of Experiments (DoE) is a field that aims at choosing the (varying) input parameters of an experiment such that accurate trends (for example, to determine optimum settings after the experiments) can be obtained without conducting a large number of experiments.

Especially for expensive and time-consuming experiments that cannot easily be repeated, the experiments must be set-up carefully. In this thesis, CFD simulations are used to obtain trends. Although a CFD simulation can be repeated easily (and even cheaply nowadays), there is still a significant amount of time required to perform a simulation. An efficient DoE is therefore required. The efficiency of an experimental design depends on 1) the number of experiments to be conducted to obtain a trend, and 2) the growth of that number when the number of parameters increases. The following discusses multiple approaches to generate a DoE.

Full-factorial grid design

The full-factorial grid design is a simple design. It takes, for each parameter involved, a series of values. Then, every possible combination of parameter is also generated. In case of a two-parameter design with three values for each parameter, there are $3 \cdot 3$ simulations to be conducted. Increasing either the number of parameters or the number of values per parameter, the total number of experiments N becomes:

$$N = n_s^{n_p}. \tag{3.1}$$

With n_p the number of parameters and n_s the number of steps per parameter. With a large number of parameters, the size of this experimental design grows quickly. For example, using a full-factorial grid for the 11 parameters described for a twin-propeller tunnel stern would require (if three steps per parameter are used) $3^{11} = 177147$ computations.

Central Composite Design

An efficient alternative to the full factorial design described above is the Central Composite Design (CCD). This approach is often used to generate regression models based on second-order polynomials. A CCD design is a combination of a hypercube with points at its corners and a (multi-dimensional) cross with a point at the end of each arm. Finally, there is a point at the center of the design. The off-center points all lie on they same (hyper)sphere. An example is presented in Figure 3.18. The number of experiments to be conducted can be computed as:

$$N = 2^{n_p} + 2 \cdot n_p + 1. \tag{3.2}$$

And is thus more efficient than the full factorial design. However, section 3.1 showed that there are at least 11 parameters, which means that a CCD would require 2071 CFD calculations, which still is a large number. Furthermore, if the trend does not resemble a second-order polynomial, the design is inadequate.

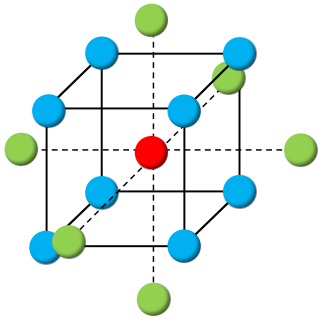

Figure 3.18: A Three-dimensional Central Composite Design. The blue points belong to a two-step full factorial design. The red dot is at the center of the design space. The green points added by the cross are at a distance from the center such that they lie on a sphere enclosing the design space. The distance from the center towards all points is equal.

Random sampling

Random sampling can lead to an additional decrease of simulations to be performed. When applying random sampling, one may choose the number of points equal to the number of unknowns in the surrogate model of interest. If this surrogate model is a second-order polynomial (with interactions), the number of unknowns can be computed by $1 + n_p + n_p + (n_p \cdot (n_p - 1))/2$, corresponding to the intercept, the linear terms, quadratic terms and interaction terms (such as $x_1 \cdot x_2$). With 11 features involved, the model consists of 78 unknowns that have to be solved. That is, if all parameters have a considerable influence on the outcomes *and* the trend of that influence resembles a second-order polynomial. If so, the number of experiments to be conducted should (at least) be 78. However, noise must be taken into account. When assuming that twice this number is sufficient to account for noise ((Rotteveel *et al.* [22]) showed that 30 points is sufficient for a four-parameter experiment, which required at least 15 points), 156 experiments have to be conducted. Comparing with a full-factorial design and the CCD, the numbers of experiments are 2071 and 177147 respectively. Random sampling thus leads to a more efficient experimental design.

A drawback of random sampling, however, is that it cannot the ensured that all portions of the design space are filled. That means that the model obtained from the results can give inaccurate predictions in regions where the design space is less dense populated. Moreover, a specific part of the design space may become more densely populated with design points. If the regression model is built using least-squares fitting, such a part will significantly influence the resulting model which will therefore yield inaccurate predictions in other regions of the design space.

Latin hypercube sampling

A Latin hypercube sampling (LHS) process solves the problems of clustering design points that may happen when using random sampling. LHS divides the range of each parameter in n_s intervals, then selects one interval for every parameter using a uniform distribution, and then places a design point in the selected intervals, again based on a uniform distribution. This process is repeated n_s times, so that all intervals are filled with design points. This ensures that every parameter is well-represented throughout the experimental design.

However, since the parameter intervals are selected with a certain probability, it can occur that all first intervals are selected for the first sample, all second intervals for the second design point, and so on. Although the chance of this occurring is low, the chance of correlation between multiple samples is certainly present (Viana [49]). There are approaches to optimize the LHS (Viana *et al.* [50]). For the present study, multiple LHS designs have been generated and the design that maximizes the distance between design points is used.

One drawback in view of the present study when using a LHS design is that it is no longer possible to isolate the effects on the 3D-flow of specific hull form aspects. However, the regression models that are generated after performing the calculations still allow to investigate the effect of one parameter on integral values such as wake fraction, resistance or propulsion power.

Despite this drawback, the LHS experimental design offers what is needed for the present study. It ensures that there is no clustering around a certain design point, and by optimization also allows the design points equally distributed across the design space. Finally, it keeps the number of required calculations relatively low, while still allowing for accurate trends to be obtained.

3.4. Summary

This chapter presented an overview of hull form aspects identified on inland ships and their implementation into a parametric model, through which hull forms are generated for the CFD calculations. Apart from main dimensions B and T, nine additional parameters have been identified for the tunnel stern while six detailed parameters have been chosen for the pram-shaped stern. Given this relatively large number of parameters, an efficient experimental design is required to limit the number of CFD calculations to be conducted. Therefore, a Latin-hypercube sampling approach is used, which ensures that the design points (i.e. ship designs to be investigated), are properly distributed across the design space.

4

Set-up for CFD calculations

The previous chapter discussed the generation of inland ship stern shapes in such a way that variations of hull form aspects are well-distributed across the design space. Each of the shapes is analyzed using computational fluid dynamics (CFD) employing a RaNS (Reynolds-averaged Navier Stokes) method to predict the flow around the ship. Ship resistance, the wake field (propeller inflow) and eventually the required propulsion power are estimated from computational results. However, these simulations are approximations of the flow of which the accuracy depends on the set-up of the simulations, which should be done adequately in order to obtain sufficiently accurate results.

This chapter therefore discusses how the CFD simulations are prepared. The following discussions include a description of PARNASSOS, the CFD code that is used, together with the computational domain and grid. As the choice of grid and domain affect the outcome of the calculations, sensitivity for both domain size and grid density are included in this chapter. Furthermore, the method of propeller modeling is discussed as well.

The first two sections, 4.1 and 4.2, describes PARNASSOS. Section 4.3 discusses the computational domain, boundary conditions and grid density. Section 4.4 presents the analyses of sensitivity to both the size of the computational domain and the grid density. Next, propeller modeling is discussed in Section 4.5. Section 4.6 discusses how resistance and the wake field are obtained. Finally, the most important information is summarized in section 4.7.

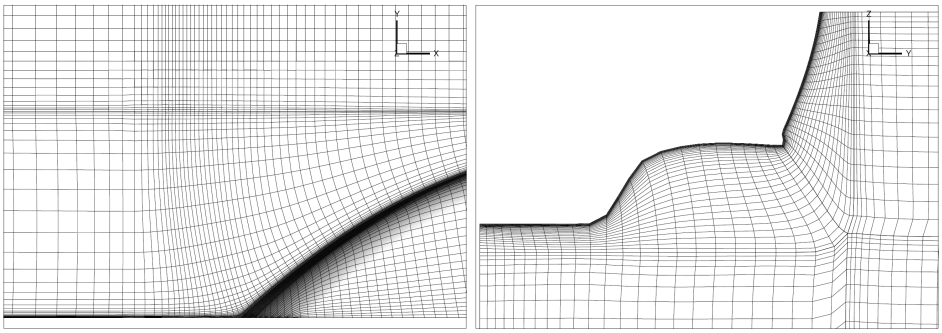

Figure 4.1: Examples of grids used in Parnassos. (a) Shows a grid around the bow from above, (b) presents a slice of the grid at a longitudinal position near the stern of the ship. Note that even with a tunnel skirt, the grid around the ship remains smooth.

4.1. Description of PARNASSOS

There are multiple programs available that are able to compute the (viscous) flow around a (partially) submerged body (Larsson *et al.* [51]). Some methods offer great flexibility with respect to the geometrical model that is to be tested, while others are able to return results quicker due to efficient solution algorithms.

For the present study, PARNASSOS has been used to obtain the flow around the ship hull. PARNASSOS is an efficient finite-difference solver for the Reynolds-averaged Navier-Stokes (RaNS) equations that Hoekstra and Eça [52] specifically developed to compute the flow around ship hulls. The solution process takes advantage of the dominant longitudinal flow component by repeatedly marching through the domain, starting upstream of the ship and solving the flow per block while moving downstream. This space-marching scheme is especially efficient with respect to memory consumption, since it is not required to solve the equations in the complete domain at once.

For the computational grid, PARNASSOS uses a multi-block topology consisting of structured grids. This has a positive effect on the computational efficiency since using structured grids simplifies the system of equations that is solved during the computations. The structured grid blocks themselves are generated by stacking a series of body-fitted 2-D grids. They are curvilinear grids which are generated by solving the Poisson equation to ensure smoothness. Two examples of the used grids are given in Figure 4.1.

PARNASSOS can simulate both double-body flows and free-surface flows. Although free-surface computations require more time, the code remains efficient by using a steady solution and applying a surface-fitting method (Starke *et al.* [53]) to capture the free-surface.

Finally, the boundary conditions used in Parnassos allow for a relatively small computational domain. Namely, the velocities and pressures on the far-field boundaries are fixed based on a potential flow simulation rather than assuming that pressure and velocities are equal to those in the free stream.

The combination of the marching scheme with the use of multi-block structured

grids allows PARNASSOS to run on a normal desktop computer. The double-body flow around an inland ship can be obtained within 6 to 7 hours using a Xeon E5 processor.

4.2. PARNASSOS in shallow water

PARNASSOS has been used in many studies for deep water, and validation studies ([53–56]) show good results. For shallow water, validation data was not available. Also, the budget for the presented study left no room for conducting model tests. However, Raven [57] used PARNASSOS to investigate shallow-water effects on various ship types, including the KVLCC2. Particularly for the KVLCC2, Raven showed that the increase of viscous resistance is in agreement with the prediction published by Millward [38], which was based on model tests.

Furthermore, the specific far-field boundary condition that is applied enhances PARNASSOS' capabilities of providing accurate results in shallow water. Namely, this boundary condition allows to specify the velocities on the far field rather than using a pressure or wall boundary condition. Therefore, wall effects are limited, whereas these wall effects would increase with decreasing water depth for the conventional boundary conditions.

Finally, the aim of this study is to address performance differences between ships and identify which parameters are responsible for these difference. Getting a most accurate estimate on the performance of a single vessel is not the main goal of the study.

Therefore, and also considering computational speed, PARNASSOS is considered a suitable flow solver for the presented study.

4.3. Computational domain and grid

The domain and computational grid both have a significant influence on the outcome of CFD calculations. If the domain is too small, the boundary conditions (the chosen velocities and pressures on the boundaries of the domain) can influence the flow near the ship and thereby affect, for instance, ship resistance. The chosen grid and especially the cell size affects convergence as well as the accuracy of computed velocities and pressures. Therefore, cell size also affects the estimate of ship resistance and wake field velocities.

This section discusses the domain and grid used for the calculations conducted. Firstly, 4.3.1 discusses the size of the domain. Secondly, 4.3.2 presents the composition of the grids within the computational domain. Uncertainty studies with regard to the domain size and grid density are presented in section 4.4.

4.3.1. Domain size

The domain size can affect the outcome of the calculations if not taken sufficiently large. If the pressure on parts of the domain boundary is fixed (and constant), the boundary must be sufficiently far away from the ship so that pressure gradient has decreased to zero. Similar constraints apply to velocities.

Guidelines by the ITTC [58] describe that the computational domain should

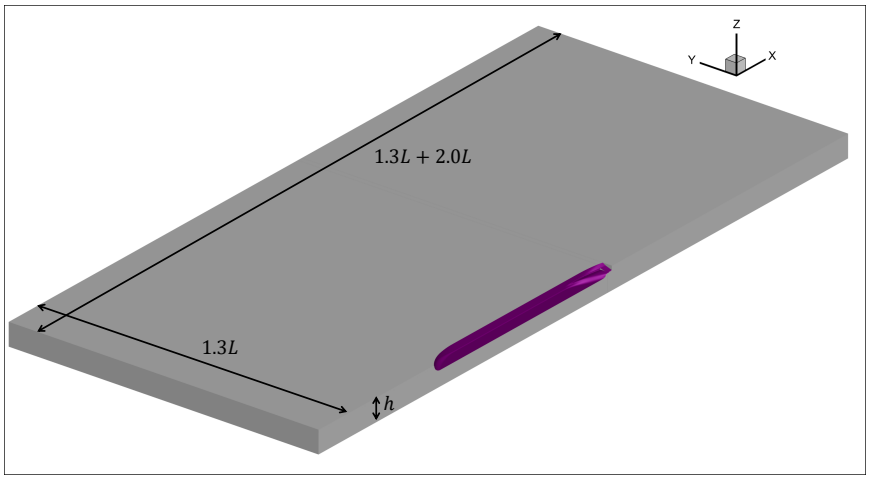

Figure 4.2: Overview of the computational domain for $h/T = 3.0$, showing the length and width of the domain relative to the ship size, while the height of the domain depends on the water depth h.

generally extend $1.0 \cdot L_{pp}$ in front of the bow, aside the ship and aft of the ship. In the current set-up, shallow water is included. In shallow water, the pressure gradients spread out further away from the ship, towards the boundaries of the domain. Therefore, fixing the boundaries of the domain at a distance of $1.0 \cdot L_{pp}$ away from the ship can be insufficient. On the other hand, PARNASSOS does not apply free-stream boundary conditions to the boundaries of the domain. Instead, a potential flow simulation is conducted prior to solving the viscous flow around the ship to obtain the velocities at the boundaries of the domain (as described in 4.1). Because of this, the size of the domain can be reduced compared to flow solvers using free-stream boundary conditions. To test which distance is sufficient, a sensitivity study has been conducted (see section 4.4) in which the distance between the ship and the boundaries of the domain has been varied.

Figure 4.2 gives an overview of the computational domain, including the dimensions and the position of the ship. The inlet boundary is positioned at $0.8 \cdot L_{pp}$ in front of the bow. The athwart ships far-field boundary is positioned somewhat further away at $1.3 \cdot L_{pp}$, which is found to be sufficient from a sensitivity study (see section 4.4). On the outflow boundary, the longitudinal pressure gradient, $\partial p/\partial x$, is set to zero. This boundary must therefore be sufficiently far away from the ship to ensure that this conditions is satisfied physically as well. Based on the sensitivity study described in section 4.4, the domain outflow is positioned at $2.0 \cdot L$ aft of midship.

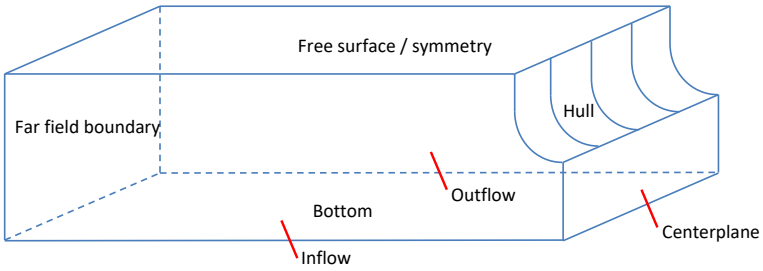

Figure 4.3: Schematic view of the computational domain around midship, with seven sides: centerplane-symmetry, freesurface-symmetry, far field, bottom, ship, inflow and outflow.

4.3.2. Grid topology

As stated in section 4.1, PARNASSOS solves the Navier-Stokes equations in a structured grid. Although this has significant advantages with respect to computational efficiency, it reduces geometrical flexibility and additional steps have to be taken for shallow water computations. Additionally, multiple blocks have to be used in longitudinal direction in order to model the transom of the ship.

Shallow-water block structure

In a conventional, deep-water calculation, the far-field boundary is shaped as the quarter of a circle, so that the domain has six boundaries. In shallow water, the domain has seven boundaries. Figure 4.3 gives a schematic overview of the domain around midship. Whereas for a deep-water calculation the bottom and far-field can be combined (usually shaped as the quarter of a circle), they are separated for a shallow-water calculation.

Although it is possible for a structured grid to have one side of the computational grid being divided over two (connected) sides of the physical grid, it decreases the quality of the grid as well as the quality of the solution describing the flow around the ship. Especially in shallow water cases where the domain width is large compared to the height, high-skew grid cells can occur which causes PARNASSOS to converge much slower or even diverge.

Therefore, the grid is divided in multiple blocks. This division is presented in Figure 4.4. The inner blocks in the top-right of the Figure are connected to the ship hull. The size of these blocks depends on the dimensions of the ship. The remaining three blocks (outer blocks) are resized if the domain size is changed.

Communication of (gradients of) velocities and pressures between multiple blocks is done by interpolation of points in adjacent blocks. This requires a smooth transition between blocks with respect to cell size. To prevent a jump in cell size when going from the inner blocks to the outer blocks, the outer blocks are generated

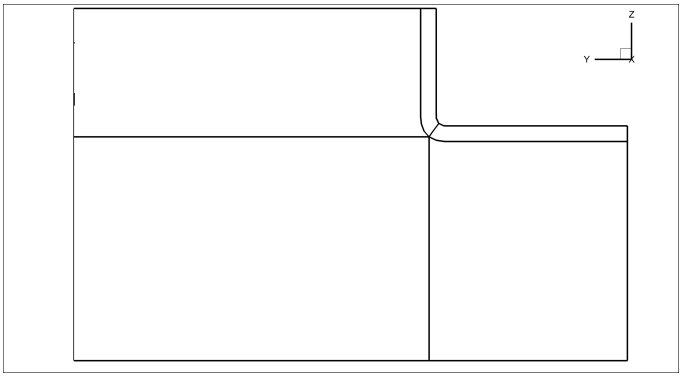

Figure 4.4: Edges between the grid blocks around midship. The two top-right blocks are connected to the ship hull. Note that there is now a point connected to all grids, for which a special treatment is required during the flow solution process.

such that the cell size varies continuously, and the points on both sides match up. An overview of the five-block grid structure is presented in Figure 4.5.

The picture shows that from the inner to the outer blocks, there is a smooth transition of cell size. Between the three outer blocks, the transitions are less smooth. In the direction of those transitions, however, gradients are small compared to derivatives normal to the hull surface. Furthermore, the cell in the lower-left block that is connected to both inner blocks (in the upper-right corner of the block) must be small otherwise the cell sizes of the other two outer blocks do not match those of the inner blocks.

Transverse split for transom modeling

Apart from the five-block structure required for shallow water computations, the grid is split in longitudinal direction as well because a structure grid cannot be fitted smoothly around a transom with sharp edges (it may be possible, but does decrease grid quality significantly). In Parnassos, the marching-scheme used to solve the flow requires such a split to extend over the full width and height of the domain.

For inland ships with a tunnel, the domain is split twice in longitudinal direction. The first split occurs at the tunnel end, which is mostly a blunt transom-like surface. The second split occurs at the transom. Figure 4.6 shows the division of the domain over multiple blocks. Furthermore, Figure 4.7 presents a close-up of the grid around the transom and tunnel end.

4.4. Uncertainty analysis

The results obtained from CFD simulations always include errors (Eça and Hoekstra, Larsson and Raven, [9, 59, 60]). The size of these errors depends on the quality of the grid, but also on the size of the computational domain. If the grid is of low quality (e.g. if the cell size is too large to capture details in the flow),

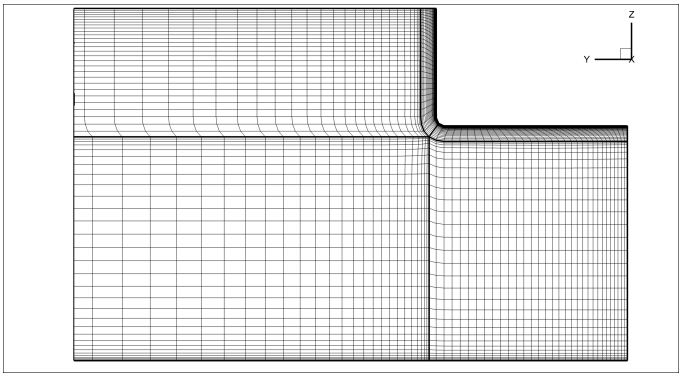

Figure 4.5: The five-block grid structure around midship, as used in Parnassos. The open space in the top right indicates the position of the vessel. Directly aside the ship, strong grid contraction is applied to capture velocity gradients in the boundary layer. The thick black lines indicate communication boundaries between the blocks. At the communication layer between the blocks connected to the ship and the outer blocks, the cell-size for the outer blocks is such that there is no jump in cell size, which would otherwise decrease the quality of the solution.

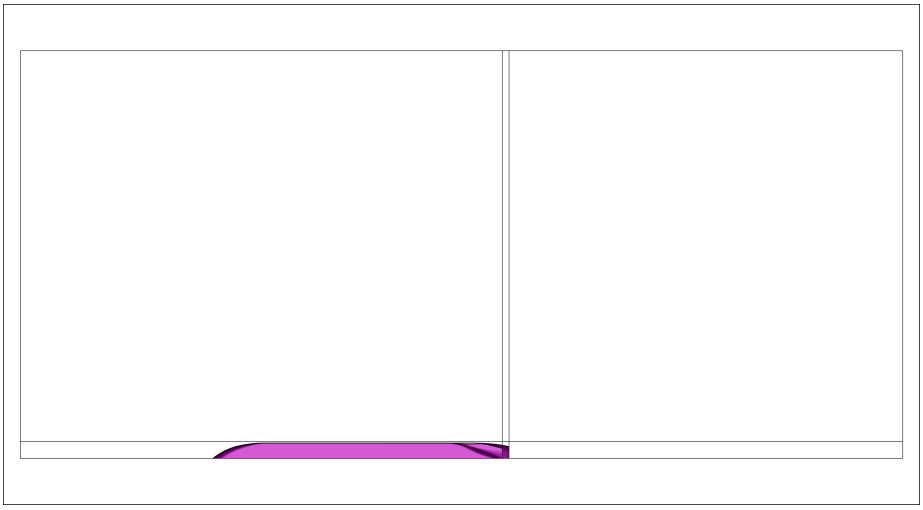

Figure 4.6: A view of the domain from above. The ship is indicated by the colored region. The two lines extending from the aft of the ship (right end of the colored region) towards the side of the domain are transverse splits. The leftmost split allows for the modeling of the transom-like tunnel end, while the second split allows for modeling of the transom area.

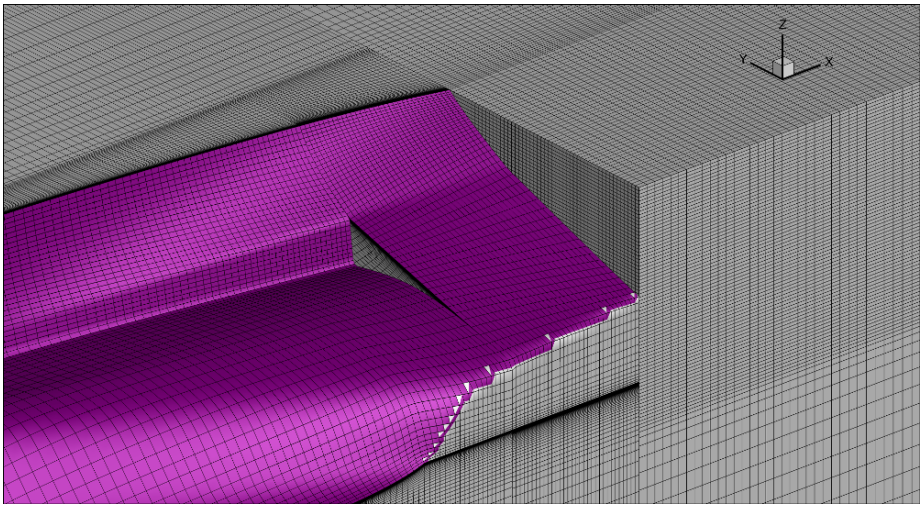

Figure 4.7: Close-up of the transverse split at the transom and the tunnel end. Directly behind the transom, Parnassos forces the velocities to be zero. The same applies to the tunnel end indicated by the gray zone inside the colored area the indicates the vessel. At the center plane, the grid cells do not exactly coincide with the ship's contour line. This is a consequence of applying body-fitted grids. To obtain an accurate estimate of resistance, Parnassos uses a contour curve to adjust the surfaces, as described in section 4.6.1.

the results can be significantly different than what they would be in reality. Moreover, it is not (always) sure whether results are either too high or too low. This is called uncertainty. Uncertainty is also introduced if the domain is not of adequate size. This section discussed the influence of both grid cell size and the size of the computational domain on the results.

4.4.1. Grid density

The grid density can significantly affect the results. If the grid cells are not small enough to capture steep velocity or pressure gradients, shear stresses or pressure variations cannot be computed accurately and the outcome of the calculation is either too low or too high. To assess grid quality, a sensitivity study for grid density has been conducted. The procedure described by Eça and Hoekstra [60] has been applied for this. In this procedure, a minimum of four grids ($n_g \geq 4$, with n_g being the number of grids) is required. The error is estimated by a multi-step procedure, which involves minimization of equation 4.1, in which ϕ_0 is the assumed CFD output (e.g. resistance) for infinite grid density, α the coefficient for a trend line fitted through the results, and p the order of grid convergence. The following steps are taken:

- First, estimate ϕ_0, α, and p from minimization of equation 4.1, both using a weighted approach ($w_i = (1/h_i)/(\sum(1/h_i))$) and a non-weighted approach ($w_i = 1$).

- Choose the values for ϕ_0, α, and p based on which method (weighted or non-weighted) gave the best fit, in which best means minimum standard deviation (for the determination of standard deviation, a formula is given by Eça and Hoekstra [60]).
- If for the chosen method, $0.5 \leq p \leq 2.0$, the error for each of the used grids can be determined by computing $\epsilon_i = \phi_i - \phi_0$.
- If p is larger than 2.0, apply equation 4.1 using $p = 1.0$ and $p = 2.0$, again using the weighted and non-weighted approaches, and chose the values for ϕ_0, p and α from the fit that gives the least standard deviation.
- If p is smaller than 0.5, apply a modified version of 4.1 which includes αh_i and αh_i^2 (a combination of $p = 1.0$ and $p = 2.0$) and select the best fit from a non-weighted and a weighted approach.
- If p is negative, data points are classified as anomalous. In this case, the options for p either being smaller than 0.5 or larger than 2.0 can still be applied. However, this will result in a large uncertainty on the error estimate.

$$S(\phi_0, \alpha, p) = \sqrt{\sum_{i=1}^{n_g} w_i \left(\phi_i - (\phi_0 + \alpha h_i^p)\right)^2} \tag{4.1}$$

The grid study consists of a series of 7 grids in which all cells inside the domain changed size with a certain factor. Figure 4.8 shows the results from this series of calculations, including uncertainty bars and a fit to extrapolate to an infinite number of cells (i.e. cell size being zero). The uncertainties have been determined following the approach described by Eça and Hoekstra [60]. As can be seen in the figure, the uncertainty at $h_i/h_0 = 1.0$ is approximately 1.6 %.

4.4.2. Sensitivity study for domain size

This study has been carried out for the case where $h/T = 1.5$, i.e. the minimum water depth considered. In that case, the influence of the boundaries is assumed to be the largest. Figure 4.9 shows the values of the total resistance coefficient at three domain widths and three domain lengths.

In Figure 4.9, it is shown that the influence of domain length (indicated by x_{out}) is small: the difference between $x_{out} = 200$ and $x_{out} = 250$ (at the same domain width) is less than 0.3 percent. The influence of domain width W is larger. This is due to the boundary layer displacement effect, which induces an additional return flow on top of the return flow that would also occur in potential flow. The potential-based return flow is accounted for by setting the velocities at the boundary based on a potential flow calculation, but that does not take the boundary layer displacement effect into account. In a viscous simulation, the boundary layer displaces the flow around the ship, so that the effective area for the flow to pass around the ship is reduced and velocities increase, eventually leading to increased resistance. For a larger domain width, resistance therefore decreases as observed from Figure 4.9.

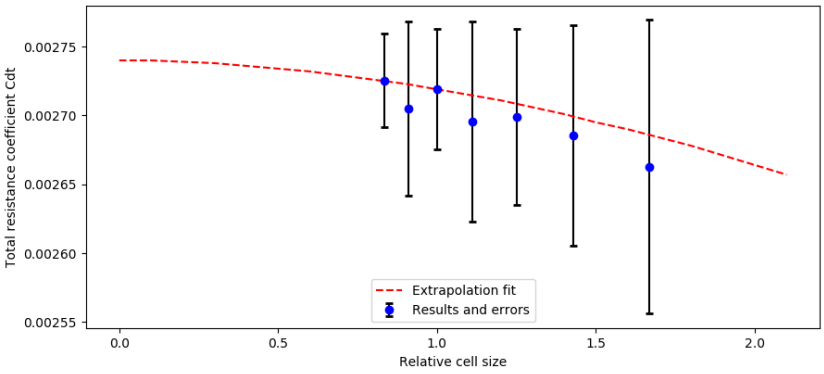

Figure 4.8: Extrapolation of ship resistance towards an infinitely fine grid (at the left end of the graph), together with the grid study results and corresponding uncertainty magnitudes per point.

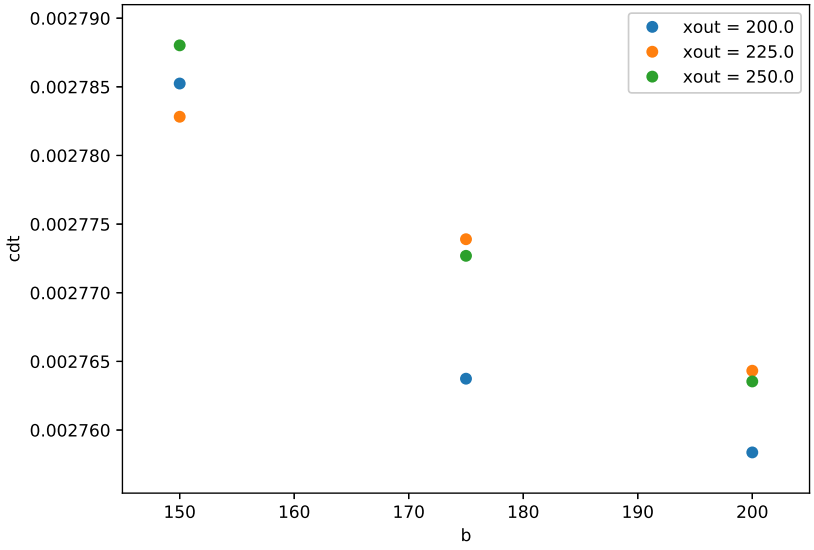

Figure 4.9: Resistance coefficient at three values for domain width (b, horizontal axis) and length (xout, grouped). The influence of domain width is larger than that of domain length, but the relative effect on the resistance coefficient is below 1.0 % (the value range on the vertical axis is small).

x_{out}	$0.5W$	C_D
200	150	2.785
200	175	2.764
200	200	2.758
225	150	2.783
225	175	2.774
225	200	2.764
250	150	2.788
250	175	2.773
250	200	2.764

Table 4.1: Resistance coefficient (multiplied by 1000.0) for various domain widths and lengths. The influence of domain length, indicated by $x_{outflow}$ is smaller than the influence of $0.5W$.

4.5. Propeller effect modeling

The complexity of the stern of an inland ship and the flow around it require that its analysis and optimization use an integrated approach that includes effects of both the propeller and the hull shape. Namely, the propeller induces a pressure change on the hull causing additional resistance, but the magnitude of this effect depends on the hull shape as well as on the produced thrust. Also, the hull shape determines the flow that the propeller operates in (i.e. the wake field), while the velocity distribution in this field also affects the propeller induced pressures that affect ship resistance.

PARNASSOS does not allow a detailed propeller geometry to be modeled, neither does it allow for the inclusion of the geometry of the propeller duct, which is commonly applied in inland ship propulsion systems (Zöllner [46]) for reasons discussed in chapters 1 and 2. To obtain information on the effect that the modeling of the ducted propeller would have on the outcome of this study, additional computations have been performed using FineMarine and ReFRESCO, two RaNS solvers that use unstructured grids and therefore allow for locally finer grids. This makes them able to include the geometry of a ducted propeller. These computations are further discussed in section 4.5.3.

This section will focus on the options for propeller modeling possible in PARNASSOS. In this study, the options considered were a coupled RaNS-BEM approach and a actuator disk applied by means of body force. Both of these are discussed below.

4.5.1. Actuator disk

A generalized actuator disk can be applied in PARNASSOS. This is done through a force distribution acting on the flow. The thrust force distribution can be determined using an equation, from a propeller calculation or can be defined by hand. The standard approach in PARNASSOS is a axissymmetric force distribution that corresponds to the formula in equation 4.2.

$$F_X(r) = F \cdot \frac{r - R_{hub}}{R_{prop} - R_{hub}} \cdot \sqrt{1.0 - \frac{r - R_{hub}}{R_{prop} - R_{hub}}} \tag{4.2}$$

The force distribution according to equation 4.2 has its maximum thrust at around $r/R_{prop} = 0.7$, which is comparable with propeller in practice. The generated force distribution is interpolated on the PARNASSOS grid at the chosen propeller position. This then results in a pressure jump over the propeller disk. The amplitude F is adjusted multiple times based on computed resistance. It is adjusted multiple times after PARNASSOS has converged for the previously set value of F.

4.5.2. RANS-BEM Coupling

An higher fidelity alternative to the actuator disk approach is to apply a coupling between PARNASSOS and software that implements the Boundary Element Method (BEM) to solve a potential flow around a propeller called Procal (Starke *et al.* [53], Rijpkema *et al.* [61]). In this approach, PARNASSOS is given a force distribution that represents the forces of the propeller on the flow. After convergence, the obtained wake field is used to determine the inflow for Procal, which then computes new propeller forces. These forces are then returned to PARNASSOS as a force distribution and a new wake field can be acquired. This process is repeated until the total thrust force, ship speed or propeller revolution rate converges. A more detailed explanation of the method is given in section 5.1.4.

The coupling approach has given results closely matching model tests (Rijpkema *et al.* [61]). A drawback of the method however is that it increases computational time significantly: the total time required to achieve a converged solution may double, depending on the number of coupling iterations required. Another drawback is the fact that RANS-BEM coupling needs a propeller geometry. Although publicly available propeller geometries exist, a certain propeller design may be optimal for one ship geometry, while being sub-optimal (or even worse) for another ship geometry. Therefore, trends can be affected if the same propeller geometry is applied to all ships. This can be overcome by using an optimized propeller for each ship, but propeller optimization is out of the scope of this study. Therefore, propeller modeling is conducting using an actuator disk as described in section 4.5.1.

4.5.3. Ducted propellers

Inland ships are regularly fitted with ducted propellers, since it reduces propeller blade loading and increases efficiency at high propeller load. Especially the former leads to the use of ducted propellers since inland ship propellers are highly loaded due to the limitations imposed on the propeller diameter.

The use of structured grids in PARNASSOS means there are limitations with regard to the modeling of complex geometry. In case of, for example, a propeller duct geometry, multiple (small) structured grids need to be fitted around the duct, which leads to a multitude of interfaces between the grid blocks. Due to the interpolation needed between the interfaces, the accuracy of the computation is reduced. Moreover, at the leading edge of the duct, the generation of a smooth grid is virtually

impossible.

However, the duct affects the propeller inflow. Due to this, the computation of the objectives of interest (propulsion power and wake field quality, see chapter 5) can be affected and the trends may differ as well. Especially the extent to which trends are affected is important, since that would affect the conclusions drawn from this thesis as well.

Effects of modeling the duct geometry

To assess these differences, a set of calculations has been performed using another flow solver, ReFRESCO. Similar to PARNASSOS, ReFRESCO is being developed and used at MARIN. Contrary to PARNASSOS, ReFRESCO employs unstructured grids and is rather a general flow solver for marine applications rather than specifically aimed at ships. The use of unstructured grids offers more flexibility for the types of geometries analyzed, and thus allows for the modeling of the duct geometry.

For the study on ducted propeller effects, a series of 25 calculations in both ReFRESCO (with duct) and PARNASSOS (without duct) has been performed, in which each calculation has been conducted at three different water depths. The ships considered in this subset vary with four parameters only. The four parameters have been chosen to include those parameter that are deemed important to the differences between open propeller flow and ducted propeller flow. Two of these parameters are the athwart-ships propeller position and the length of the stern region. Both have a large influence on the propulsion performance as presented in chapter 7. The other two parameters are the bilge radius in the stern region and the shape of the bottom plane (which can be either s-shaped or v-shaped, as discussed in chapter 3).

From the calculations, propulsion power is calculated by an integration of the thrust force distribution multiplied by the velocity distribution across the propeller disk (see 5.1). From the data, surrogate models (see chapter 6) are constructed in order to compare the trends between PARNASSOS and ReFRESCO. Figure 4.10 shows that for an h/T ratio of 3.0, the trend is similar. The difference becomes larger at $h/T = 2.0$ and slightly larger at $h/T = 1.5$.

Figure 4.10 shows that the most important trends are similar between PARNASSOS and ReFRESCO. The ReFRESCO calculations discussed so far are double-body calculations (no wavemaking) in which the propeller has been modeled as a volume of body forces inside the duct. The applied distribution of the bodyforces in the duct is axisymmetric but varies in radial direction such that it resembles the force distribution occuring in a real ducted propeller. Namely, the outer radii of the propeller produce more thrust in ducted propellers [62].

Impact of the force distribution

The axisymmetric distribution is too optimistic. In reality, the velocity deficit in the wake closer to the hull is stronger. Because of this, the local angle of attack is larger, and therefore the local thrust force is larger as well. Figure 4.11 shows the force distribution extracted from a moving-grid calculation in which a moving propeller was modeled inside a duct.

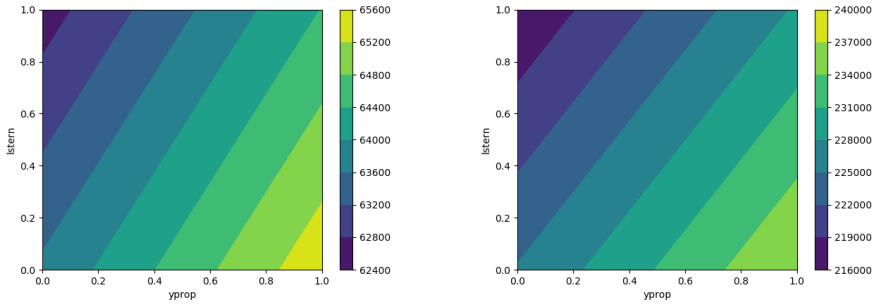

(a) Parnassos

(b) ReFresco

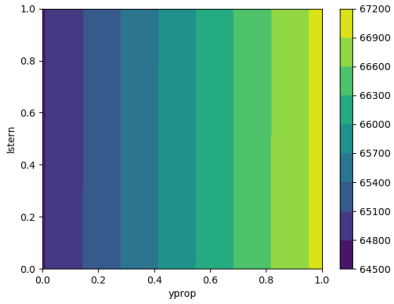

(c) Parnassos

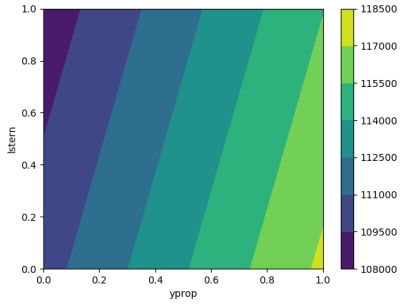

(d) ReFresco

Figure 4.10: Contour plots of the trends of propulsion power estimates based on data from Parnassos (left) and ReFresco (right), at h/T ratios of 3.0 and 2.0. For the first case, the trends are clearly similar. The differences are larger for $h/T = 2.0$. The horizontal and vertical axis are the normalized values for the athwart-ships propeller position and the stern length respectively.

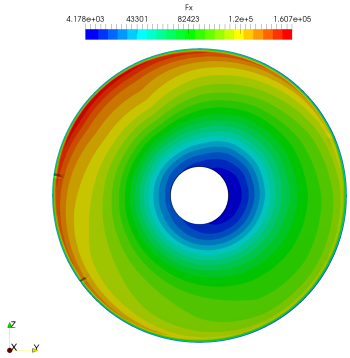

Figure 4.11: Thrust force distribution extracted from a ReFresco simulation with a rotating propeller in a duct.

The use of an axisymmetric force distribution rather than a circumferentially varying distribution has two effects: firstly, the thrust produced by the duct is larger in the former case, since the duct is loaded more uniformly. Secondly, the non-uniform loading of the duct causes open-water efficiency to drop, as is shown by Ghassemi *et al.* [18] through calculations with ducted propellers in oblique flow. Finally, the non-uniform force distribution can affect the calculation of power (discussed in section 5.1), since that is an integral of velocity and force. However, a stronger velocity deficit (thus lower velocity) leads to a larger angle of attack and thus a locally larger thrust force. Therefore, this effect of the nonuniform thrust distribution is being compensated.

In the PARNASSOS calculations (and in the set of 25 ReFRESCO calculations) performed for the present study, axisymmetric force distributions have been used. The effects mentioned above therefore influence the results with respect to reality. However, the impact on the trends that this thesis focuses on is limited. Namely, the wake fields produced from PARNASSOS all have a similar composition per stern type considered. The non-uniformity of each force distribution is therefore similar across the ships considered, and the main effect is a shift of values, while the trends (the differences between ships) are assumed to be not affected significantly.

Details of ducted propeller flow

That the effect on the trends may be limited can further be explained by presenting a cut-through of the flow around the duct. To this end, two calculations have been performed in FineMarine, a software package developed by Numeca. FineMarine is, similar to ReFresco, a CFD solver aimed at marine applications. It uses unstructured grids, which allows for propeller ducts to be modeled. The two calculations performed are equal ships but one is equipped with a ducted propeller while the other is equipped with an open propeller.

Figure 4.12 shows the pressure distribution around the duct. The strongest

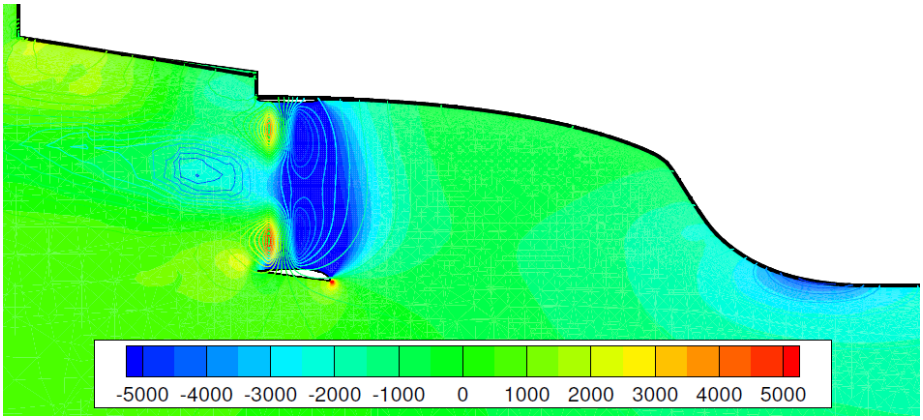

Figure 4.12: Pressure distribution in a cut-through of the flow perpendicular to the athwart-ships direction. The filled contours indicate the pressure distribution for the case *with* duct, while the colored lines show the distribution for a non-ducted case.

differences occur inside the duct. The pressures in the duct are lower, due to the acceleration effect that the duct has on the flow. Therefore, the pressures downstream of the propeller do not reach the high levels obtained by the non-ducted propeller. Furthermore, the low-pressure area induced by the propeller is shifted upstream by the duct, but these differences are very small already at half a diameter upstream of the duct. Small differences can also be observed at the bilge (far right in the figure), but these differences are so small that they are assumed to be within the error range of the calculation.

4.6. Results

The next chapter discusses the estimation of propulsive performance. This involves two objectives, propulsion power and the quality of the wake field. The estimates of these objectives requires that two types of data are obtained from the CFD simulations. These are ship resistance and the wake field. This section discusses how this data is obtained from Parnassos.

4.6.1. Resistance

The resistance of a ship is obtained in Parnassos by integration of the forces that act on the hull of the ship. In Parnassos, three types of stress/pressure affect the resistance of a ship: the hydrodynamic pressures, hydrostatic pressures and and shear stresses. The second, hydrostatic pressures, should integrate to approximately zero since double-body calculations are used. The hydrodynamic pressure integrates to the viscous pressure resistance, while the shear stresses integrate to the frictional resistance of the ship.

Since Parnassos applies body-fitted structural grids, the geometry of a ship is not exactly represented by the shape of the grid. At the bow, for example, grid

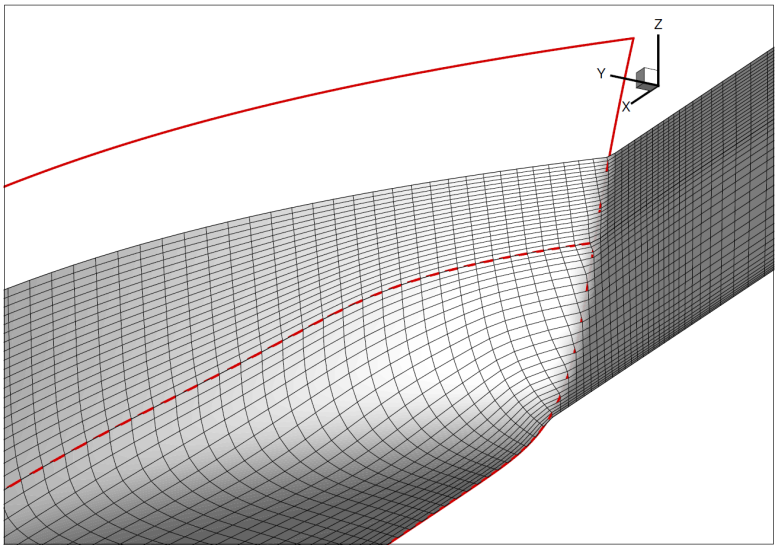

Figure 4.13: Example of a ship contour curve used to precisely integrate the resistance of the ship. Since a five-block topology is used, a contour dividing the ship hull in two sections is also used since the resistance is integrated for both parts separately.

cells may be attached to both the symmetry plane at $y = 0$ and the hull of the ship. To overcome the effect on the accuracy of force integration that this may cause, two precautions are taken: first, the grid is refined at both the bow and the stern, where cells intersect with the contour of the ship. Second, a curve that accurately described the ship's contour is used to capture the ship geometry in a post-processing step. An example of this curve is given in Figure 4.13.

In chapter 5, resistance with and without propeller is needed in order to estimate the thrust deduction factor needed for the estimation of propulsion power. This is performed in a two-step approach: first, a simulation without propeller is conducted. In this way, the nominal (or towed) resistance R_T is computed. Next, an actuator disk producing a thrust force equal to R_T is enabled. The thrust force is iteratively adjusted for the effect of thrust deduction, until the total resistance, R is obtained.

4.6.2. Wake field

The second result obtained is the wake field. The wake field is used to determine the wake fraction, the quality of the wake field, and to obtain estimates on propulsion power (see chapter 5). The wake field is extracted by interpolating the velocities and pressures from the flow field obtained by PARNASSOS onto a two-dimensional circular grid. The interpolation occurs at the propeller position. Figure 4.14 gives an example of a wake field underneath a ship as for which a computation has been conducted in PARNASSOS.

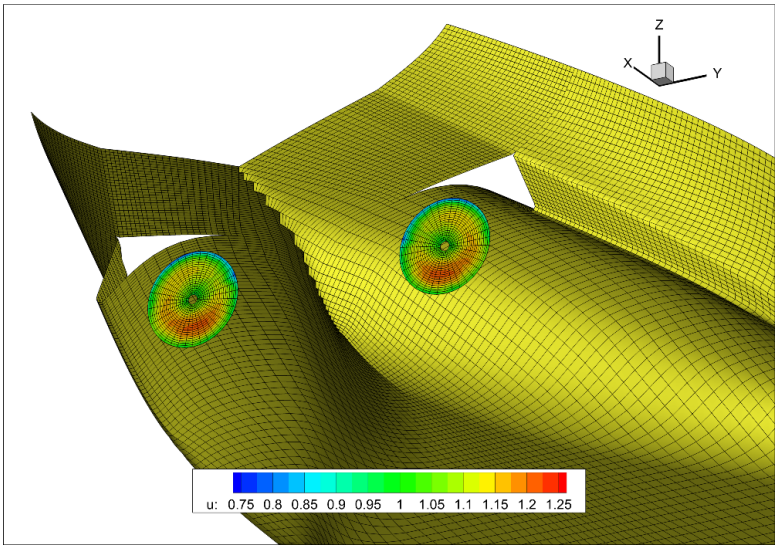

Figure 4.14: For the extraction of the wake (mirrored in the ship center plane), a two-dimensional, circular wake field grid is generated. From the flow field obtained from PARNASSOS, data on velocity and pressure is extracted through bi-linear interpolation.

4.7. Conclusions

This chapter discussed the set-up of CFD calculations. It described the used flow solver PARNASSOS, including the use of double body calculations, the space-marching solution technique and structured grids. The size of the computational domain was presented, as well as the multi-block grid topology that is used to model shallow water flow. Furthermore, a sensitivity study for domain size and grid density is presented. Propeller modeling methods as well as the effects of a ducted propeller have been discussed, and finally the methods to obtain ship resistance and the wake field have been presented.

The size of the domain is increased over the size advised by guidelines given by the ITTC [58] since shallow water leads to pressure gradients extending to further away from the ship. Propeller modeling is done through body forces, with a distribution that is circumferentially uniform but varies in radial direction. A ducted propeller can not be modeled in PARNASSOS, and it is shown that this simplification leads to differences in the flow. However, the most important trends are well captured, and it is shown that the differences in the flow are mostly local and within one diameter distance from the duct.

The next chapter discusses how the results obtained from PARNASSOS are processed to obtain estimates that describe propulsion performance.

5

Objectives for propulsion performance

Ship resistance and the wake field are calculated using CFD simulations as described in the previous chapter.The goal of this thesis, however, is determine which stern form aspects are relevant to the propulsive performance of an inland ship. Two objectives related to propulsive performance are investigated in this thesis. The first one is the required propulsion power. The second is a measure of the wake field quality. The quality of the wake field determines to a large extent the hindrance due to propeller induced vibrations and cavitation.

For the first objective, a traditional method for estimation is using self-propelled model tests and open-water propeller tests. In the present study, shaft RPM is not available but necessary to compute propulsion power following the conventional method. An alternative means to estimate power is therefore needed. The second objective, wake field quality, is a measure for the risk vibration hindrance and cavitation. The quality of the wake can be measured by analysis of the wake peak or the variance of the angle of attack.

This chapter discusses the estimation of both the aforementioned objectives. Section 5.1 elaborates on the prediction of shaft power. This section also discusses the relevant factors such as thrust deduction (section 5.1.3), the wake fraction (section 5.1.4), and propeller efficiency (section 5.1.5). Assessment of wake field quality is discussed in section 5.2. Finally, the used approach is summarized in section 5.3.

5.1. Propulsion power estimation

With a direct relation to fuel consumption and thereby the ship's emissions, the amount of required propulsion power is an important objective in the present study. For one propeller, the required shaft power is defined by:

$$P_D = 2\pi n Q \tag{5.1}$$

In which both Q and n, respectively torque and shaft rotation rate, depend on the required amount of thrust, the propeller geometry, the advance speed (i.e. the flow velocity at the propeller). Furthermore, the torque Q depends on the revolution rate n as well.

Traditionally, an estimate for delivered power P_D is obtained from model tests using the following formula:

$$P_D = \frac{R_T \cdot V_S}{\eta_H \eta_O \eta_R} = \frac{1 - w_T}{1 - t} \cdot \frac{R_T \cdot V_S}{\eta_O \eta_R} \tag{5.2}$$

In which V_S is the ship's speed, R_T the towed resistance (without propeller), η_H the hull efficiency, which itself follows from the Taylor wake fraction w_T and the thrust deduction fraction t. Furthermore, η_O is the open-water efficiency (the propulsive efficiency of the propeller in open water with uniform inflow) and η_R is the relative rotative efficiency.

In equation 5.2, an estimate for P_D involves using the thrust-identity condition. For this, the thrust of the propeller is required, which follows directly from a self-propelled test ($T = R_T/(1-t)$). Together with a measurement of n, the thrust coefficient K_T can be computed ($K_T = T/(n^2 D^4 \rho)$). Using this K_T, the corresponding advance coefficient J in open-water is obtained from a propeller diagram or open-water tests with the same propeller. From J, the effective inflow speed $V_A = nDJ$ can be computed, finally leading to the wake fraction w_T from $V_A = (1 - w_T)V_S$. The wake fraction obtained in this way is the Taylor wake fraction (Newman [63]). Furthermore, t follows from the known thrust force and η_O is calculated from the propeller diagram. Finally, η_R accounts for the difference between torque from the open-water test and torque applied in the model test with propeller.

In the present study, both the propeller revolution rate n and shaft torque Q are not available, so that this approach can not be used. A different means of estimating P_D or the components in equation 5.2 is therefore needed. This section discusses two methods. The first (section 5.1.1) is based on actuator disk theory, since this approach has the closest relation to the propeller modeling approach used in PARNASSOS, where a circular field of body forces is applied in the flow to simulate the propeller effect. The second method focuses on obtaining the components in equation 5.2 and applies actuator disk theory to obtain the wake fraction w_T while using propeller diagrams for η_O.

5.1.1. Actuator disk model

An actuator disk is a simplified, one-dimensional model of a propeller. The velocity and the force distribution are assumed to be uniform. In PARNASSOS, a similar

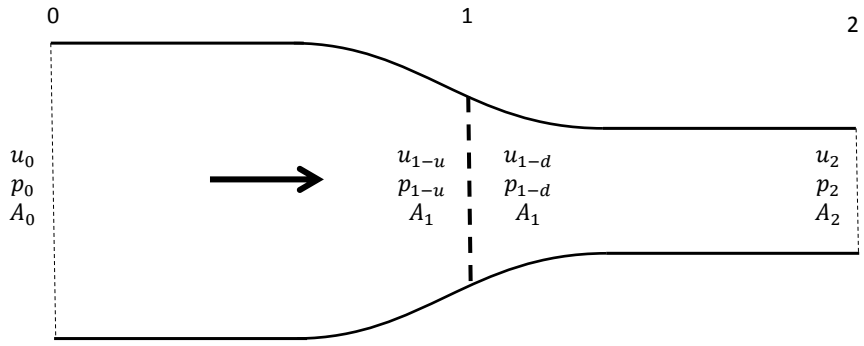

Figure 5.1: Schematic overview of the flow through an actuator disk propeller.

model is used to model the effect of the propeller on the flow. The differences lie in the fact that the propeller model uses a non-uniform force distribution (an axisymmetric distribution has been applied, see equation 4.2) and that the flow through the disk is non-uniform as well. But also for a non-uniform force and velocity distribution, conservation of energy can be used to compute the power delivered to the disk. This section discusses the formulations needed to compute power directly from the actuator disk as used in PARNASSOS. Furthermore, it presents an additional property of the theory that is used in section 5.1.4, but is discussed here to keep the derivation together.

A control volume is presented in Figure 5.1. Four locations are specified: the inflow side of the volume (with u_0, p_0 and A_0 the flow velocity, local pressure and inflow area respectively), just upstream of the propeller disk, just downstream of the disk, and the outflow side. u and p are specified at the axial position, but can vary in radial and circumferential position. Furthermore, no flow passes through the upper and lower bounds of the control volume. From this, the energy added to the flow can be computed using the conservation of energy:

$$P_D = \int_{A_2} u_2 \left(p_2 + \frac{1}{2}\rho u_2^2 \right) dA_2 - \int_{A_0} u_0 \left(p_0 + \frac{1}{2}\rho u_0^2 \right) dA_0 \tag{5.3}$$

In which the upper and lower bounds are not included because no flow passes through these bounds, and the energy flux through these bounds is therefore zero. The power delivered to the disk is thus equal to the amount of energy leaving the volume through A_2, minus that entering the volume through A_0. If the areas A_0 and A_2 are taken sufficiently far from the propeller disk, p_2 becomes equal to p_0. Equation 5.3 then reduces to:

$$P_D = \int_{A_2} u_2 \frac{1}{2}\rho u_2^2 dA_2 - \int_{A_0} u_0 \frac{1}{2}\rho u_0^2 dA_0 \tag{5.4}$$

Since all planes are part of the same streamtube, mass continuity gives $u_0 dA_0 = u_1 dA_1 = u_2 dA_2$ (Wald [15]). Therefore, both integrals in 5.4 can be computed at A_1. This leads to:

$$P_D = \int_{A_1} \frac{\rho}{2} u_1 (u_2^2 - u_0^2) dA_0 \tag{5.5}$$

$\rho(u_2^2 - u_0^2)/2$ can be related to the force distribution as applied in PARNASSOS using two Bernoulli equations. When applying one equation to the half of the volume upstream of the propeller disk, and a second one to the other half downstream of the disk:

$$\begin{aligned} \frac{1}{2}\rho u_0^2 + p_0 &= \frac{1}{2}\rho u_{1-u}^2 + p_{1-u} \\ \frac{1}{2}\rho u_{1-d}^2 + p_{1-d} &= \frac{1}{2}\rho u_2^2 + p_2 \end{aligned} \tag{5.6}$$

Equation 5.6 can be reduced by the fact that due to continuity, $u_{1-u} = u_{1-d}$ and $p_{1-d} = p_{1-u} + \Delta p$, with Δp being the pressure jump induced by the body forces in PARNASSOS. By substituting this into equation 5.6 and subtracting the first equation in 5.6 from the second, the relation aimed for emerges:

$$\frac{\rho}{2}\left(u_2^2 - u_0^2\right) = \Delta p \tag{5.7}$$

Before continuing to derive the estimate for delivered power, an additional property of actuator disk theory is used here for use later in the discussion of wake fraction estimation. This property involves the conservation of momentum (where again no flow crosses the upper and lower bounds of the control volume in Figure 5.1), from which the thrust force can be computed.

$$F = \int_{A_2} \left(p_2 + \rho u_2^2\right) dA_2 - \int_{A_0} \left(p_0 + \rho u_0^2\right) dA_0 \tag{5.8}$$

Using again that A_0, A_1 and A_2 are all part of the same streamtube, and that $p_0 = p_2$ sufficiently far away from the disk, equation 5.8 can be rewritten as

$$F = \int_{A_1} \rho u_1 \left(u_2 - u_0\right) dA_1 \tag{5.9}$$

Next, integrating equation 5.7 across the propeller disk A_1, the thrust force F is obtained. Substituting that into the last equation, and assuming that the integrands are equal:

$$\rho u_1 \left(u_2 - u_0\right) = \frac{1}{2}\rho\left(u_2^2 - u_0^2\right) \tag{5.10}$$

From which the following relation can be obtained:

$$u_1 = \frac{1}{2}\left(u_2 + u_0\right) \tag{5.11}$$

This relation is later used in section 5.1.4, because together with the Bernoulli equations presented in equation 5.6, it allows to estimate the effective wake velocities based on the velocities in the total wake field.

Continuing with the estimate for delivered power, equation 5.7 can be substituted in equation 5.5 to obtain an estimate for the amount of delivered power P_D:

$$P_D = \int_{A_1} u_1 \Delta p dA_1 \tag{5.12}$$

The P_D value in equation 5.12 can be computed from the results of a PARNASSOS simulation. Namely, u_1 can be obtained from the wake field with an active propeller, while Δp is known from the chosen thrust force and distribution according to equation 4.2. The P_D estimate in equation 5.12 does include hull efficiency η_H as well as part of the open water efficiency η_O. This part is the ideal efficiency η_I and certain losses due to a non-uniform flow and force distribution (since η_I is defined for a uniform velocity). Namely, hull efficiency multiplied by the ideal efficiency can be written as (Kerwin and Hadler [64]):

$$\eta_H \eta_I = \frac{R_T V_S}{TV_A} \cdot \frac{TV_A}{TV_{disk}} = \frac{R_T V_S}{TV_{disk}} \tag{5.13}$$

In which the TV_{disk} represents P_D in equation 5.12, with the exception of equation 5.12 applies to non-uniform flow while TV_{disk} applies to uniform (or averaged) flow only.

5.1.2. Semi-empirical model

The power estimate P_D described above is affected by hull efficiency and part of the open-water efficiency which is the ideal efficiency. Still, rotational losses that are included in open-water efficiency are not included but may be affecting the power estimate P_D as well as differences of this estimate among ships considered in this study. Therefore, the second method to obtain a power estimate from PARNASSOS calculations is to estimate the components in equation 5.2, which is repeated here:

$$P_D = \frac{1 - w_T}{1 - t} \frac{R_T \cdot V_S}{\eta_R \eta_O} \tag{5.14}$$

Where w_T is the Taylor wake fraction (Newman [63]) obtained from thrust identity, t the thrust deduction fraction, R_T the towed resistance, V_S the ship speed, η_O the propeller open-water efficiency and η_R the relative rotative efficiency.

The relative rotative efficiency η_R follows from the approach to obtain the Taylor wake fraction from thrust identity. It is the ratio between shaft power for the model test and the propeller open-water test. Usually, this ratio is around 1.0 (Kerwin and Hadler [64], Carlton [65]). Lewis *et al.* [66] found that the relative rotative efficiency, for a specific ship in still water, varies between 1.04 and 0.96 when increasing propeller thrust from bollard pull to full speed and also showed that η_R differs if either torque or thrust identity is used [66]. Because shaft power is not obtained directly (there is no propeller geometry included) from the CFD calculations, the value of η_R is kept constant at a value of 1.0 in the present thesis.

The estimation of t, w_T and η_O is discussed in further detail in following subsections. As discussed earlier, the thrust-identity method used to obtain w_T requires that the propeller revolution rate is known. This is not the case for present study, which means that w_T must be obtained using a different approach. An alternative way to compute w_T is discussed in 5.1.4.

5.1.3. Thrust deduction

The thrust deduction factor is a measure of the added resistance that is induced on the hull by propeller action. When the propeller is active, it creates a low-pressure field upstream, while increasing the pressure downstream of the propeller. The low-pressure field will, depending on the shape of the stern, result in additional pressure resistance. This is partly compensated by the high-pressure field downstream of the propeller, but only partly because the surface on which the high-pressure field can act is much smaller and not behind the propeller (while upstream, the hull is in front of the propeller). Additionally, the acceleration of the flow induced by the propeller increases friction at the stern, which also adds up to the negative force in longitudinal direction.

Once resistance and thrust force are known, the thrust deduction factor is computed as follows:

$$t = 1 - \frac{R_T}{T} \tag{5.15}$$

In which R_T is the resistance of the ship in an unpropelled or towed condition, and T is the required thrust force in a propelled condition, i.e. the resistance including the suction of the propeller on the stern. Both are obtained by conducting two calculations per case: a calculation without the propeller force distribution, and one including this force distribution.

5.1.4. Wake fraction

The wake fraction, w_T in equation 5.2 represents the velocity deficit relative to the ship speed in the propeller plane. It is the averaged value of axial velocities in that plane. This plane is called the wake field. This is different from the ship wake (or wake of the ship), which is the overall reduction of flow velocities around and behind the stern. Three different wake field can be defined: the nominal wake field, the total wake field and the effective wake field. The following discusses these three wake fields, along with the Taylor wake which is used in equation 5.2.

Nominal wake field

The nominal wake field is the velocity field at the propeller plane in case there is no propeller present. According to Wald [15], this wake field may be separated into two parts: a potential wake field and the viscous wake field. If no propeller is present, the potential wake field is restored aft of the ship, leaving no velocity disturbance in the flow far downstream of the ship (the resistance is then zero, a phenomenon called the Paradox d'Alembert). The viscous wake field, on the other hand, persists downstream of the ship.

The potential wake can be considered relatively small (Carlton [65]), but the average velocity reduction in the viscous wake can become significant. The viscous wake emerges due to boundary layer growth at the stern. Around the stern, the pressure gradients that follow the flow direction are positive. This decelerates the flow and increases the area that the flow must pass through. At the propeller plane, the ship wake can take up a significant portion of the flow cross-section. In case of too severe pressure gradients, flow separation occurs.

Total wake field

If an active propeller is added to the flow, this propeller accelerates the flow upstream and downstream of it. Due to this acceleration, streamlines that pass through the vicinity of the propeller are contracted (which follows from mass conservation in a streamtube). Also, a low-pressure region is generated upstream of the propeller, while a high-pressure region emerges downstream of the propeller. The flow therefore starts accelerating ahead of the propeller already, since it is attracted by the low-pressure region.

If the propeller is close to the hull of the ship, the low-pressure region affects the pressure distribution on the hull surface, leading to the thrust deduction effect described in section 5.1.3. The pressure gradients on the hull are affected as well. For example, the pressure gradient along a curve aligned with the flow near the hull decreases because of the low-pressure region upstream of the propeller. This suppresses growth of the boundary layer and the ship wake. Suppressed growth of the ship wake lowers chances of flow separation and flow separation existing in a nominal wake field may even be absent in a total wake field.

An example of this is given in Figure 5.2, where the non-propelled flow shows a large low-velocity region which is close to flow reversal, while this region is absent in the propelled case. The figure also shows the suppression of the growth of the ship wake.

Effective wake field

The effective wake field is a theoretical concept and is an intermediate field between the nominal wake field and the total wake field. It is defined as the total wake field, minus the potential flow effects of propeller-induced velocities (Kerwin [67]).

The effective wake field does not exist in reality, nor physically, but is useful for propeller designers or serves as input propeller calculations since it can be regarded as the wake field that the propeller effectively operates in and which determines blade loading, for example.

Compared to the total wake field, viscous effects such as the suppressed boundary layer and reduced viscous velocity deficit remain in the effective field. Therefore, velocities in an effective wake field are commonly higher than those in a nominal wake field. The effective wake field is the wake field that is being used in the remainder of this thesis to compute the wake fraction used in equation 5.2 instead of w_T.

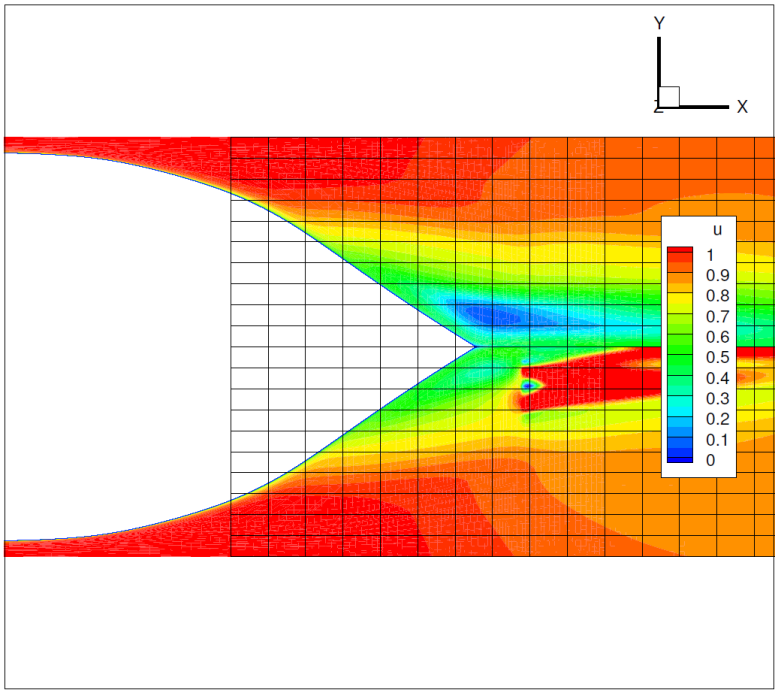

Figure 5.2: Differences between the flow velocities with (bottom) and without (top) propeller action, in an x-y plane at the z-position of the propeller shaft, for an inland ship at $h/T = 1.2$.

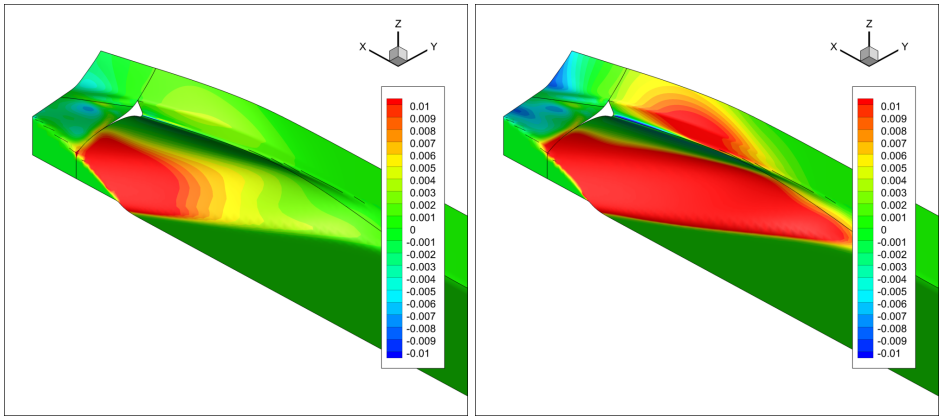

Figure 5.3: Distribution of added resistance, relative to the nominal resistance distribution, due to thrust deduction in (left) deep water and (right) shallow water at $h/T = 1.2$.

Selection of wake field for wake fraction estimation

The wake fraction that should be used in equation 5.2 is the effective wake field. Using the nominal wake field would yield larger wake fractions since the nominal wake field may include significant flow retardation in some cases (an example of which is shown in Figure 5.2). A wake fraction that is too large leads to a high propulsive efficiency and an estimate of propulsion power that is too low. This is particularly important in shallow water, where the velocity deficit in the nominal wake field can increase significantly (Rotteveel *et al.* [22]) due to increased pressure gradients around the stern of the ship. Together with an increase of the extent to which propeller suction affects the pressure gradients on the hull in shallow water (see, for example, Figure 5.3), the difference between the nominal wake field and the effective wake field increases in shallow water compared to deep water. This has also been shown by Kulczyk *et al.* [43]. Using the nominal wake fraction in shallow water may even result in the power requirement being lower in shallow water than in deep water [22], which is incorrect as shown by experiments (Lackenby [35], Kulczyk *et al.* [43]). On the other hand, using the total wake field to compute the wake fraction yields a negative wake fraction in most cases (i.e. the flow speed in the wake field exceeds the ship speed V_S).

Estimation of the effective wake fraction

In order to determine the effective wake field from a measured or computed wake field, two approaches are described by Carlton [65]. The first is to adjust the nominal wake field with flow interactions while the second subtracts the propeller-induced wake field from the total wake field.

Methods that are available using the first approach are the V-section method and the force-field method. In the first method, the flow is divided into multiple V-shaped sections and using actuator disk theory, the induced and effective flow field are obtained. The interaction in this method emerges as a reduction of boundary layer thickness. The second method solves the Euler equations in the vicinity of the

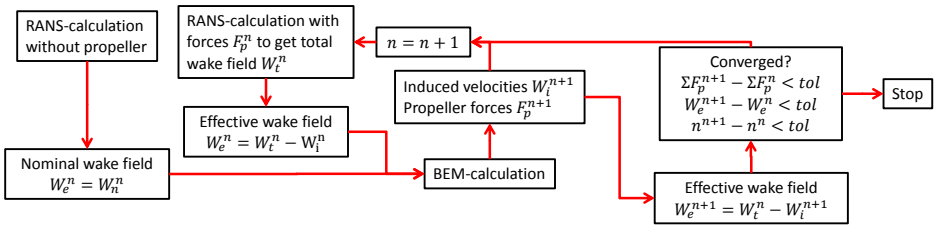

Figure 5.4: Flow-chart describing the procedure in a hybrid RANS-BEM method as proposed in [61]

propeller to estimate the total wake field based on the nominal wake field. From the equations, induced velocities can be computed and subtracted from the total wake field to obtain the effective wake field and the effective wake fraction.

The second method can be used by measuring the flow in several planes upstream of the propeller, and extrapolating the values in these planes to obtain the total wake field. Then, iterative procedures can be applied to determine which inflow field is required to produce the required thrust force and total wake field. Measurement of the total wake field is difficult from model tests due to the time dependent disturbances that the propeller induces has on the nearby flow. With CFD simulations, however, a measure of the total flow field can be extracted from the computed flow field directly.

Rijpkema *et al.* [61] describes a hybrid method that couples RANS-simulations with a potential flow solver to estimate the effective wake field. The method follows the procedure depicted by Figure 5.4. It starts with a computation without propeller forces to obtain the nominal wake field. This nominal wake field is used as input for a boundary element method to solve the potential flow around a propeller. This yields the induced velocity field as well as a force distribution. The force distribution is now put into the RANS-simulation, resulting in a total wake field. Subtracting the previously computed induced velocity field from the newly acquired total wake field gives an effective wake field, which is now used as input for the propeller simulation to obtain a new force distribution and a new induced velocity field. This process is iterated until - depending on the convergence criterion - the change of either the propeller revolution rate, total thrust force of the effective wake field becomes sufficiently small. According to [61], the method yields more accurate results than a force-field method as described above.

For the present study, two important drawbacks of the hybrid RANS-BEM method are the computational requirement and the need for a propeller geometry. The second drawback affects the trends of propulsion power with regard to the varied hull form aspects. This can be overcome by applying a (near-) optimal propeller to each tested ship geometry but the added computational effort to determine for each ship which propeller must be applied is undesirable for the initial design stage that this study focuses on.

An alternative is therefore applied. This method has been used by Rotteveel *et al.* [22] and is based on actuator disk theory. Using the total wake field as

obtained from CFD simulations and the applied force distribution (see equation 4.2), it computes the effective wake field. The computational method follows from the derivations made in section 5.1.1. The following conditions (equations 5.11 and 5.7) are used:

$$\Delta p = \frac{\rho}{2}\left(u_2^2 - u_0^2\right)$$
$$u_1 = \frac{1}{2}\left(u_2 + u_0\right)$$

By substituting u_2 based on the second equation into the first, and rewriting, the following equation results:

$$u_0 = \frac{u_1^2 - \frac{\Delta p}{2\rho}}{u_1} \tag{5.16}$$

Equation 5.16 is applied to each element of the discretized propeller plane. Finally, the effective wake fraction w_e is computed by averaging over de resulting wake field.

The method does involve certain important assumptions. Namely, transversal velocities are not taken into account. However, axial velocities are considerably stronger than transversal velocities, so this should not affect the result significantly. Also, effects of the pressure distribution on the ship hull that normally affect the accelerations in the flow if the propeller is active, are absent in the current method.

To assess the accuracy of the results, a small set of ship geometries has been selected to be analyzed using the RANS-BEM approach described above. The comparison between effective wake fractions obtained using RANS-BEM and the actuator disk method is presented in Figure 5.5, showing that the trend is similar to what is obtained from calculations using the hybrid RANS-BEM method.

An advantage over the RANS-BEM method is that the method from equation 5.16 does not require a propeller geometry. Compared to methods such as the force-field method or the V-shape section method, this method employs the total wake field which includes the viscous interaction effects between the ship wake and the propeller induced pressure field. Furthermore, using the total wake rather than the nominal wake ensures that effects of propeller suction on the effective wake field are included. Therefore, strong velocity deficits that normally occur in the nominal wake field in shallow water are prevented as well.

5.1.5. Open water efficiency

The remaining variable in equation 5.2 is the open-water efficiency η_O. The open-water efficiency is the relation between the effective power provided by the propeller to the ship and the power that is applied to the propeller shaft:

$$\eta_O = \frac{TV_A}{2\pi nQ} \tag{5.17}$$

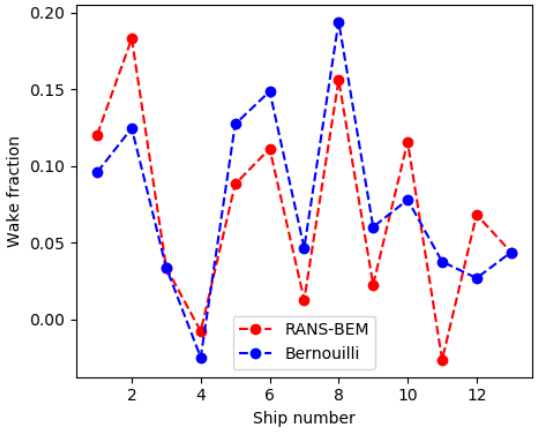

Figure 5.5: Comparison effective wake fraction between estimation using RANS-BEM coupling and estimation using equation Bernoulli equations (see equation 5.16)

The denominator can be split into a part that represents the axial losses in the flow, a part that accounts for blade friction, and a part indicating the rotational losses in the flow. The first part is already included in equation 5.12 as the ideal efficiency.

An additional alternative to equations 5.2 and 5.12 would therefore be to use equation 5.12 together with a ratio between ideal efficiency and open-water efficiency to obtain a power estimate.

Open-water efficiency can be determined from open-water diagrams, constructed based on measurements with propeller series. In the present study, ducted propeller series described by Oosterveld [17] are used. These are Kaplan-type propellers fitted in a 19A nozzle. The choice for a ducted propeller series is based on the wide usage of ducted propellers among inland ships, since the relative small propeller benefits from a decrease of propeller loading due to the addition of the duct, which increases efficiency (Kerwin and Hadler [64]) and increases the maximum power that can be delivered to a propulsion unit of certain diameter (Zöllner [46]).

Estimation of η_O starts by estimating V_A using equation 5.16. Next, the propeller rate of revolutions, n is iteratively adjusted such that the thrust of the propeller is equal to the required thrust as computed in the CFD simulations. With estimates n and V_A, and D as corresponding to the ship of interest, η_O can be computed from the formulation provided by Oosterveld [17].

5.2. Wake field quality

For ships, especially under heavy propeller loading such as is the case for inland ships, the velocity differences in flow towards the propeller can affect propulsive performance significantly. Preferably, the inflow should be circumferentially uniform, so that the angle of attack of a propeller blade is constant. In such a wake field, a propeller designer can adjust the blade design such that optimal lift-to-drag ratios are obtained around the propeller circumference, and the propeller performs efficiently. However, the wake field is (nearly) always non-uniform due to the boundary layer and the viscous wake that has formed around the ship.

For ships with a single propeller, a v-shaped velocity deficit in the top of the wake field is usually observed. This velocity deficit emerges because the flow passing through the top half of the propeller disk is not from the free-stream, it is flow that has been part of the boundary layer around the ship and just left the ship hull at the end of the skeg. For twin-propeller ships, on the other hand, the incoming flow enters the propellers slightly from aside: the flow is a combination of flow coming from underneath the ship and flow coming from aside the ship. Also, the ship wake has grown and therefore leaves a velocity deficit in the top half of the propeller disk. Moreover, the propeller shafts of double-propeller ships usually have to be supported by struts. Although these should be positioned such that their effect on the wake field is limited, they still leave a velocity deficit in the wake field.

The propeller blades, therefore, pass through regions of varying axial velocity. Apart from axial velocity deficits, vortical structures are produced by the propeller shaft, the hub of the shaft, and the bilge. Thereby, transverse and vertical velocity are also affected and changing across the propeller disk. As the angle of attack on a propeller blade is a combination of the axial velocity and the tangential velocity, the propeller blades will therefore encounter varying angles of attack around their circumference. Too strong variations can cause the angle of attack to exceed the stall angle, cavitation can occur or the exitation of the blade pressure on the hull can cause strong vibration hindrance. It is therefore important to assess the quality of the wake field.

One specific variation of the angle of attack is that occurring in a wake peak. For a single propeller ship, a wake peak may occur in the top quarter of a circular wake field, since the flow in that part has been affected by the friction along the ship hull the most. In the wake peak, an increase of the angle of attack can occur, causing locally increased blade loading. The pressure field produced by the increased blade loading extends towards the hull close to the propeller, for example that right above the propeller. If the wake peak is too strong, vibration hindrance can occur. Based on statistics, a formula, called the *propeller design difficulty index*, has been developed that can be used as an objective measuring the quality of the wake field.

$$WOF_{DI} = \frac{T \cdot N_P^2 \cdot \Delta w^5 \nabla^{3/4}}{5 \cdot 10^7 \cdot Z \cdot \frac{A_E}{A_O} \cdot \sqrt{C}} \tag{5.18}$$

The formula has been developed for single-propeller vessels specifically. In the formula, T is the propeller thrust, N_P the revolution rate, Δw the wake deficit

$(= w_{max} - w_{min})$, C the clearance between the propeller blade tip and the hull, ∇ the ship's displacement, A_E/A_O is the expanded area ratio of the propeller and Z the number of blades for a propeller. The quality of the wake field is considered to be sufficient if WOF_{DI} in equation 5.18 does not exceed a value of 7.0. The importance of the wake deficit is shown by the formula: the difficulty index increases exponentially at the 5th power relatively to the wake deficit.

Other difficulty design indices have been developed as well. For example, [68] present the formula:

$$WOF_{DI} = \frac{T + 0.61\left(N \cdot D^3 \cdot V_S \cdot \Delta w_{0.8R}\right)}{(h + 10) \cdot D^2} \tag{5.19}$$

The value of the formula by Jonk and Beek [68] should not exceed a value of 740.0. Additionally, another method has been proposed by Jonk and Beek:

$$WOF_{DI} = \frac{C_P}{\sigma_0} \tag{5.20}$$

$$C_P = \frac{P \cdot 75}{0.5\rho V_A^3 0.25\pi D^2} \tag{5.21}$$

$$\sigma_0 = \frac{p_0 - p_v}{0.5\rho V^2} \tag{5.22}$$

While equation 5.22 is proposed as a method that can be used in an earlier stage of ship design, it does require the propeller advance velocity V_A and an estimate of the cavitation number σ_0.

A drawback of the methods presented by formulas 5.18 and 5.19 is that the parameter representing the wake is the (normalized) difference between the minimum and maximum velocity in the wake field. Under the assumption that most of this difference is produced by the wake peak, the formulas provide useful estimators for the wake field quality. However, if the difference is caused by a smooth transition of the velocity deficit from the bottom to the top of the wake field, the indices yield the same result whereas the actual vibration hindrance may be different. This effect may occur for double-propeller ships, which are also included in the present study.

Furthermore, both 5.18 and 5.19 rely on a parameter indicating the head clearance of the propeller (either the distance to the water surface or the distance to the hull). For inland ships, ducted propellers are commonly applied, where the effect of head clearance will be different. Additionally, inland ship propellers are fitted inside a propeller tunnel, which also alters the influence of the clearance parameter as the tunnel virtually increases the distance between the propeller and the water surface.

A different approach has been described by van der Ploeg [69]. Is is a measure of the non-uniformity in the wake field by computing the variance of the angle of attack in a wake field. A suggestion for using local gradients or variance was made by Wilson [70]. The indicator proposed by van der Ploeg is computed using:

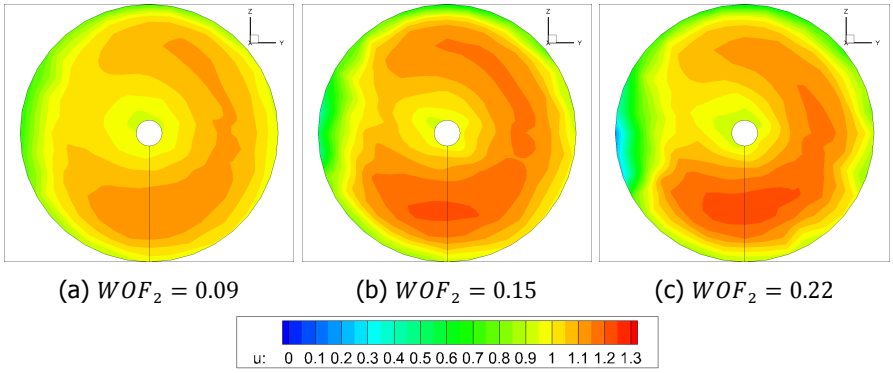

(a) $WOF_2 = 0.09$ (b) $WOF_2 = 0.15$ (c) $WOF_2 = 0.22$

Figure 5.6: Examples of wake fields from PARNASSOS. These wake fields are obtained from calculations for a double-propeller ship with a tunnel stern.

$$WOF_2 = \frac{\int_{R_H}^{R_P} \int_\theta |\partial\beta/\partial\theta| f(\theta,r) d\theta r dr}{\int_{R_H}^{R_P} \int_\theta f(\theta,r) d\theta r dr} \tag{5.23}$$

In which β is the angle of attack, as computed from:

$$\beta = \arctan\left(\frac{u}{\omega \frac{r}{R_P} - v_t}\right) \tag{5.24}$$

Where u is the axial velocity in the wake field, R_P is the propeller radius, R_H the radius of the propeller hub, v_t the tangential velocity (computed from the transverse and vertical velocities), ω is the rotation rate of the propeller. In equation 5.23, $f(\theta,r)$ is a weighting function which can put more emphasis on variations of β in, for example, the top of the propeller disk.

An important remark on equation 5.23 is that WOF_2 is still relatively small if there is one large peak while it can be higher if there are multiple smaller peaks. Moreover, there is no single value of WOF_2 that should not be exceeded so that wake field quality remains acceptable. Namely, if propeller thrust is low, operation in a wake field with multiple variations of the angle of attack can be without problems. The same applies to the propeller design difficulty index (equation 5.18), since lower ship speed would reduce the outcome of the formula as well. The WOF_2 formula presented in equation 5.23 can be used as a minimization objective for both single- and twin-propeller ships, and will therefore be used in the remainder of this thesis.

Equation 5.23 is computed from the total wake field as defined in section 5.1.4. Namely, the axial velocity has a significant influence on the angle of attack, making relative differences between different angles of attack smaller and limiting the influence of transverse velocities. In Figure 5.6, three examples of wake fields and their corresponding WOF_2 value are presented.

5.3. Conclusions

This chapter presented multiple options to estimate propulsion power and wake field quality from CFD calculations. For the estimate of delivered power, two methods have been presented. The first is based on actuator disk theory and does not involve a propeller geometry: the power estimate is directly obtained from the flow through the propeller disk and the force field imposed on it. The second is based on the traditional approach for estimation of P_D, with the influencing factors determined using an alternative approach. Next, methods to assess wake field quality have been discussed as well.

For the first, a semi-empirical approach is used. This approach is based on the traditional method used with model tests (equation 5.2), but the Taylor wake fraction w_T is replaced by an effective wake fraction w_e obtained from equation 5.16, which is based on actuator disk theory. For the relatively rotative efficiency, η_R, a value of 1.0 is used. Other factors influencing the power estimate, namely the thrust deduction fraction t, and open water efficiency η_O, are obtained from CFD and open-water propeller diagrams respectively.

The Wake Object Function (see equation 5.23) is used as a measure for the quality of the wake field. This measure mainly depends on circumferential changes of the angle of attack, which are an indicator for the risk that cavitation can occur.

In the next chapter, estimates of propulsion power and wake field quality are used for trend analysis through surrogate modeling. The models obtained in this way are later used for optimization and to derive guidelines from.

6

Trend analysis by surrogate modeling

The previous chapter described the method to estimate the propulsive performance, shaft power and wake field quality. These results are obtained on a non-structured experimental design as described in chapter 3. In order to derive design guidelines, the trends between the performance objectives and the hull form parameters must be retrieved from the data. These trends can be obtained by means of so-called surrogate modeling. Surrogate models are cheaper replacements for more expensive models (such as CFD) or experiments. In this thesis, they are used to predict the outcome of a CFD simulation that was not performed yet, based on results of formerly performed simulations. The models provide a means to find trends with regard to the propulsive performance and identify the most important stern shape aspects.

Different types of surrogate models exist, each with a different ability to accurately represent the underlying data. Also, there is the risk of over-fitting in surrogate modeling, which causes unwanted high variance and oscillations. To investigate which surrogate model fits best to the present study, multiple options are investigated. Furthermore, the method to determine which hull form parameters are most important to propulsive performance is not straightforward.

This chapter therefore discusses the methods used to find trends within the database of results and chooses the approach that is used for the remainder of the present study. First, section 6.1 describes multiple surrogate models. Next, methods to assess the influence of a hull form parameter on propulsive performance are presented in section 6.2. In section 6.3, methods to assess model quality and parameter influence are discussed and different models en parameter influence analysis methods are compared. 6.4 gives examples of the results obtained with the methods. Main findings are summarized in section 6.5.

6.1. Surrogate models

A surrogate model predicts the outcome of an experiment, the result of a simulation (e.g. a CFD calculation) or the consequence of an action in the real world. It makes a prediction for a case or situation for which no data is available yet, and uses formerly acquired data to make the prediction. The surrogate model is supposed to be cheaper (cheaper may be from an economical viewpoint, but can also mean faster or more easily repeatable) in obtaining results, at the cost of accuracy because the prediction is an estimate based on the data that was obtained already and the real data remains unknown. Surrogate models can be used to obtain trends for specific parameters or to assess the importance of a parameter to the outcome (i.e. predicted power). This is particularly useful when the number of parameters is relatively high and experiments/calculations are expensive so that varying each parameter in a structured way is unfeasible: surrogate models can be used to show the trend for the variation of a single feature only.

Surrogate models are divided in two groups: classification models and regression models. The former predicts if the input belongs in a certain class or group (e.g. categorizing articles where the input is the text) while the latter yields a continuous output depending on the input. Since this study focuses on the trend of propulsion performance objectives (see chapter 5), regression methods are used.

Three commonly used methods for regression are linear models, kernel-based models and neural networks. Linear models multiply parameters with weights and sum the resulting products in order to get an estimate of the outcome for a certain choice of feature values. Kernel-based methods first transform the design space spanned by parameters into so-called kernel-space, and fit weights to the kernel functions corresponding to each data point. In neural networks, input values 'propagate' through multiple layers of functions called hidden layers. In each layer, a weighted sum of inputs is fed through a function, of which the output is again fed to another hidden layer or (if the network consists of a single hidden layer) used as output of the model. Linear models, kernel-based models and neural networks are discussed in sections 6.1.1, 6.1.2, and 6.1.3.

In the discussions, y is used for the observations (i.e. results of a CFD calculation), while $\hat{y}$ represents a prediction. Similarly, y is the vector with all observations and $\hat{y}$ is the vector of all predictions. x_i is used for the feature values of a single data point, while X is the matrix of all data points such that $X = [x_1, x_2, \ldots x_n]^T$, with each row representing a single data point and each column the values for a specific feature in all n_o data points. For an untried location, x' is used. $x_{i,j}$ is the jth feature value of the ith data point, while x'_j is the jth feature value of the untried location. A matrix of untried locations is represented as X'. The following table summarizes the nomenclature for this chapter:

6.1.1. Linear regression models

Linear regression models are the most widely used type of surrogate models. They provide a transparent predictor in which coefficients are multiplied with parameters. Therefore, the impact that a certain parameter has on the outcome of the prediction

Symbol	Explanation
y	Observation of a result
$\hat{y}$	Prediction from surrogate model
y	Vector of multiple observations
$\hat{y}$	Vector of multiple predictions
x_i	Parameter values for single data point
x'	Parameter values for untried location
X	Matrix of parameter values of all data points
X'	Matrix of parameters for untried locations
$x_{i,j}$	Parameter value for observation i, parameter j
x'_j	Parameter value j for an untried location

can be read from the model itself. In general, a linear model can be formulated as:

$$\hat{y} = \sum_{j=1}^{n_f} \beta_j x'_j \tag{6.1}$$

With $\hat{y}$ being the predicted value, x'_j the value of parameter j for the data point to be predicted, and β_j the coefficient corresponding to feature j. It is important to note that the number of parameters n_f is not limited to the number of hull shape parameters defined in chapter 3. Additional parameters can be defined by taking combinations (divisions, products, additions) of the primary parameters.

The next section discusses the surrogate model that uses equation 6.1 without adaptations, which is least-squares regression. Variants of the linear model are Ridge regression, Lasso regression, and Elastic Net regression, which are also discussed in this section.

Least-squares regression

One of the more basic models, and probably most widely used model, is the linear regression model. The model computes the outcome based on a sum of products with features and weights, optionally including an intercept:

$$\hat{y} = \beta_0 + \beta_1 x'_1 + \beta_2 x'_2 + ... \tag{6.2}$$

With β_0 representing the intercept. It is also possible to include squares and products of features, so that a quadratic response surface results. The following gives an example of a quadratic response surface with two parameters and an intercept:

$$\hat{y} = \beta_0 + \beta_1 x'_1 + \beta_2 x'_2 + \beta_3 (x'_1)^2 + \beta_4 (x'_2)^2 + \beta_5 x'_1 x'_2 \tag{6.3}$$

Although equation 6.3 is called a quadratic response surface, it is still a linear model if squares and products of features are considered as new features. It is possible to extend the number of features further, using multiple consecutive operations including division and multiplication. The weights $\beta_j, j \in [1, ...p]$, are obtained using minimization of the residual sum of squares:

$$RSS = \sum_{i=1}^{n} (y_i - \hat{y}(x_i))^2 \tag{6.4}$$

The RSS can be minimized by the least-squares method, which sets the derivatives of RSS with respect to the weights β_j to zero. Least-squares fitting performs well in over-determined situations, where there are more observations than unknowns. It is not possible to introduce more features than the number of observations, since that would render the system of equations that must be solved under-determined. This can be a drawback of linear regression and therefore limits the flexibility.

Lasso regression

By extending the minimization objective in equation 6.4, the procedure of finding the weights in equations 6.2 and 6.3 is such that unrelevant features can be removed from the regression formula:

$$C_{Lasso} = \sum_{i=1}^{n} (y_i - \hat{y}(x_i))^2 + \alpha \|\beta\|_1 \tag{6.5}$$

Where RSS has been replaced by C_{Lasso} to indicate that it is a cost function rather than a measure of residuals. When equation 6.5 is used as the objective function to determine the weights β_j, the method is called Lasso regression (Tibshirani [71]). The Lasso regression approach does not only minimize the error between the observations and the predictions, but also minimizes the sum of absolute values of the weights, which is the 1-norm of the weight vector. The balance between minimization of the RSS or the 1-norm of the weight vector depends on the model parameter, α. For $\alpha = 0$, Lasso regression reduces to linear regression as described above. If $\alpha \to \infty$, all weights become zero and the model always predicts 0 for the outcome.

If α is chosen correctly, Lasso regression has the advantage of performing parameter selection: if a parameter $x_{:,j}$ only has a small effect on the data, reducing β_j does not significantly affect the RSS part of equation 6.5. Since Lasso tries to minimize the 1-norm of β, β_j is set to zero. The Lasso approach requires that the feature values are normalized. Otherwise, large-value features would remain in the model, despite being unimportant, since the corresponding weight would be low.

Ridge regression

The Lasso objective can be modified such that not the 1-norm of the weights vector, but the 2-norm of the weight vector is minimized together with the RSS:

$$C_{Ridge} = \sum_{i=1}^{n} (y_i - \hat{y}(x_i))^2 + \gamma \|\beta\|_2 \tag{6.6}$$

The 2-norm of the weights vector is the sum of squares of vector entries. In comparison with Lasso regression, Ridge regression will keep all parameters inside the model, even if multiple parameters are correlated with each other. Namely, if parameters j and $j+1$ are correlated, β_j^2 is larger than $(0.5\beta_j)^2 + (0.5\beta_{j+1})^2$.

Elastic Net Regression

A combination of Lasso regression and Ridge regression forms the Elastic Net regression approach [72]. Similar to Lasso regression, Elastic Net performs parameter selection as well. Meanwhile, it also provides accurate estimates due to the combination with the Ridge regression minimization objective.

$$C_{Elastic-net} = \sum_{i=1}^{n} (y_i - \hat{y}(x_i))^2 + \gamma \|\beta\|_2 + \alpha \|\beta\|_1 \tag{6.7}$$

6.1.2. Kernel-based models

Kernel-based models first transform the parameters using kernels. The transformed parameters are a measure for similarity or correlation between data points. Then, multiplying the transformed parameters with weights, an estimate of the outcome is achieved. The predictor of a kernel-based method can be written as follows:

$$\hat{y} = \sum_{i=1}^{n_o} \gamma_i \Phi(x' - x_i) \tag{6.8}$$

With γ_i being the weight corresponding to data point i, and x indicating a vector of parameter values, with the prime indicating the vector for an untried location and x_i the parameters of an available data point. Comparing equations 6.1 and 6.8, an important difference is that a linear model has a number of coefficients equal to the number of parameters, while kernel-based models have a number of coefficients equal to the number of data points. This is an important advantage of kernel-based models with respect to estimation of the coefficients: a linear model does not allow the number of parameters to exceed the number of observations, while this is allowed for a kernel-based model.

In this thesis, basic Kernel regression, the Kriging Response Surface, Support Vector Regression, and Kernel Ridge Regression are discussed.

Kernel regression

As stated in 6.1, Kernel-based methods firstly transform the feature space into kernel space (the kernel trick) before fitting the function to the features. A basic form of kernel-based regression is that proposed by Nadaraya [73]:

$$\hat{y} = \frac{\sum K(x' - x_i) y_i}{\sum K(x' - x_i)} \tag{6.9}$$

It is a weighted average of all observations, in which the weights are determined with a kernel function K. For the estimate of the outcome at an untried location x',

a weighted average of all data points is used. The weights per point depend on a function K of the distance to the location of interest. This function can be such that only a certain number of points is allowed to be taken into account. If, in that case, only a single observation - the one closest to the location of interest - is allowed to affect the prediction, Kernel regression reduces to Nearest Neighbor interpolation.

The basic form of Kernel regression given in equation 6.9 is not applied for this thesis, as it cannot provide suitable predictions at the boundaries of the design space: given the formulation, the estimates obtained by equation 6.9 always go to zero.

Kriging response surface

The Kriging response surface, or a Gaussian Process regression method, uses the transformation from feature space to kernel space to compute the correlation between data points. Based on this correlation, the Kriging response surface represents predictions as Gaussian processes. A prediction drawn from the Kriging response surface is the mean value of the local distribution, while the model also provides an error estimate at any location in the design space.

In most applications of the Kriging model, the observations are splitted in a trend and a deviation of this trend. The trend may be fitted with a linear model such as described in section 6.1.1, while for the deviation, a Kernel-based approach is used. After fitting of the model, a prediction $\hat{y}$ is obtained using the following formula:

$$\hat{y} = \sum_{i=0}^{p} \beta_i f_i(x') + z(x') \tag{6.10}$$

The fitting approach used for the deviation in equation 6.10 is not to minimize the overall error (such as RSS or RMS) between predictions and observations at known data, but to minimize the size of the error across the complete design space (thus, instead of minimizing $y_i - \hat{y}(x_i)$, $y(x) - \hat{y}(x)$ is minimized. The procedure is described by Kim *et al.* [74] and Vesting and Bensow [75] and is referred to a maximization of the likelihood.

A surrogate model build using Kriging can be tuned using two additional parameters. The first one represent an error or uncertainty estimate for each data point. This parameter allows the predictor to slightly deviate from the data points rather than exactly interpolating them, leading to smoother predictions. The second is a length-scale parameter for the used kernel function. The used Kriging model relies on a radial basis function kernel to compute correlation between data points, wherein the chosen length-scale is a measure for the number of points taken into account for the prediction of a new, unknown output.

Support vector regression

Support vector regression (Smola and Schölkopf [76]), similarly to the Kriging method, a kernel function to first estimate the correlation between data points before fitting coefficients. In support vector regression, one feature is that it allows

for an error between the observations and the predictions. This is realized by not increasing the cost function in the fitting process until the specified amount of error, ϵ, is exceeded. This forms an ϵ-tube around the prediction function. Outside the tube, the cost function increases, thus forcing the prediction function to lie within a certain range of the data points.

Another feature of support vector regression is that its fitting process also aims at producing a flat predictor. That means, it also minimizes the coefficients corresponding to each data point i. This feature prevents outliers (or an incorrect data point) to have a large effect on the predictions. In fact, predictions obtained from a Support Vector Regression model do not take all data points into account: the model is sparse. The points that remain in the prediction model are called the Support Vectors.

Similar to Lasso and Ridge regression, a regularization parameter decides the trade-off between obtaining a flat predictor or one that is more attracted to data points (and may be more accurate, but more prone to over-fitting). Another parameter used for the support vector model is ϵ, describing the size of the error-tube and finally, similar to the Kriging model, there is a length-scale parameter used to set the number of points taken into account by the radial basis kernel function.

Kernel ridge regression

Kernel Ridge regression (Vovk [77]) is similar to Ridge regression discussed above (the difference is well explained by An *et al.* [78]), however it first transforms the features into kernel space using the kernel trick (where the kernel function again is a distance/correlation metric between points). The advantage here is that non-linearities in the data can be fitted.

Kernel ridge regression also incorporates resemblance to support vector regression by basically using the same fitting approach. The main difference is that Kernel ridge regression does use the error-tube, which means that the penalty function immediately depends on the errors between predictions and observations. This leads to a faster fitting process, but also reduces the flatness of the predicting function since small errors are now affecting the prediction, while they were smoothened out in the support vector regression approach.

The similarity with a support vector model extends to the available parameters as well. Namely, the Kernel Ridge model allows setting the parameters for the kernel length scale as well as a regularization parameter that sets the trade-off between a model that may capture more details or one that is less affected by local deviations.

6.1.3. Neural Networks

In a neural network, input 'propagates' from the input, through a series of neurons, towards the output. An example is presented in Figure 6.1. In a Neural Network, there is at least an input layer, one hidden layer consisting of multiple neurons and an output layer. Each of the inputs in the input layer is fed to the first hidden layer. In each neuron of this layer, a weighted sum of the parameter values is computed (the weighted sum is most commonly used, but other options exist) and the result of this is processed by an activation function (e.g. a hyperbolic tangent or sigmoid

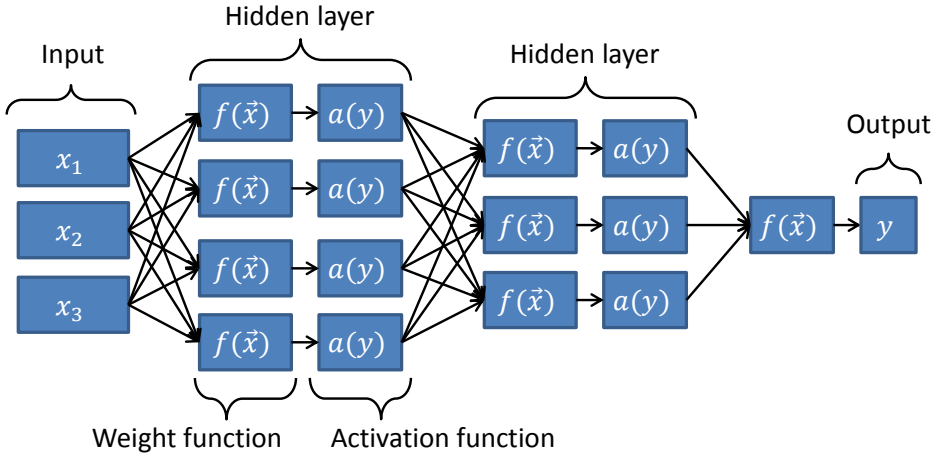

Figure 6.1: Example of a neural network with two hidden layers.

function) to obtain the output of the neuron. Next, all outputs from neurons in one hidden layer will either propagate through additional layers or are fed to the output layer, where again a weighted sum is used to compute the final output of the neural network.

The complexity of neural networks can vary. In the example shown in Figure 6.1 is a feed-forward neural network, in which the information propagates in one direction only. It is possible to have the information propagating forth and back or maybe iteratively passing through the same layer multiple times. Depending on the complexity, neural networks are able to represent highly non-linear or discontinuous behavior.

Neural networks have been used for propeller optimization by Vesting and Bensow [75]. They firstly showed that in general, a kernel-based method is more successful in prediction of multiple objectives regarding propeller performance. Furthermore, the stochastic process that is used in fitting/training of neural networks significantly affects the prediction accuracy (in fact, only an averaging model using the mean prediction of an ensemble of networks was able to yield good predictions) and renders it unfeasible to assess the influence of parameters, since each run of the process yields different results. Hence, neural networks are not further considered for the present thesis.

6.1.4. Summary

The former discussed a variety of surrogate models that are considered for this study. Two groups of models have been discussed: linear regression models and kernel-based regression models. The main difference between the two groups is that the former directly takes the features and outcomes, and uses least-squares minimization to fit a multi-variate polynomial to the data such that the error between

the predicted points and the data is minimized, while the second first transforms the input so that the distances (or correlations) between points are treated as the features. Next, weights are addressed to each point so that the prediction, which is a summation of the products between the data, weights, and function of the distances, comes closest to the original data.

The linear methods offer good insight in the effects that features have on the output, because each feature is given a coefficient (which is larger in magnitude if the feature has more influence). The kernel-based approach results in less transparent models, but is better at capturing non-linear behavior in the data.

The next section discusses methods that can be used to assess the influence of a feature on the data. Then, section 6.3 analysis the predictive performance of models so that a choice can be made for the model that is used in the remainder of the study.

6.2. Assessment of hull form aspect influence

One goal of this thesis is to indicate which stern shape aspects have a large influence on the propulsive performance of an inland ship, and which do not. Such insight gives direction to which stern aspects to improve. Surrogate models can provide this information in multiple ways. This section discusses methods to estimate the influence of hull form aspects (i.e. parameters) on the outcome.

The purpose is to find a subset of parameters that, when used with a certain surrogate model, gives a sufficiently accurate representation of the data on propulsion power or wake field quality. For example, if four parameters x_1, x_2, x_3, x_4 have been used as input, and y is the output (e.g. propulsion power), a possible subset can be $\{x_1, x_3\}$. If extending this subset with x_2 and x_4 does not significantly improve the quality of the prediction of y, it can be said that x_1 and x_3 are important parameters while x_2 and x_4 are less relevant.

The example above contains only four features. In such a case, searching over all possible subsets (exhaustive search) is feasible and can yield the optimal parameter subset in limited time. For this study, ship geometries have been generated as combinations of up to 16 variants, i.e. 16 parameters are involved. A search across all possible subsets would mean that the surrogate model is fitted $16 \cdot 15 \cdot 14 \cdot \ldots \cdot 1 = 16!$ times, which is possible but heavily time-consuming.

Efficient methods for the assessment of parameter influence are therefore investigated. Overviews of available methods are discussed by Guyon and Elisseeff [79] and Karagiannopoulos *et al.* [80]. Three groups of methods can be distinguished. First, there are filter methods, which make a sub-selection of parameters based on their correlation with the outcome of the simulation, interdependence, and correlation among parameters. Filter methods work independent of the surrogate model to be used. Second, wrapper methods use the predictive performance of a surrogate model to choose which parameters should be included in the parameter set. The third group of methods are embedded methods, which perform parameter selection while the model is being fitted to the data. The Elastic Net regression and the Lasso regression methods fall in this third group, since these methods will set certain coefficients to zero in order to reduce the sum of the coefficients, thereby

effectively removing parameters from the model.

In the present thesis, only wrapper methods are investigated. Filter methods are not applied since these can rule out parameters if correlation with the simulation outcome is small, which does not necessarily mean that correlation is still small if the parameter would be combined with another parameter in a fraction or product form (Guyon and Elisseeff [79]). Embedded methods are only available for certain types of surrogate models, and furthermore do not show the influence of a single parameter, but only assesses the influence of a certain contribution of the parameter (i.e. its linear, quadratic contribution, or the contribution of itself multiplied with another parameter).

Wrapper methods can be applied to any type of surrogate models and show the complete contribution of a parameter to the model. The following subsection discusses greedy algorithms, parameter scaling optimization and parameter selection. The various methods are compared in section 6.3.

6.2.1. Greedy algorithms

Greedy algorithms iteratively add or remove parameters from the model depending on the effect of these parameter on the error between observations and predictions. Since it uses this error, it is considered as a wrapper method. Greedy algorithms can start from an empty model and iteratively add features to the model (a forward step approach), or start with a complete model including all parameters and stepwise removing a feature (backward step). Greedy algorithms are greedy in the sense that once a feature is added or removed, it remains inside or outside the model parameter set. An example of the working principle in a forward-step method is presented in Figure 6.2. At each iteration (the first iteration starting with an empty model), each available (e.g. which is not already in the model) feature is added to the model and the model is tested. The feature that leads to the best predictions upon being added to the model, is kept in the model and the next iteration starts searching over the remaining features. The procedure is terminated once all features have been added or if the maximum number of features to be added has been reached.

Greedy algorithms can also be combined with a navigation-planning procedure. This is called a best-first approach. While the method described above discards any model that does not yield the best predictions, a best-first approach will keep them in memory. It does, however, still continue expanding the model with that yields the best prediction, but will always compare the predictive quality will all models in memory. If, at a certain moment, one of the earlier created models yields better predictions than the model currently being expanded, the best-first algorithm will continue expanding the best model, despite it was not the best model earlier. The best-first approach will, if not stopped earlier, search over all possible combinations (Karagiannopoulos *et al.* [80]). Therefore, an adequate stopping criterion must be used.

Greedy algorithms are relatively efficient [80], since especially if stopped at a maximum number of parameters, the number of surrogate model constructions is limited. On the other hand, it should be noted that a model with three features

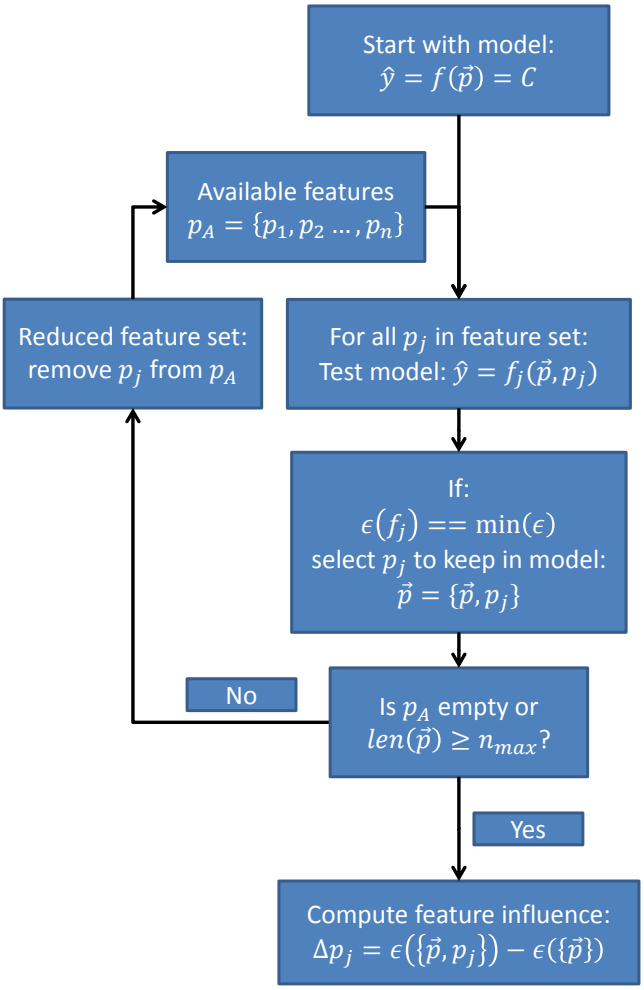

Figure 6.2: A forward-step greedy algorithm for feature selection. Starting with an empty model, it searches across available features and adds that feature to the model that leads to the lowest prediction error. This is repeated until either all features are added to the model, or a limit of features to be added is reached.

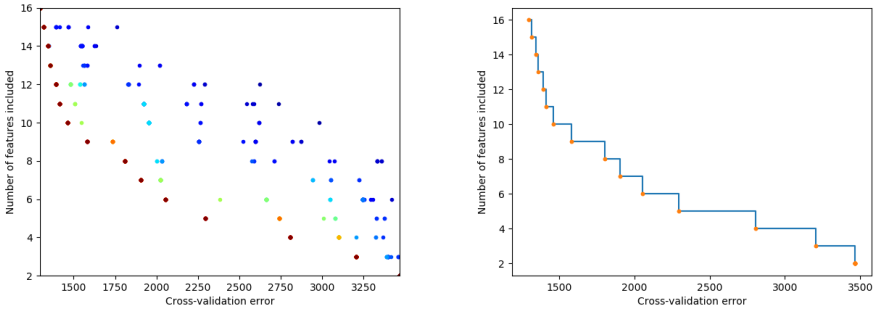

Figure 6.3: Example of feature selection through genetic algorithms. The graph on the left shows data for both the error computed in cross-validation and the number of features in the model. On the right, the Pareto-front is shown. The front shows that once multiple features are included, further addition of features has a smaller influence on the decrease of prediction error.

automatically inherits the features from the two-parameter model, while a different subset of three features may have performed better.

6.2.2. Parameter selection

As stated earlier, performing exhaustive search is too costly from a computational perspective. However, the search can be guided using genetic algorithms. This approach has been used by multiple authors and for multiple applications (Raymer *et al.* [81], Yang and Honavar [82], Frohlich *et al.* [83]). Commonly, both the number of enabled features as well as the error between the predictions from the model and the real data are used as object functions. As constraint, authors have introduced a minimum value of features to be included.

In the present thesis, the NSGA-II algorithm developed by Deb *et al.* [84] is applied to this end. As object functions, the cross-validation error as well as the number of included features is used. The genes are a series of n_p ones or zeros (or a combination), with a one indicating that a parameter is included. Since the NSGA-II algorithm is a multi-objective optimization algorithm, the procedure leads to a Pareto-front showing the trade-off between a model with less features but a larger deviation from the data. Moreover, the Pareto-front shows how much features should at most be in the model. Namely, if a higher number of features is included but the error increases, the result is no longer part of the Pareto-front.

In Figure 6.3, an example of the results of feature selection through the NSGA-II algorithm is presented. The graphs show both multiple generations in the algorithm and the resulting Pareto front. The Pareto front shows that there is a trade-off between the number of features and the accuracy of the model.

In greedy algorithms, the most important features are those that have been added first (in case of a forward-step method). When using genetic algorithms, a model with 6 features does not necessarily include all features from the model with 5 feature. In order to determine which features are most important, one should

look at the frequency of inclusion: if a feature is included in most (if not all) models, the parameter is more important.

To compute the (relative) influence of a certain feature (e.g. ship hull form parameter) on the power requirement, a different approach has to be used than that for a greedy algorithm because a model with a higher number of features can consists of entirely different features than the one with one less feature. The solution is to firstly compute a matrix consisting of ones and zeros indicating whether a feature is included in the model or not. Next, by subtracting adjacent rows a matrix is obtained with values 1.0, 0.0 and -1.0. A -1.0 indicates that a specific feature was added, 0.0 means that it is either included or excluded in the previous as well as the next model, while -1.0 means that it is in the model for n^i features, but not in the model with n^i+1 features. Next, multiplying this matrix with the error differences from models with n^i features to those with n^i+1 features, a matrix results that shows the positive or negative influence of certain features when increasing the number of included features. Taking the sum of values per feature, the result is the overall effect that the specific feature has on the data.

$$\begin{pmatrix} x_1 & x_2 & x_3 & x_4 & n_i \\ 0 & 0 & 0 & 0 & 0 \\ 0 & 1 & 0 & 0 & 1 \\ 0 & 0 & 1 & 1 & 2 \\ 0 & 1 & 1 & 1 & 3 \\ 1 & 1 & 1 & 1 & 4 \end{pmatrix} \rightarrow \Delta\epsilon \cdot \begin{pmatrix} x_1 & x_2 & x_3 & x4 \\ 0 & 1 & 0 & 0 \\ 0 & -1 & 1 & 1 \\ 0 & 1 & 0 & 0 \\ 1 & 0 & 0 & 0 \end{pmatrix} = \begin{pmatrix} \Delta\epsilon_{x_1} \\ \Delta\epsilon_{x_2} \\ \Delta\epsilon_{x_3} \\ \Delta\epsilon_{x_4} \end{pmatrix}^T \tag{6.11}$$

6.2.3. Feature scaling

A similar approach to feature masking is to scale the features (Punch III *et al.* [85], Weston *et al.* [86]). The same genetic algorithm can be used, but whereas for parameter masking the gene of an individual consists of ones and zeros indicating if parameters are included or not, parameter scaling uses genes with n_p continuous values ranging from, for example, 0.0 to 5.0.

The method only works for kernel-based models, since linear models will address a higher coefficient to feature that has been scaled down. The working principle of feature scaling for kernel-based models can be explained using Figure 6.4. In case the features are as provided, hence not scaled, both x_1 and x_2 affect the distance measure (or correlation) between the red data point and the blue data points. After downscaling of parameter x_2, the distance between the red and blue data points is (almost) entirely dependent on x_1, and x_2 does no longer affect the data set.

An advantage of the feature scaling approach is that it adjusts the relative effect that features have on the correlation between points. Namely, a kernel-based model assigns weights to data points rather than to features in order to construct a predictor for the power requirement of a ship. This means that any feature has the same effect on the correlation between data points after feature normalization. Feature scaling adjusts the effect that features have on the correlation and will attach lower weights to less important features.

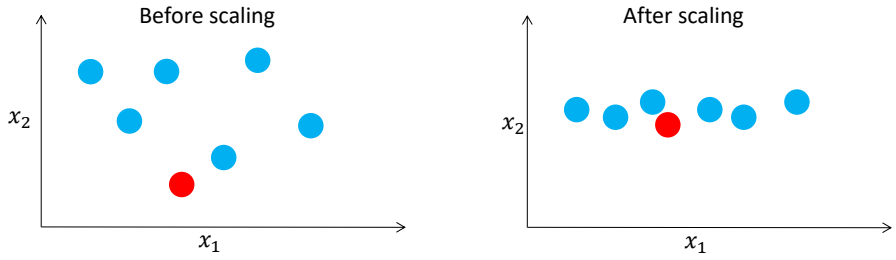

Figure 6.4: Effect of feature scaling on the correlation / distance measure between data points.

One drawback of the feature scaling method is that it requires a larger computational effort, compared to feature masking, to find the Pareto-front that shows the trade-off between a smaller number of features or a closer representation of the dataset. Furthermore, as stated earlier, the feature scaling approach cannot be applied to linear models.

6.2.4. summary

This section discussed multiple methods to assess the importance of features on the data. Greedy algorithms sequentially add more features to the model, while keeping those added previously. The influence of a feature is indicated by the drop of the RMSE at each step. Feature masking methods, and features scaling methods, can be applied through an optimization algorithm, for which NSGA-II is used in this study. These methods adjust the inclusion of features by turning them on or off, meanwhile tracking the RMSE of the model. Finally, model fitting regularization methods have been discussed as well. Regularization methods force the coefficient of linear models to decrease during the fitting process, and thereby limit the extent of over-fitting.

The advantage of feature scaling and masking methods is that they will observe if the effect of the one feature in a single-feature model can also be explained by two different features in a two-feature model. A greedy algorithm, in that case, would show that the two other parameters are redundant, while the feature masking/scaling methods instead show that the first parameter is redundant.

Section 6.3.4 compares the different methods based on their applicability to multiple surrogate model types and their ability to represent the influence of features on the data.

6.3. Comparison of surrogate models and feature selection methods

In order to select which surrogate model is well suited for identifying important hull form aspects as well as for finding relations between these aspects and ship propulsive performance, the surrogate modeling methods described in the previous

section are compared with each other. Furthermore, the methods available to select which features are important to the hydrodynamic ship design are also discussed.

For this comparison, the criteria mostly focused on is the predictive performance of the model, i.e. how well it represents the underlying data. To measure the predictive performance, multiple methods can be used to compute this performance parameter. These are discussed in the following sub-section. After that, multiple models are compared for the datasets generated during the present research.

After the model comparison, multiple methods to analyze the feature importance to propulsive performance are discussed. This discussion is limited to only the models that are deemed useful based on the predictive performance comparison. At the closure of this section, the selected model and applied feature analysis methods are stated as they are used in the remainder of the study.

6.3.1. Assessment of predictive performance

The predictive performance is a measure of how well a surrogate model is able to represent the underlying data. To do this, multiple methods are available. Before discussing these methods, it is important to stress that predictive performance should not be tested or computed using the data onto which the surrogate model has been fitted. Namely, the fitting procedure focuses on minimizing the error between that data and the predictions produced by the model. It is therefore obvious that the predictive performance is good.

To circumvent this problem, and obtain a more realistic measure of model performance, the predictive performance of a surrogate model should be tested with data that has not been used during the fitting process. This data is called *test data*. For the present study, a test data set is obtained by splitting the data gathered from CFD simulations with a 20/80 division, such that the test data comprises 20 percent of the total data set. The remaining 80 percent is then used for surrogate model fitting and optimization, and is called *training data*.

The predictive performance is thus measured using test data. It can be computed in multiple ways. A common approach is to use the R^2-value, which is a value that has a maximum value of 1.0, that is when the model exactly represents the data points. Another commonly used measure the the Root Mean Squared Error (RMSE), which has the advantage of being in the same units and order of magnitude as the data itself. The R^2 and the RMSE are defined as follows:

$$R^2 = 1 - \frac{\sum(y_i - \hat{y}(x'))^2}{\sum(y_i - \bar{y})^2} \tag{6.12}$$

$$RMSE = \sqrt{\frac{1}{N}\sum(y_i - \hat{y}(x'))^2} \tag{6.13}$$

For the present study, the RMSE value is used. It has a relation with the spread and variance in the data because the RMSE is equal to the standard deviation if the model only consists of a constant value, the mean of the underlying data. A better model yields a lower RMSE, and the ratio between the standard deviation and the

RMSE is thus a useful measure that generalized to multiple data sets with differing spread of propulsion power and wake field quality.

6.3.2. Optimizing predictive performance

As stated in the previous sub-section, the 80 percent split of the data is used for surrogate model optimization, apart from fitting. This optimization process is required since most of the models discussed in section 6.1 allow choosing of either regularization parameters or smoothing parameters. For example, the Kernel Ridge model uses an radial basis function as kernel. In this function, the relevant length scale affecting the weights of data points can be set. If this scale is either too low or too high, the predictive performance of the model is suboptimal.

Therefore, each of the models that include additional parameters is optimized. Since the performance of the model across the parameter space may have multiple local optima, the NSGA-II algorithm (Deb *et al.* [84]) is applied.

For the fitness function used in the optimization process, the RMSE with respect to the training data cannot be applied. Namely, the RMSE error is minimized if a model exactly passes through all data points, which means that smoothing parameters for kernel-based models, and regularization parameters in the Lasso and Elastic Net models, are set to zero. Although this seems preferable, a model that exactly fits to the data points may have very high variance and shows unrealistic behaviour between data points.

Instead, cross-validation is used. In cross-validation, a subset of the training data is set aside and the model is fit to the remaining data. Then, an RMSE value is computed with respect to the subset. This is done for multiple subsets, and the average of RMSE values for all subsets is used as the objective. In the present study, more specifically, k-fold cross-validation is performed, with k set to 10.

Alternatively, leave-one-out cross-validation can also be used (which in fact is k-fold cross-validation with k set to m, the number of data points) but that approach requires the fitting of much more models while the accuracy of the RMSE value does not increase that much. Also, a *validation set* can be split off from the training set so that three separate sets exist: a *test* set, a *validation* set and a *training* set. This approach, however, decreases the size of training set significantly, and may lead to high-varying models depending on how the split is made. Using cross-validation, this effect is smoothened out, giving a better fitness function for the optimizer to use.

As a final note, one may question why the full data set (before splitting in *test* and *training* data)is not directly used in the optimization procedure. With that approach, however, the model parameters would be optimized such that the model represents the full data set very well, but the model may exhibit strong variance between data points. Therefore, the test/training split needs to be made in order to assess whether the model really performs well on *new* data points.

6.3.3. Effects of data split and cross-validation

As discussed, splitting data into a test set and a training set, and furthermore using cross-validation, are required in order to assess predictive performance in a realistic

manner and to optimize the model parameters. Both steps, however, require that a certain split is made between *test* data and *training* data, while the latter is split in k subsets for cross-validation. The location of these splits may affect the resulting model and its predictive performance, as it changes the data on which the model is trained as well as the data with which the model is tested.

To assess the effect of the split location on the resulting models, the split positions are varied using random generators. However, per iteration, the random generator is given a fixed seed to ensure that cross-validation, used as the fitness function during model parameter optimization yields consistent results. In each iteration, a different seed is used so that a distribution of predictive performance can be generated.

Overall, the effect is relatively small. For a dataset consisting of 300 calculations, the spread of the power estimate varies between 110 kW and 150 kW (i.e. a spread of 40 kW). Meanwhile, the distribution of RMSE values from test data has a mean of 2.6 kW and a standard deviation of 0.4 kW.

6.3.4. Predictive performance comparison

The previous subsections discussed how the predictive performance of a model can be assessed, and how the outcome of this assessment can be affected. This section presents the predictive performance for multiple models.

In the present study, CFD simulations have been performed in multiple sets. Included ship types are a double-propeller ship with tunnels, a single-propeller ship with tunnels and double-propeller, pram-shaped ships without tunnels. The sets remain separated given the nature of the parametric model, which combines multiple ship geometries (variants) based on coefficients ranging from 0.0 to 1.0. The variants are different for each ship type considered, and it is not possible to combine the data sets into one large set.

Therefore, surrogate models are created for each data set separately. To test the predictive performance of the models, one dataset has been used. This is a dataset consisting of 300 double-propeller ships, all with main dimensions of $L_{pp} \times B \times T = 110.0 \times 11.40 \times 3.5$. The models have been created for the two objectives discussed in chapter 5, propulsion power and the quality of the wake field (WOF). The predictive performance of each model considered is presented in the table 6.1. The variational range of propulsion power in the used dataset was 40 kW, while WOF varied from 0.05 to 0.18. Furthermore, the presented values in the table are RMSE values on test data, which are computed *after* model optimization based on cross-validation errors. Additionally, the standard deviation of the RMSE values (following from multiple settings for the training data / test data split) is included as well.

The table shows that for the prediction of propulsion power, most models considered perform equally well, except for the Quadratic polynomial model and the Ridge Regression model, which both yield higher error values. For the wake field quality, the Kernel Ridge and Support Vector models perform best, while the Kriging model yields slightly worse results. Overall, the predictive performance for wake field quality is worse than for propulsion power. This is explained by the higher non-

	Power prediction [W]		WOF prediction [-]	
Model Type	$\overline{\text{RMSE}}$	$\sigma(\text{RMSE})$	$\overline{\text{RMSE}}$	$\sigma(\text{RMSE})$
Quadratic Fit	3568	348	4.311e−3	5.02e−4
Lasso Regression	2622	390	4.434e−3	5.30e−4
Ridge Regression	2960	263	4.332e−3	5.26e−4
Elastic Net Regression	2627	393	4.236e−3	5.17e−4
Kriging Model	2597	310	3.017e−3	7.41e−4
Kernel Ridge Regression	2598	311	2.816e−3	6.29e−4
Support Vector Regression	2573	339	2.776e−3	6.46e−4

Table 6.1: RMSE values on the test data set consisting of propulsion power and wake field quality estimated derived from 300 CFD calculations. For propulsion power, the standard deviation of all data equals 8.7 kW, while for wake field quality, the standard deviation is 0.0255.

linearities in the WOF data, since WOF is more dependent on the local hull shape close to the propeller, whereas such local effects tend to even out for propulsive power. Table 6.1 therefore also shows that kernel-based models are better at covering nonlinear behavior compared to linear models.

Based on predictive performance, the Kriging model is selected for further use in this thesis. The next section discusses feature selection methods. Despite the choice for the Kriging model in this section, the Quadratic Response Surface model is also used in the comparison of feature selection methods.

6.3.5. Comparison of feature selection methods

In this section, several of the models investigated before are used for feature selection, in order to compare which features are selected using various methods for feature selection, and using various surrogate models. Given that the Kriging model performed best with regard to predictive performance, that model is included in this analysis. Futhermore, the Elastic Net, being the linear model with the best predictive performance, is used as well.

Figure 6.5 shows a comparison between multiple feature selection methods for the basic quadratic model as well as for a Kriging model. The left graph shows that the forward-step greedy algorithm selects the same parameters for each model as the genetic algorithm. For the Kriging model, however, the greedy algorithm yields different results. From the 2-feature model to the 3-feature model, the error increases. This does not happen in both other feature selection methods and the quadratic model. The explanation, however, lies in the fact that the model parameters (which for the Kriging model are the error estimate and the radial basis kernel length scale) need to be optimized for every different set of features and results. As discussed in section 6.3.2, the NSGA-II algorithm can be used for this. In Figure 6.6, the greedy algorithm has been adjusted to optimize model parameters in each step.

As shown in Figure 6.6, all three feature selection methods roughly yield the same results. However, combining a greedy algorithm with an optimization proce-

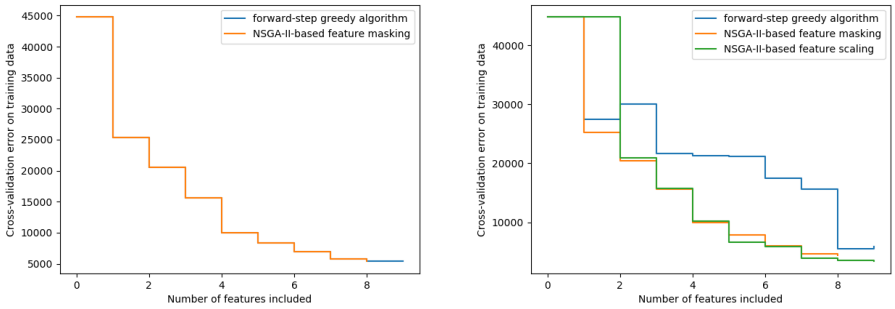

Figure 6.5: Comparison of feature selection algorithms when using a quadratic response surface (left) and a Kriging response surface (right). The graphs show that NSGA-II based feature masking gives similar results for both models, while a greedy algorithm is dependent on the choice of the underlying surrogate model.

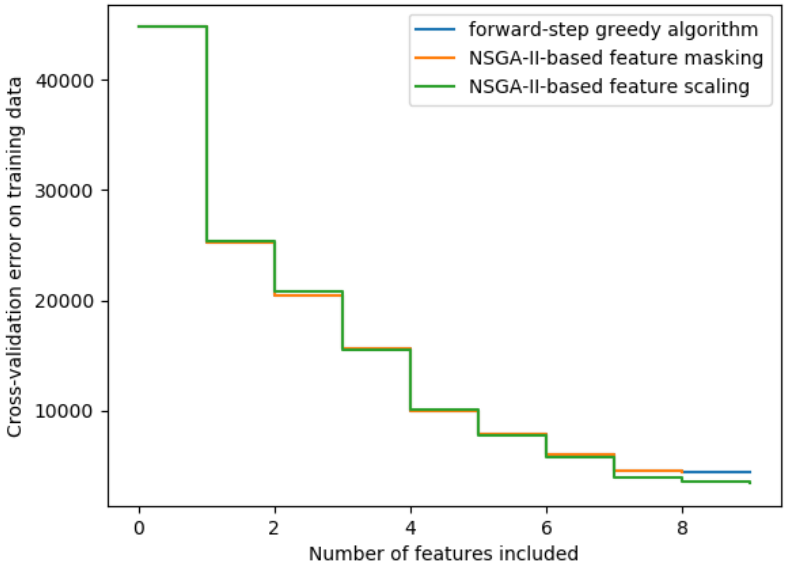

Figure 6.6: Comparison of three feature-selection methods applied to a Kriging model. All approaches yield the same result, while the NSGA-II based feature masking approach obtains this result with minimal computational effort.

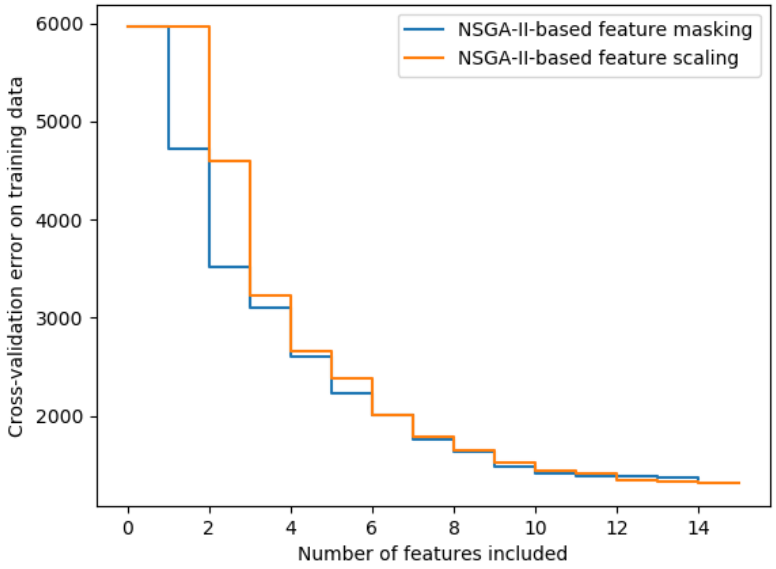

Figure 6.7: Comparison of feature masking and feature scaling for a Kriging model based on a 17-feature data set. Both methods obtain similar results for models with a high number of features, but feature scaling does not - within the same computational effort as masking - find a single-feature model at the Pareto-front.

dure for every model considered (which leads to $n \cdot (n-1) \cdot (n-2) \cdot (n-3) \cdot \cdots \cdot 1$ optimization runs). Therefore, the feature scaling or feature masking approach is more efficient, especially because model parameter can be optimized simultaneously. The greedy algorithm, in fact, is only more efficient for quadratic models that expose no additional parameters.

Figure 6.7 shows a comparison between feature masking and feature scaling for the Kriging model, working with a 17-feature dataset. For models with a higher number of features, both the scaling and masking methods yield similar results. For smaller models, however, the feature scaling method has not yet found any feasible models. With these results, it is difficult to assess the importance of the five most important features, while this can be determined from the feature selection procedure using feature masking.

6.4. Example of hull aspect influence

This chapter discussed the approach to answer one of the key questions posed in chapter 1: *What are the most important hull form aspects for inland ship propulsive performance?*. Using the parameter influence analysis method discussed in 6.2, the importance of hull form aspects for a Class Va inland ship (main dimensions L, B

and T being 110.0, 11.40 and 3.50 meter) has been determined and is presented here. The data involved 16 hull form parameters, and a total of 300 variants has been analyzed.

Figure 6.8 shows a diagram indicating which hull form aspects are most important for propulsion power and the wake object function (see chapter 5). For both performance objectives, the stern length is the most important. The next most important aspect, also for both objectives, is the athwart ships propeller position. For the estimate of propulsion power, additional aspects of importance are the tunnel entrance design (tunnelinward in Figure 6.8), the propeller diameter and the bilge radius (narrowbilge). For the wake object function, the influence of the stern length and the propeller position are significantly more important than other aspects. Propulsion power is thus sensible to more hull form details than the quality of the wake field.

If possible, a ship designer should address stern length and the athwart ships propeller position first: a too short stern leads to larger propulsion power, while it also decreases the quality of the wake field. The influence of the athwart ships propeller position is opposite for both objectives. Placing the propeller closer to the ship center leads to a reduction of propulsion power, but also decreases the quality of the wake field.

These two variables, however, may be fixed (due to design requirements such as ship displacement and machinery room arrangement) so that they can not always be adjusted. The propeller diameter also affects propulsion power significantly, but is usually kept small to ensure it remains well submerged in case of limited ship draft. Despite this, stern length, athwart ships propeller position and the diameter of the propeller are of key importance to propulsion power, as well as for the wake field quality (except for the propeller diameter).

6.5. Conclusions

This chapter discussed multiple surrogate modeling methods and multiple approaches to determine feature influence on the propulsive performance objectives. The purpose of both is to be able to determine which hull form aspects are most important to the propulsive performance of the inland ships considered, as well as to quickly assess which aspects mostly influence the optimal hull shape when optimizing for a specific displacement or water depth.

From the assessment of predictive performance of multiple surrogate models, the Kriging response surface shows the best performance. The error with respect to a test data set is smallest and the variance of that error also is smallest. Meanwhile, other surrogate models including linear models with squared features perform good as well. For feature selection and importance determination, a feature masking approach is selected because it is able to simultaneously optimize the feature mask as well as the model parameters (which, for the Kriging model, are the kernel length scale and the error estimate).

Therefore, the Kriging model combined with feature masking for hull form aspect selection are used in the next chapter, where the derivation of hull form design guidelines is presented.

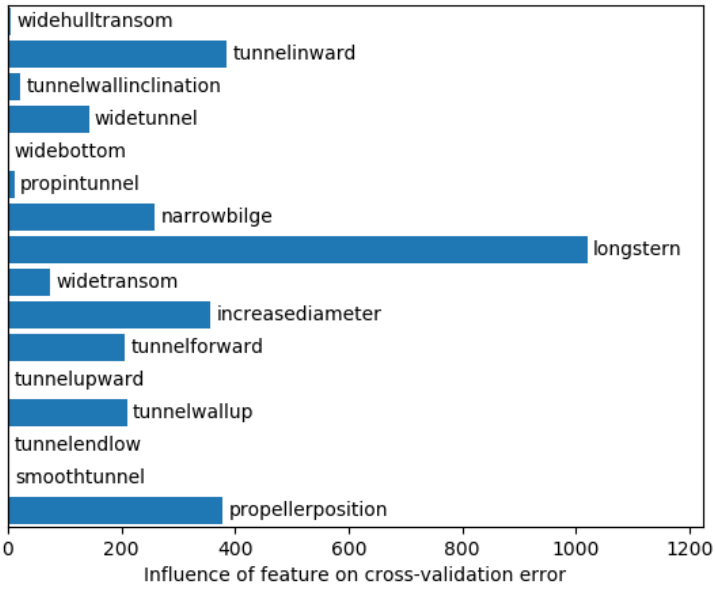

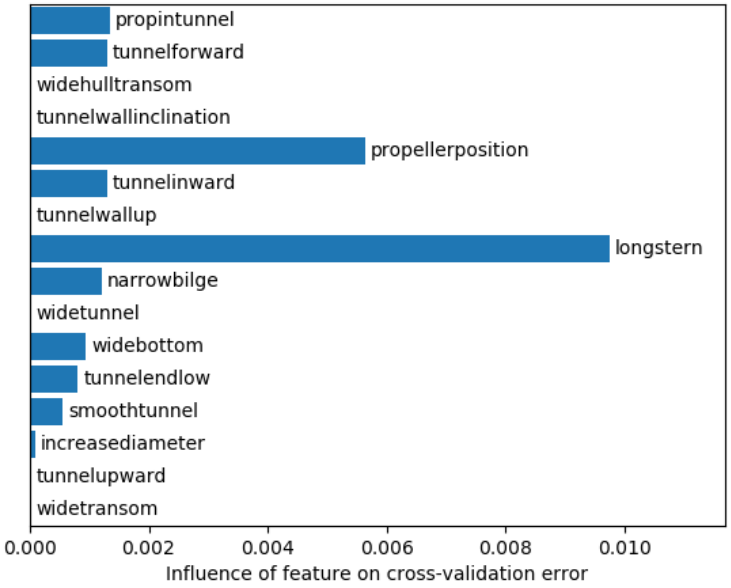

Figure 6.8: Influence of hull form aspects on the error between prediction models and power estimates or wake field quality obtained from CFD. On the horizontal axis, the influence on the error (in the same units as the objective itself) are given. The diagrams show that stern length and the athwartships propeller position both have a significant influence on both objectives, while for example the diameter of the propeller only affects propulsion power.

7

Derivation of design guidelines for inland ship sterns

The goal of this thesis is to gain insights in the relations between water depth, propulsive performance and inland ship stern shape aspects. These insights can be obtained using the CFD simulations discussed in chapters 4 and 5 and the surrogate models presented in chapter 6. Multiple design problems can be approached with the data. In this chapter, the use of the data is demonstrated for the following design case: given a CEMT-class (i.e. specific L, B, T) and water depth, find a stern shape design with optimal propulsive performance that provides the needed displacement. This problem is chosen because it involves the trade-off between fuel consumption and cargo capacity, which affects an operators competitive position.

This design case should not be solved for a single design. To show the relations between performance and shape aspects, a series of stern shapes with varying displacement, with optimal propulsive performance at the water depth of interest, must be found. The search for this series of stern shapes can be conducted using optimization and the surrogate models discussed in chapter 6. The differences between the found stern shapes can then serve as guidelines showing how the optimal shape changes if the displacement requirement changes.

This chapter presents a method to derive design guidelines using surrogate-based optimization of an inland ship stern. A set of 300 stern shapes for twin-propeller class Va ($L_{pp} = 110.0$, $B = 11.4$, $T = 3.5$) inland ships is used as a test case. Propulsive performance has been determined at three water depths for each stern shape. Section 7.1 describes the method to achieve guidelines for choosing stern parameters depending on displacement and water depth. Next, section 7.2 shows the resulting guidelines for the test case. Finally, conclusions are drawn in section 7.3. Results for other inland ship stern types are presented in chapter 8.

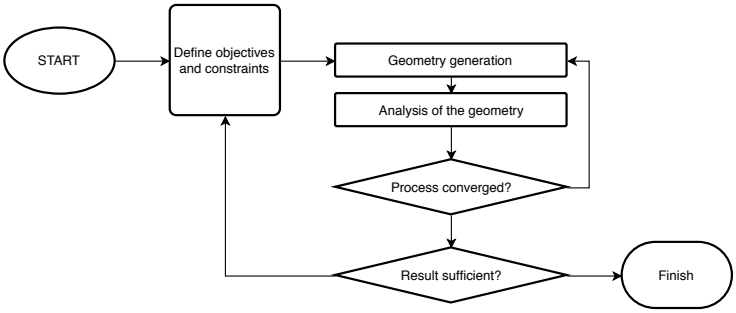

Figure 7.1: Example of an optimization process. Generally, objectives are defined while constraints (or requirements) are set. The process (which may be an algorithm or people adjusting the design) then sequentially generates geometries and analysis the performance of each geometry. When no more changes are possible or further adjustments would no longer improve the design, the process terminates. In case the resulting optimal performance is not adequate, requirements or constraints may be altered and the process restarts.

7.1. Guideline derivation approach

To obtain a ship with optimal propulsion performance (thus minimal propulsion power with a good quality wake field), a designer can follow the process presented in Figure 7.1. For a specified set of requirements (e.g. displacement and interior space constraints), the optimization process produces a ship design that performs optimally. The impact of changing design requirements can be analyzed by repeating the process for multiple sets of requirements. However, that increases the number of analysis steps needed. The same applies to incorporating multiple operational conditions such as water depth. This leads to a significant increase of expenses, which is unfavorable in regard to the limited budget (see chapter 1) that is available for the design of an inland ship.

The purpose of design guidelines is to omit high costs and still obtain a ship design with good propulsion performance. Guidelines by Heuser and Müller [3] describe certain limits to geometrical aspect of the hull form. Not exceeding the limits should result in a inland ship hull form design that operates with decent performance. However, the goal of this thesis is to also show the impact of varying requirements and, vice versa, to show the impact of changing the design on its performance. With that, guidelines are developed that aid designers in understanding the impact of choosing requirements and in making the trade-off between propulsion performance and ship displacement.

Such guidelines can be used according to the diagram presented in Figure 7.2. At the beginning of the process, certain requirements for the design are chosen. Next, the designer may adapt an existing design. In that case, the guidelines should be able to tell the designer which hull form aspects to adjust. Also, the guidelines should show the impact of the required adjustments to propulsion performance. If, on the other hand, the designer has no design available, the guidelines can provide

the hull parameters that lead to a hull form that fulfills the chosen requirements. The impact of the chosen requirements should also be made clear by the guidelines. In both cases (with or without an existing hull form), the guidelines should provide the designer with the means to make the trade-off between requirements and performance (i.e. displacement versus propulsion power).

The requirements set for the guidelines can be translated into a search for a set of ships with varying displacement, in which each ship has optimal propulsive performance at the water depth of interest. This search can be performed using optimization. More specifically, multi-objective optimization can be applied because displacement and propulsive performance can both be regarded as objectives. For the estimation of propulsive performance, the surrogate models discussed in chapter 6 can be used. The result is a Pareto front: a set of feasible (i.e. a ship does not sink) solutions for which there are no other solutions better at *all* objectives.

Each point on the Pareto front corresponds to a ship with an optimal combination of parameter settings. Presenting the parameters values for all ships contained in the Pareto front shows which hull form aspects are critical for the displacement to power ratio, and also shows which hull form parameters should be adjusted first if displacement is to be increased. Finally, the parameter settings can be used in the parametric model discussed in chapter 3 to generate a series of hull forms with varying displacement, and displaying those.

In this section, the set-up of the optimization method and the presentation of the guidelines are discussed. The results of the approach are presented in the section 7.2, for a Class Va (L, B and T being 110.0, 11.40 and 3.50) inland ship of which 300 variants have been analyzed with PARNASSOS at two different water depths: $h/T = 3.0$ and $h/T = 1.5$.

7.1.1. Optimization method

Multi-objective optimization has been used in this thesis to search for a series of ships with varying displacement but optimal propulsive performance. To incorporate varying displacement in the optimization problem, displacement can be used as an objective as well. Together with propulsion power and the wake object function (which are conflicting objectives as discussed in chapter 5), this results in an optimization problem for three objectives. The optimization problem is also subject to certain constraints. The first is parametric model feasibility, which is a check if the hull form has a realistic shape. Secondly, the distance from a point of interest, x', to the centroid point of the experimental design used to generate the data underlying the surrogate models is limited to 90 percent of the maximum distance between a point in the set and the centroid. This second constraint prevents the optimization algorithm from placing solutions in sparsely populated extreme regions of the design space.

For the optimization itself, the NSGA-II algorithm (Deb *et al.* [84]) is applied. This algorithm is capable of handling multiple objectives and can thus produce a Pareto front from an optimization problem with multiple objectives, which in this case are ship displacement, propulsion power and wake field quality. The resulting Pareto front of one optimization run is presented in Figure 7.3. In the graph, the

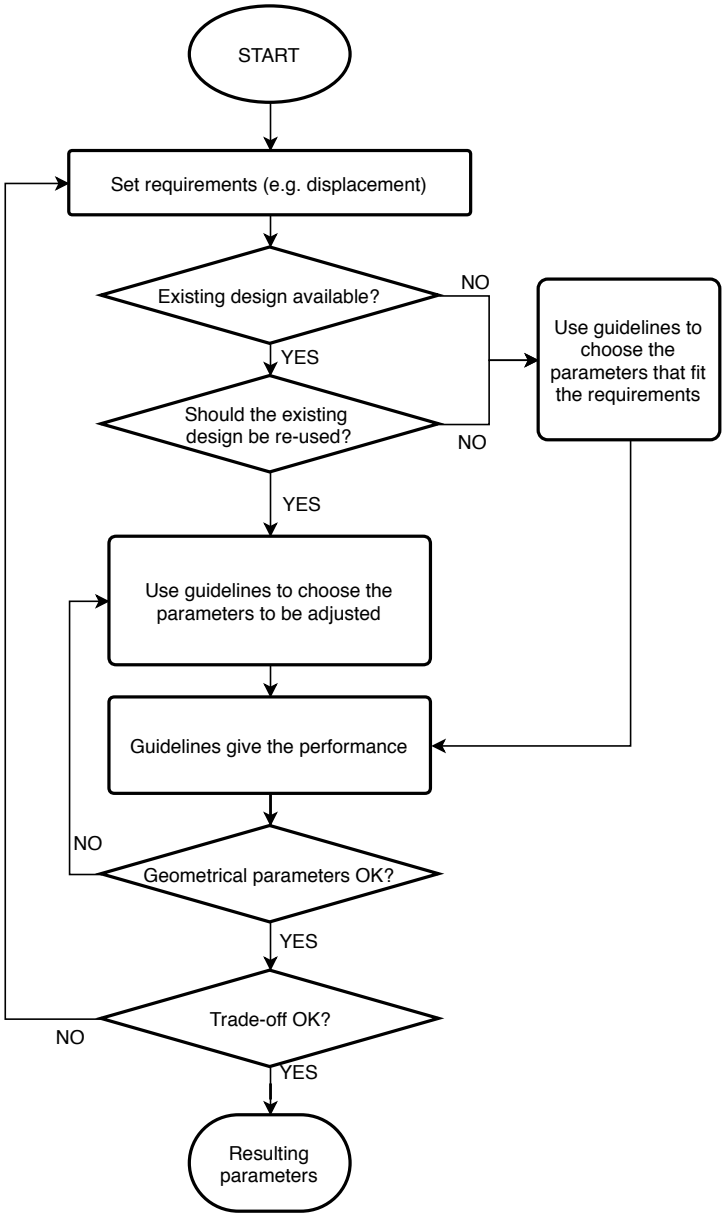

Figure 7.2: Diagram showing the proposed use case for the guidelines. The designer's aim is to obtain a ship hull that fulfills the needed requirement and provides optimal performance. The designer may start with or without an existing design, and the guidelines also allow to make the trade-off between chosen requirements and performance.

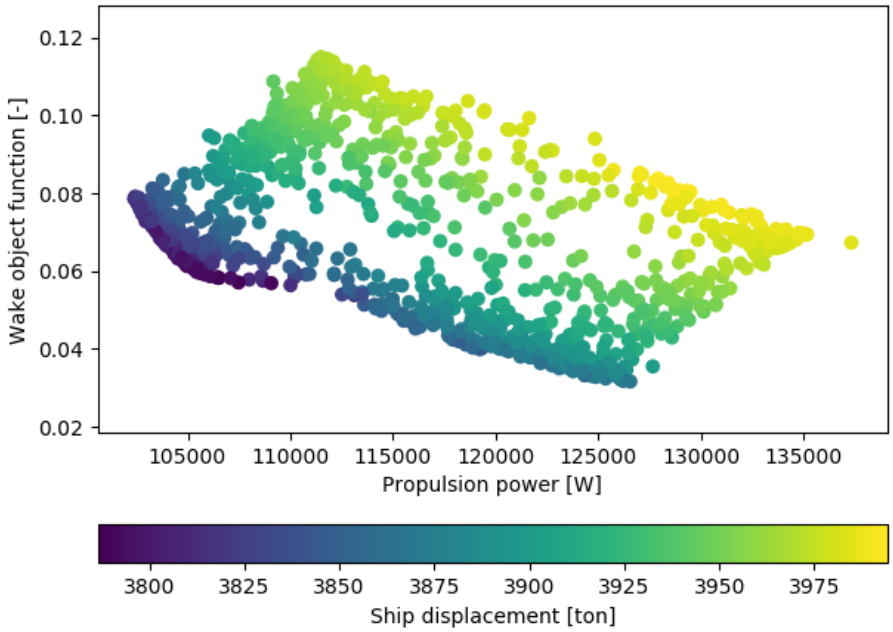

Figure 7.3: Resulting Pareto front from a three-objective optimization process using NSGA-II. The horizontal and vertical axis show propulsion power and wake quality respectively. The amount of displacement is represented by the colors of the dots.

horizontal axis depicts propulsion power, while the vertical axis represents the wake object function. The amount of displacement is shown by the color of the dots.

To find and show which parameters are adjusted in order to increase displacement, a selection of multiple points from the Pareto front in Figure 7.3 must be made. By comparison of the solutions (i.e. ships) corresponding to those points, the preferred changes to hull form aspects following from an increase of required displacement can be found. However, it can not be guaranteed that specific values of displacement are included in the Pareto front in Figure 7.3. Also, the Pareto front is less dense in the center, making it difficult to extract the needed points (solutions not being well-distributed across the Pareto front is a drawback of optimization algorithms when used for 'many' objectives (Deb and Jain [87])).

Due to the aforementioned problem, the optimization problem is reduced to one with two objectives only, a problem that is handled well by the NSGA-II optimization algorithm. To reduce the number of objectives by one, the objective representing wake field quality, the Wake Object Function (WOF), is used as a constraint instead of as an objective. This choice is made because for a WOF below a certain value, vibration hindrance is acceptably low, while it should never exceed a certain value for the ship to remain operable. The constraint is therefore such that the WOF value is not allowed to exceed a fixed value. The resulting optimization problem is

a two-objective problem, in which a trade-off is made between propulsion power and displacement.

The relation between the WOF value and operability depends on (as discussed in chapter 5) ship speed, propeller design and loading draft. Therefore, there is no single value that is adequate for all ships. For the present study, the maximum value allowed for the WOF value is set to the 75 percentile value of all data acquired in the calculations.

The optimization procedure is conducted separately per water depth, so that effects of choosing a water depth of interest can be shown. Moreover, taken multiple water depths into account at once implies that a water depth distribution is chosen, which depends on the operation of the ship and is therefore for the designer to choose. Furthermore, each optimization run is conducted multiple times. This is needed due to the stochastic nature of the optimization algorithm (mutations and combination happen by chance and the initial settings are generated randomly), and the parametric model inputs not being entirely independent to each other due to feasibility constraints: adjustment of a single input (that would lead to better performance) may require that another input (which does not have much effect on performance, but does have effect on feasibility) is adjusted as well to prevent constraint violation. Pareto fronts are averaged over all runs.

7.1.2. Presentation of guidelines

The aforementioned two-objective optimization approach produces a Pareto front. Ship design solutions with varying displacement and propulsion power are distributed along this front. Each ship design has different parameter values (that is, it needs different inputs to the parametric model described in chapter 3). For example, ships with lower displacement on the Pareto front will have a longer, more slender stern while those with high displacement have a shorter stern.

The effect of the length of the stern is relatively straightforward in the sense that a shorter stern leads to higher resistance (due to increased curvature) and therefore higher propulsion power, while displacement is higher as well. However, the length of the stern is not the only parameter to adjust when increasing displacement. Other parameters affect displacement as well, and simultaneous adjustment of multiple parameters may lead to a lower increase of propulsion power upon increasing displacement.

Therefore, it is chosen to present the result by plotting the change of parameter settings against ship displacement. A simplified example is presented in Figure 7.4. This shows how parameters (p_1, p_2, p_3) are adjusted when changing displacement. For example, the optimal parameter value may be adjusted proportionally with changing displacement. On the other hand, a parameter value can stay at its minimum across most of the displacement variation range, while only being increased when that is the only way to increase displacement.

In such a graph with parameter change depending on displacement, only the parameter settings for the most relevant hull form aspects are provided. Namely, the acquired settings for less important parameter is a consequence of the optimization algorithm searching for the very best solution, thereby also changing settings

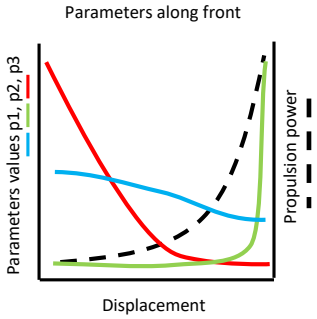

Figure 7.4: Example of plotting parameters settings as used in the Pareto front after optimization against ship displacement. By picking a position with a fixed displacement in the graph, the parameter values can be obtained for a ship that should provide decent propulsion performance for the selected displacement.

to parameters that are of limited influence to propulsive performance or displacement (even if the difference is practically negligible, the algorithm still favors a ship design with lower propulsion power and/or more displacement). Including such parameters in the design guidelines leads to a false idea of accuracy. The choice of which parameter to show is based on parameter selection as discussed in chapter 6. The most influential parameters for the test case are presented in section 7.2.1.

From these graphs, it is possible to extract parameter settings at a certain value of displacement. This leads to an estimate of the most important parameters to an inland ship stern. Additionally, these settings can be used in the parametric model (see chapter 3) to generate a series of hull forms for all displacement values included in the graph. By presenting this series (in sketches showing the stern frames), the changes that lead to an optimal ship with increased displacement can be presented graphically.

Following the diagram in Figure 7.2, a graph such as Figure 7.4 can be used in two ways. If a ship designer already has a hull form available, but needs to increase displacement, the graph shows which parameters can be adjusted while maintaining the ships propulsive performance. If a designer has no hull for available, the sketches described above help the designer selecting an optimal stern shape design. Additionally, the designer can see the effect of further increasing displacement (or decreasing it) and make the trade-off between cargo capacity and propulsion power.

7.1.3. Summary of the approach

In Figure 7.5, a graphical representation of the aforementioned approach is shown. Initially, multiple optimization runs are conducted for a specified water depth with two objectives: propulsion power and displacement. The wake object function is constrained to not exceed a maximum value. Because of the stochastic nature in the used optimization algorithm, the Pareto front is slightly different each run, and an

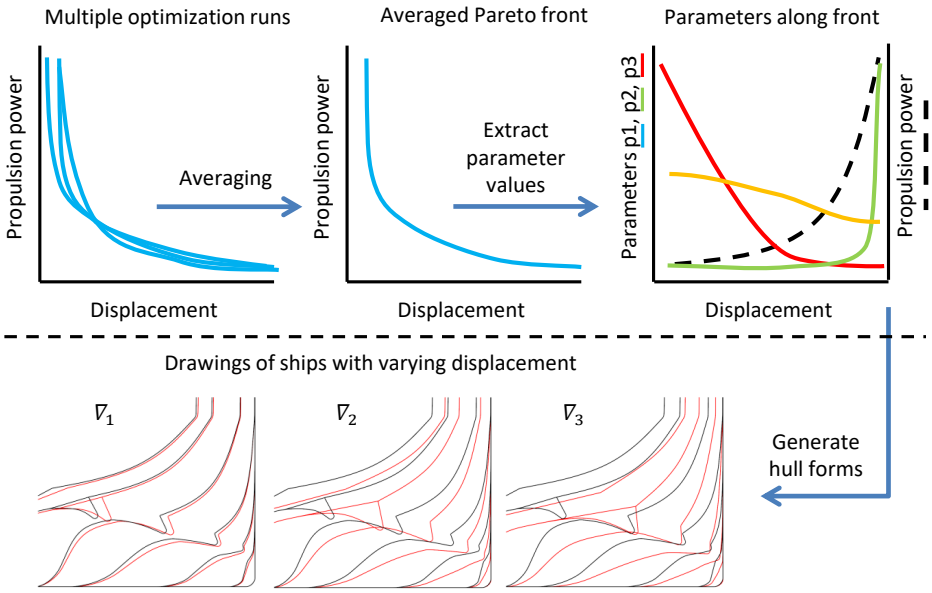

Figure 7.5: Used approach for guideline derivation. 1) Run optimization multiple times, 2) create an averaged Pareto front, 3) Extract parameter settings and display them against ship displacement and 4) take specific displacement values and use the corresponding parameter setting to generate hull forms.

averaged Pareto front is created. From this averaged Pareto front, the input values (parameter settings) for each solution on the front are plotted against displacement for each solution. This is only done for the most important parameters. The result is a parameter trajectory. For a certain displacement, the parameter values can be applied in the parametric model to generate hull forms for visual presentation of changes due to displacement adjustments.

The approach used here aimed at solving a specific design problem: finding a ship with optimal propulsion performance for the water depth of interest, and a required amount of ship displacement. However, if a different objective would be included (such as propeller outflow speed to guarantee adequate rudder forces for maneuverability, for example), the approach is applicable as well. The limitation is that only two objectives can be addressed simultaneously, additional performance indicators for (depending on the design problem) should be included as constraints.

7.2. Design guidelines for a Class Va inland ship

Using the approach described above, it is possible to show how hull form aspects change with increasing displacement. Per displacement value, it is also possible to extract the hull form aspect settings and obtain a ship design that provides adequate

propulsive performance. The presented information serves as a guidelines that can aid designers in obtaining a ship design that has the desired propulsive performance.

The importance or sensitivity of the aspects is determined using parameter selection as discussed in chapter 6. The results of this method are presented in section 7.2.1. The results presented there correspond to a class Va inland ship (L, B and T are 110.0, 11.4 and 3.5 respectively), and are presented for two water depths corresponding to $h/T = 3.0$ and $h/T = 1.5$. In sections 7.2.2 and 7.2.3, the resulting guidelines are presented for the same two water depths.

7.2.1. Hull form aspect sensitivity

In Figure 7.6, the importance of hull form aspects at $h/T = 3.0$ for propulsion power and the wake object function is presented. It shows that for the wake object function, stern length and the athwartships propeller position are of largest importance. Additionally, the curvature of the bottom plane as well as the submergence of the tunnel skirt contribute to the WOF value as well.

Propulsion power is affected by more parameters. Similar to the wake object function, stern length is the most important parameter. Other important parameters are the propeller diameter, bilge radius, the athwartships propeller position, the tunnel entrance design and the curvature of the tunnel top curve.

The sensitivity analysis shows that a ship designer should, if possible, address the stern length and athwartships propeller first in order to improve propulsive performance. Additionally, the bilge radius contributes to both objectives as well and should not be too small (see van der Meij and Raven). However, stern length and propeller position may be fixed by other design requirements such as a required length for the cargo hold or the arrangement of the machinery room.

At the tunnel start, the designer may have the freedom to locally make the hull form smoother, without affecting interior space or displacement significantly. It does, however, affect propulsion power as shown in Figure 7.6. A more detailed explanation is given using Figure 7.7. In this figure, distribution of the local resistance contribution over the hull is presented for two different ships in the dataset. In the right image, the tunnel entrance is sharp, and the local resistance contribution is high. In the left image, the entrance is much smoother, resulting in a lower contribution to resistance, and therefore a more efficient ship.

Figure 7.7 also shows the effects of two other parameters. First, the aft end of the ship is inclined for the ship in the left image. This results in a decreased contribution to resistance (as indicated by the blue colors). The contribution is decreased due to the surface normals having a larger horizontal component, while local pressure is high. The result is that the ship is 'pushed' forward locally. In the right image, the aft end is not inclined, because of which the locally high pressure does not result in a reduction of resistance.

Secondly, the bilge is sharper at the tunnel entrance in the right image. This increases resistance as well as required propulsion power. Moreover, it affects the magnitude of vortices ending up in the propeller wake field and thus affects the wake object function as well.

Figure 7.8 shows the sensitivity of propulsive performance to hull form aspects

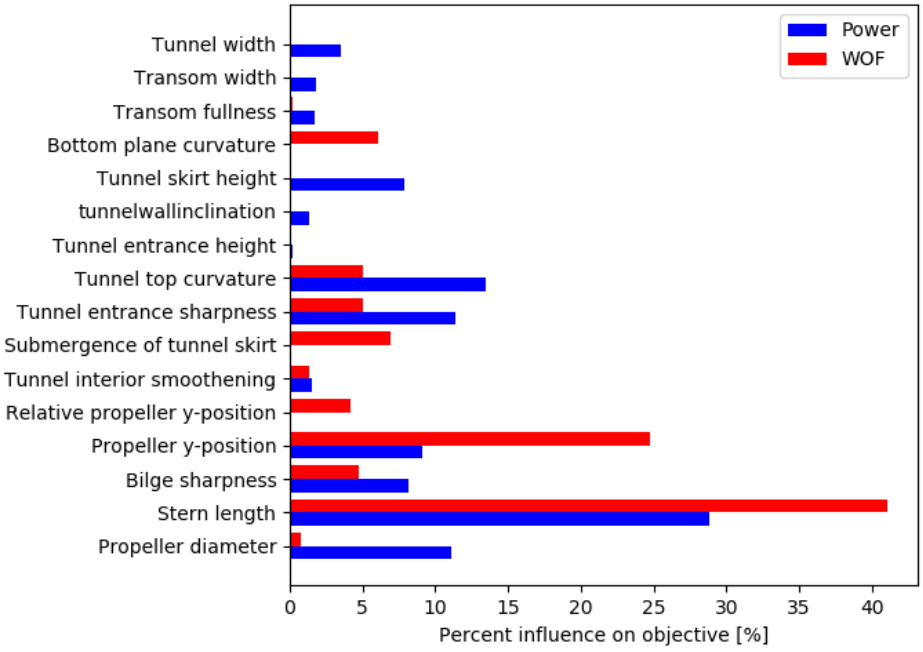

Figure 7.6: Influence of hull form aspects on power estimates or wake field quality at $h/T = 3.0$, showing the percentage of variation explained by each aspect.

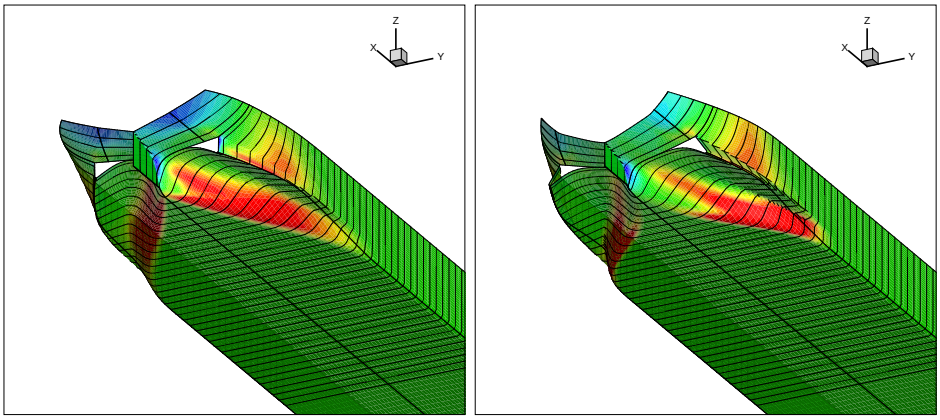

Figure 7.7: Distribution of the local resistance contribution for two ships of the 300-ship set. The left ship has a stern rise just before the transom, lowering resistance. Furthermore, the tunnel starting point is smoother, and the bilge radius is larger. These three differences make that the ship in the left Figure has lower resistance and requires less propulsion power.

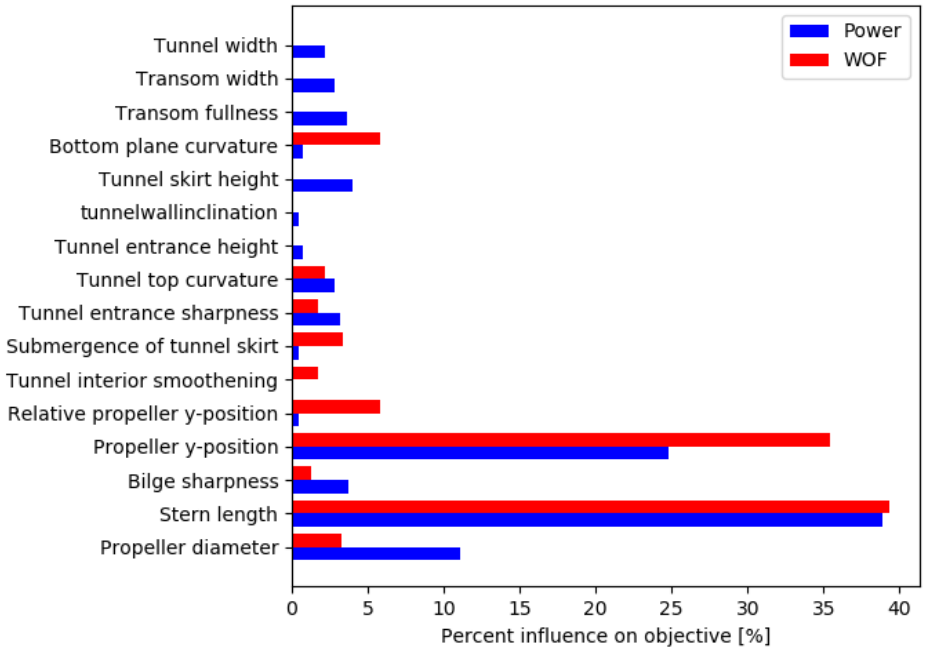

Figure 7.8: Influence of hull form aspects on power estimates or wake field quality at $h/T = 1.5$, showing the percentage of variation explained by each aspect. Compared to deep water (see Figure 7.6), stern length and the athwartships propeller position have a larger influence on both objectives.

for shallower water, $h/T = 1.5$. In this case, propulsive performance is largely affected by three parameters only: stern length, athwart ships propeller position and propeller diameter.

Figures 7.6 and 7.8 showed that the most important parameters to propulsive performance are stern length, athwart ships propeller position and the propeller diameter. These three parameters become even more important in shallow water. Additionally, designers should pay attention to the design of the tunnel entrance and the shape of the aft end of the ship: a smooth tunnel entrance reduces propulsion power and leads to a better propeller inflow, while an inclined aft end reduces resistance, thereby reducing propulsion power as well.

The next sections discuss design guidelines for the Class Va inland ship in two water depths. Design guidelines are given through the change of parameter settings for increasing displacement. Based on the sensitivity of propulsive performance to hull form parameters, these guidelines are given for the following parameters:

- Stern length
- Athwart ships propeller position
- Propeller diameter

- Tunnel top curvature
- Tunnel entrance sharpness
- Bilge radius
- Height of the tunnel skirt

The presented graphs show parameters settings between 0.0 and 1.0. To indicate how such settings affect the hull form, the body plans as presented in chapter 3 are shown in Figure 7.9 for the parameters in this list.

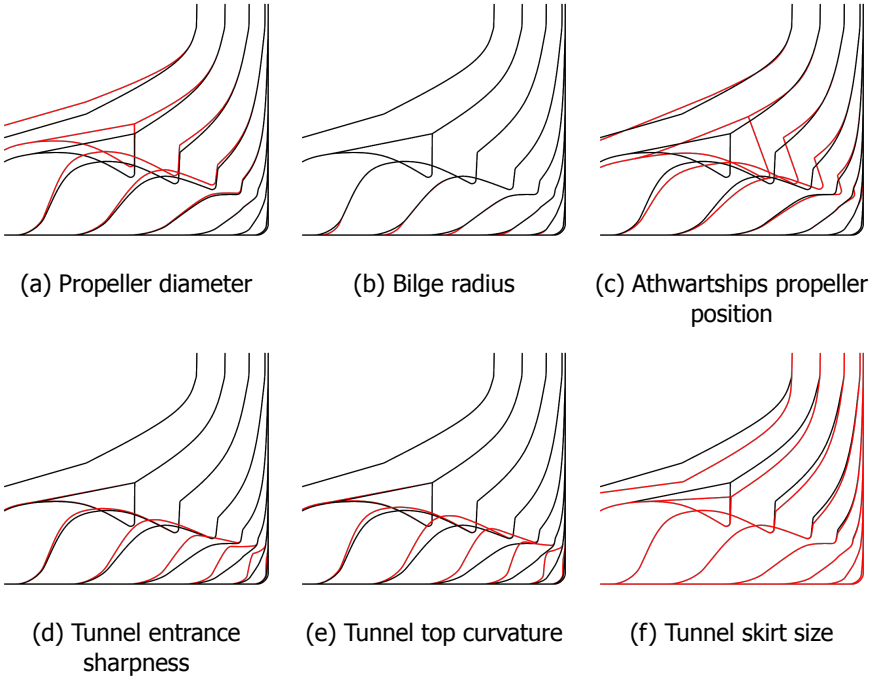

(a) Propeller diameter (b) Bilge radius (c) Athwartships propeller position

(d) Tunnel entrance sharpness (e) Tunnel top curvature (f) Tunnel skirt size

Figure 7.9: Bodyplans for hull form parameters used in presentation of design guidelines. The black lines correspond to a parameter setting of 0.0, while the red lines correspond to a value of 1.0.

7.2.2. Design guidelines for h/T = 3.0

Using the approach summarized in section 7.1.3, graphs are created that serve as a design guideline, showing optimal (i.e. minimum propulsion power at a certain displacement, while ensuring adequate wake field quality) combinations of parameter settings depending on ship displacement. These graphs are presented in Figure 7.10. Additionally, the generated body plans are given in Figure 7.11.

Figure 7.10 shows that to increase displacement, stern length and propeller diameter are decreased. The length of the stern is decreased immediately, while

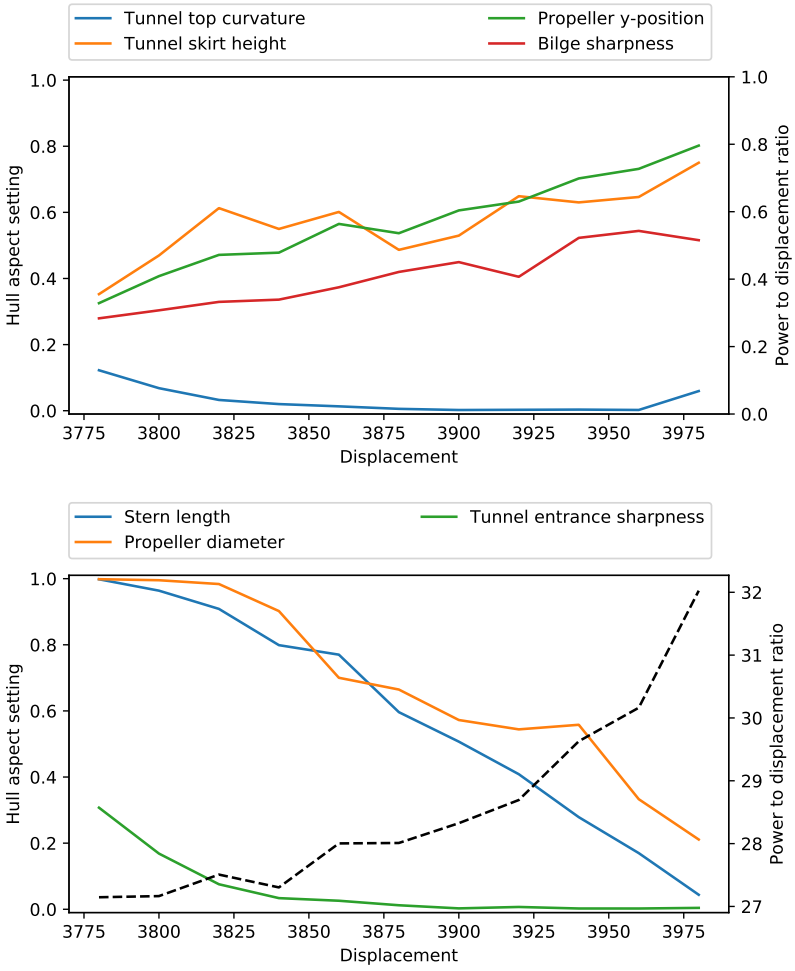

Figure 7.10: Change of hull form aspect settings depending on ship displacement, extracted from Pareto fronts created by multi-objective optimization for propulsion power and certain level of displacement, while the wake object function is constrained to a maximum value. The figures show that both stern length and the propeller diameter are decreased to accommodate for more displacement. The sharpness of the tunnel entrance is kept at a minimum. Furthermore, the bilge radius is decreased and the tunnel skirt is made larger.

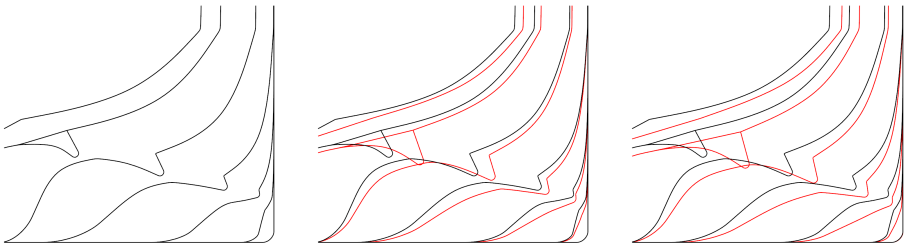

(a) $\nabla = 3770.0$ tons (b) $\nabla = 3805.0$ tons (c) $\nabla = 3840.0$ tons

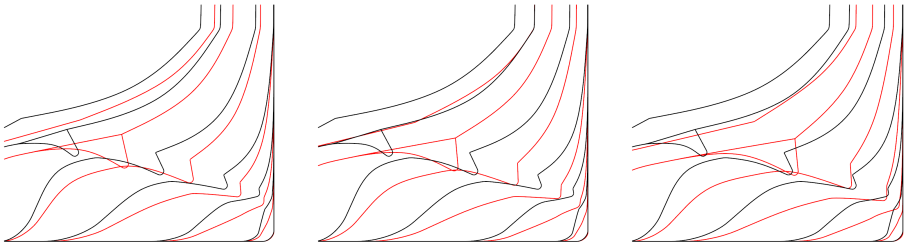

(d) $\nabla = 3875.0$ tons (e) $\nabla = 3910.0$ tons (f) $\nabla = 3945.0$ tons

Figure 7.11: A series of lines plans for ships created for hull aspect parameters settings obtained from Figure 7.10, each for an increasing amount of displacement. The tunnel starting position is lowered as much as possible and the entrance of the tunnel is made smooth. Also, the athwartships propeller position is increased to accommodate for the needed displacement.

propeller diameter is kept larger until the additional displacement is required to achieve an optimal design. Furthermore, the parameter for the tunnel top curvature is minimized along the whole displacement range. This indicates that the algorithm favors a tunnel design with a smooth entrance, and a tunnel top curve that is inclined with respect to the ship center plane at the end of the tunnel. This is also represented by the minimization of the tunnel entrance sharpness parameter: it is minimized.

Based on these results, a designer who needs to increase the displacement of a twin-propeller inland ship is advised to first attempt to decrease the length of the stern as well as to decrease the propeller diameter (which means that the space available for the propeller must be reduced). Furthermore, the entrance of the tunnel should be smooth (see Figure 7.9 (d)). The changes to other parameters are limited. However, a smooth bilge is advised. Also, the tunnel top curve should have minimal curvature - it is allowed to have the propeller inflow entering the propeller inclined.

7.2.3. Design guidelines for h/T = 1.5

The impact of shallow water on the design choice is investigated as well. Since the wake object function generally increases in shallow water (stronger velocity and pressure gradients, more separation), the optimization constraint puts stricter limits to region where designs can be found. In Figures 7.12 and 7.13, the change of hull form parameter upon increasing displacement and the corresponding lines plans are presented respectively.

Compared to deep water, especially the settings for tunnel top curvature, propeller y-position and propeller diameter show different behavior. Namely, the parameter for tunnel top curvature maintains a larger value until its effect on displacement outweighs that on propulsion power. Therefore, the tunnel becomes more pronounced in shallow water, and is also more aligned with horizontal inflow. The propeller y-position is reduced in shallow water to prevent separation near the ship center which is more likely to occur in shallow water. Separation can be suppressed by the propeller-induced pressure decrease upstream of the propeller, because it suppresses boundary layer growth. Furthermore, propeller diameter is kept larger. The loss of displacement due to this is compensated by a faster decrease of stern length compared to deep water.

In Figure 7.13, especially more horizontal-flow design of the tunnel can be observed, when comparing the lines plans to those for deep water in Figure 7.11. Similar to deep water, the sharpness of the tunnel entrance is minimized.

For a designer, this shows that care must be taken when the ship is supposed to be optimal at shallow water ($h/T = 1.5$ and under). In shallower water, the propeller diameter should maximized if possible. Additionally, it is important that the flow towards the propeller does enter the propeller horizontally, whereas inclined inflow is allowed in deeper water ($h/T = 3.0$). Finally, if the displacement requirement allows it, the propellers should be positioned closer to the ship's center. In order to increase displacement, the designer can reduce the length of the stern and increase the propeller's athwartships position (assuming that leads to increased displacement).

7.2.4. Observations

Based on the graphs and lines plans presented in sections 7.2.2 and 7.2.3, various observations can be made. These observations are outlined in the following list:

- The optimization procedure always shifts the starting point of the tunnel skirt downward when displacement increases. Due to this, the tunnel skirt rises upward from the midship towards the transom. Also, it decreases the curvature of the transversal frames at the bilge. This occurs at the whole displacement range.
- In deep water, the tunnel top curve is smoothened. Instead of being s-shaped such that it is aligned with the axial direction at the propeller position, the optimization procedure lowers the tunnel top curve from the start to the end of the tunnel. In shallow water, on the other hand, the optimization algorithm favors a more 'pronounced' tunnel, with an s-shaped top curve ending in axial

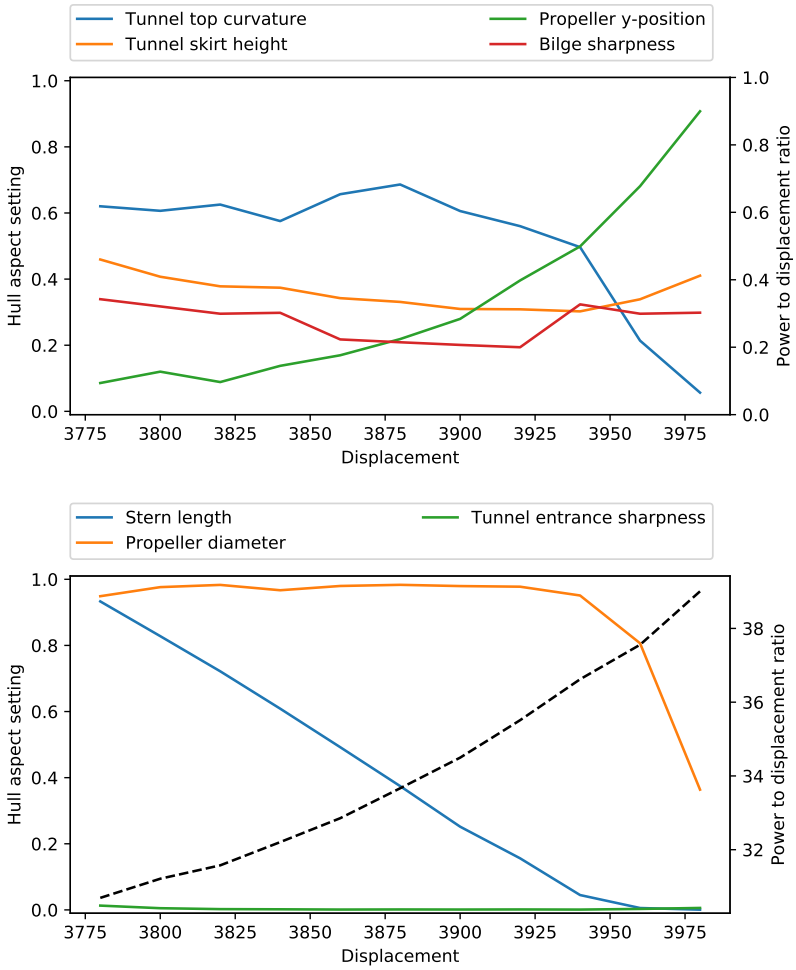

Figure 7.12: Change of hull form aspect settings depending on ship displacement, extracted from Pareto fronts created by optimization for wake quality and propulsion power at a certain level of displacement, for $h/T = 1.5$. In comparison with $h/T = 3.0$ (see Figure 7.10), mostly the propeller diameter is kept as large as possible, and other hull form aspects are adjusted in order to gain displacement. For example, the length of the stern is reduced earlier (i.e. at lower displacement) than in deeper water.

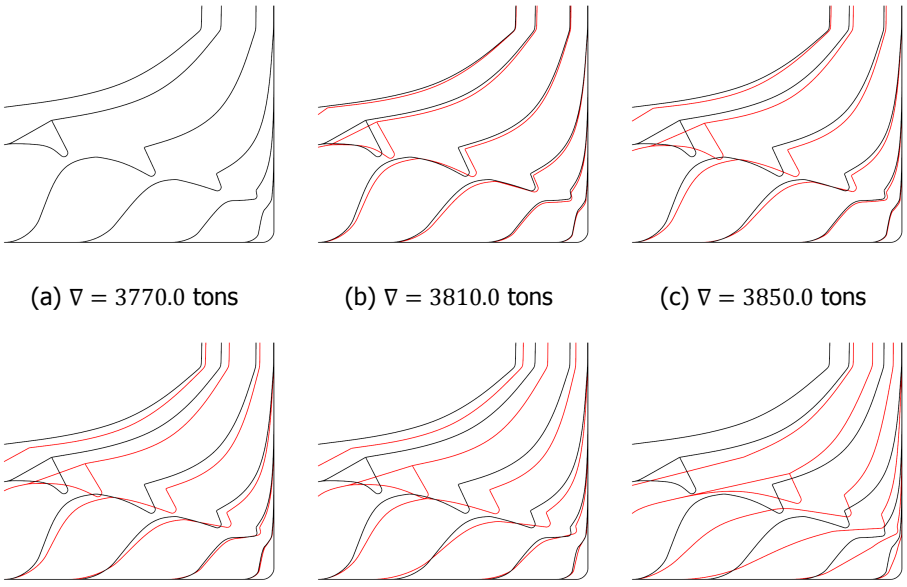

(a) $\nabla = 3770.0$ tons (b) $\nabla = 3810.0$ tons (c) $\nabla = 3850.0$ tons

(d) $\nabla = 3890.0$ tons (e) $\nabla = 3930.0$ tons (f) $\nabla = 3970.0$ tons

Figure 7.13: A series of lines plans for ships created for hull aspect parameters settings obtained from Figure 7.12, each for an increasing amount of displacement. Comparing to the lines plans optimized for $h/T = 3.0$, the optimization process clearly returns a different tunnel design. Only at the maximum displacement, the tunnel top curve is pulled downward. Also for the tunnel skirt, the starting point is lowered at $h/T = 3.0$ water while it remains at the initial height for the present case. These changes are a consequence of two-dimensional flow in shallow water, for which the hull form gets better suited using the high tunnel and high tunnel skirt.

direction at the propeller position. Figure 7.14 shows the difference between both tunnel top curves.

- At both water depths, tunnel entrance sharpness is minimized. The starting point of the tunnel should therefore, as discussed in section 7.2.1, be as smooth as possible.
- The tunnel skirt would normally only show its performance at limited draft in order to prevent the propeller from ventilating. In any other case, it leads to more resistance [19]. However, the optimization process used in this thesis favors additional displacement provided by a slightly larger tunnel skirt (and can thereby optimize other hull form aspects to reduce resistance). Apparently, if the tunnel skirt is required, its size does not significantly affect the amount of required propulsion power.
- Bilge radius is mostly affecting propulsion power. A large bilge radius is more important in deep water than it is in shallow water. This is due to water

coming from underneath the vessel in deep water, while in shallow water a larger portion comes from aside the ship.

- In shallow water, multiple aspects change. The increased importance of the propeller diameter (as observed in Figure 7.8) is reflected by the fact that it is maintained at its maximum until there is no other option to add displacement than to reduce the diameter. Furthermore, the tunnel top curve is not pulled downward as it is for deep water, and the starting point of the tunnel skirt remains at its height, while is was shifted down in deep water. Furthermore, the propeller y-position is kept lower in shallow water.

The above observations discuss, among others, the starting point of the tunnel. From the results, this point should be designed such that the curvature of waterlines is minimized, while also the curvature near the bilge of transverse frames is reduced as much as possible. Furthermore, designers should limit the curvature of the tunnel top curve: instead of ensuring that the tunnel top curve ends at the propeller parallel to the horizontal plane, allowing it to be inclined reduces propulsion power while it does not harm the wake field quality. This, however, only applies in deep water. In shallow water, the optimization procedure favors a pronounced tunnel significantly pulls into the hull (see Figure 7.13).

The hull form becomes significantly different in shallow water, especially for the tunnel top curve which is more pronounced and the tunnel is much more integrated into the hull instead of being an appendage. Meanwhile, the entrance point of the tunnel should still remains smooth, but whereas the tunnel skirt is shifted down in deep water, it starts higher in shallow water. These observations should be taken into account if a ship is expected to regularly navigate in shallow water with h/T less than 1.5.

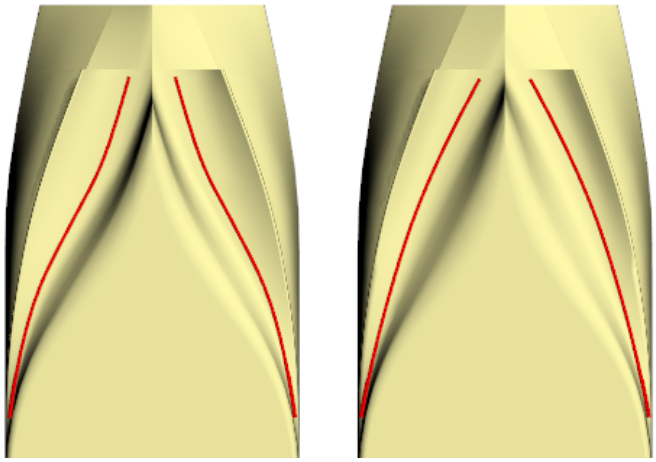

Figure 7.14: Difference between an s-shaped tunnel top curve (indicated by the red line) that is closer to axially aligned inflow, and a single-curved tunnel top curve that approaches the propeller disk inclined.

7.3. Conclusions

This chapter discussed the approach to derive design guidelines from the computations conducted in PARNASSOS and presented results for a dataset consisting of 300 double propeller inland ships with main dimensions of $L = 110.0$, $B = 11.40$ and $T = 3.50$. The results presented are the relative influence of each hull form aspect on propulsion power and wake field quality, as well as choices of hull form aspects that lead to a hull form with a specific amount of displacement and minimal power.

The first part, which is the relative influence of hull form aspects, applied the feature influence analysis approach described in chapter 6. It is found that the main contributors to propulsion power are

- the length of the stern region,
- the athwart ships propeller position,
- the propeller diameter,
- the curvature close to the starting point (near parallel midbody) of the tunnel,
- the curvature of the tunnel top curve,
- the size of the tunnel skirt,
- and the bilge radius.

While the main contributors to the wake object function (i.e. quality of the wake field) are mostly the length of the stern region and the athwart ships propeller position. Furthermore, the curvature of the starting point of the tunnel affects the quality of the wake field as well.

Next, optimization using the NSGA-II algorithm and the surrogate models discussed in chapter 6 have been applied in order to find how an inland ship should be designed if is should have a certain amount of displacement. Using multi-objective optimization with propulsion power and displacement as the objectives, the resulting Pareto front has been used to investigate the change of hull form aspects depending on displacement.

The main observations from these optimization procedures have been discussed in section 7.2.4. At any water depth, designers should attempt to minimize curvature at the starting point of the tunnel. The optimization procedures favors this regardless of displacement. In deep water, the starting point of the tunnel skirt as well as the tunnel top curve was moved downward, which both reduce curvature and increase displacement. In shallow water, the tunnel top curve remains pronounced and is not moved downward. Instead, the length of the stern is reduced faster in order to gain displacement.

For a designer, this shows that care must be taken when the ship is supposed to be optimal at shallow water ($h/T = 1.5$ and under). In shallower water, the propeller diameter should maximized if possible. Additionally, it is important that the flow towards the propeller enters the propeller horizontally, whereas inclined inflow is

allowed in deeper water ($h/T = 3.0$). Finally, if the displacement requirement allows it, the propellers should be positioned closer to the ship's center. In order to increase displacement, the designer can reduce the length of the stern and increase the propeller's athwartships position (assuming that leads to increased displacement).

The next chapter will present results for single-propeller ships and ships with a pram-shaped stern. The same method is used as for the present chapter.

8

Design guidelines for single-propeller tunnel and pram-shaped stern types

The previous chapter discussed the derivation of design guidelines using optimization and feature influence analysis. In that chapter, results have been presented for a class Va ship ($L_{pp} \times B \times T = 110.0 \times 11.40 \times 3.5$). The conclusions discussed multiple useful observations that give insight in differences between optimized ship designs depending on the displacement and water depth.

In this chapter, the same approach is applied to obtain the same type of results for inland ships with a pram-shaped stern and single-propeller ships with a tunnel stern. Width (B) and draft (T) are equal to the case in chapter 7, being 11.40 and 3.50 respectively.

Section (8.1) discusses single-propeller inland ships. Next, section 8.2 discusses ships with a pram-shaped stern. Both sections are structured as follows: first, the sensitivity of propulsion power and wake field quality to each of the hull form parameters is discussed. Then, the optimization approach discussed in chapter 7 is used to show how parameters should be adjusted in order to increase displacement while maintaining optimum propulsion power. This is presented for water depths corresponding to $h/T = 3.0$ and $h/T = 1.5$. Both sections finish with a summary of the main observations made. The findings are summarized in section 8.3.

8.1. Single-propeller tunnel sterns

For single-propeller ships including a propeller tunnel, a data set of 300 ships has been generated. Apart from variation of hull form details, main dimensions have also been varied. Furthermore, water depth has been included in the initial experimental design, by using the h/T ratio as a parameter. The main dimensions used are those for a Class Va inland ships, with length, breadth and draft being 110.00, 11.40 and 3.50 respectively.

This section discusses the sensitivity of the objectives (Propulsion power and the wake object function) to the hull form parameters as well as design guidelines for a Class Va single-propeller inland ship. Similar to the discussion of guidelines for double-propeller ships in chapter 7, the most important observations are mentioned as well.

8.1.1. Hull form aspect sensitivity

In Figure 8.1, the importance of hull form aspects for propulsion power and the wake object function is presented. Three aspects are most important to the wake object function: stern length, smoothness of the tunnel entrance, and the bilge radius (as indicated by *Bilge sharpness*). Additionally, the height of the tunnel entrance as well as the curvature of the bottom plane play a smaller, but still significant role for the wake object function.

Propulsion power is affected by more parameters. Similar to the wake object function, stern length is the most important parameter. Additionally, the width of the tunnel, size of the tunnel, transom dimensions, bilge radius and the smoothness of the tunnel entrance are important as well.

The sensitivity analysis shows that a ship designer should, if possible, address the stern length first to improve propulsive performance. Additionally, the bilge radius contributes to both objectives as well and should not be too small (van der Meij and Raven, [19]). The same applies to the smoothness of the tunnel entrance (see chapter 3, Figure 3.3), which affects both the wake field quality and propulsion power. The effect of this hull form aspect has been discussed in chapter 7, and an example of its effect on the flow around the ship is presented in Figure 7.7. Finally, propulsion power is also affected by the size of the tunnel skirt and the width of the tunnel (at the propeller position).

Figure 8.2 shows the sensitivity of hull form aspects for shallower water at $h/T = 1.5$. In this case, propulsive performance is largely affected by three parameters only: stern length, bilge radius and smoothness of the tunnel entrance. Stern length has significantly more influence than bilge radius and tunnel entrance smoothness. Propulsion power thus becomes dependent on fewer hull form aspects in shallow water. This is similar to what is found in chapter 7. The same applies to the wake object function, which in shallow water almost solely depends on the smoothness of the tunnel entrance and the length of the stern.

Figures 8.1 and 8.2 showed that for propulsive performance, the most important hull form aspect is the length of the stern region. This parameter becomes even more important (relatively to other hull form aspects) in shallow water. Additionally, designers should pay attention to the design of the tunnel entrance: if it is smooth,

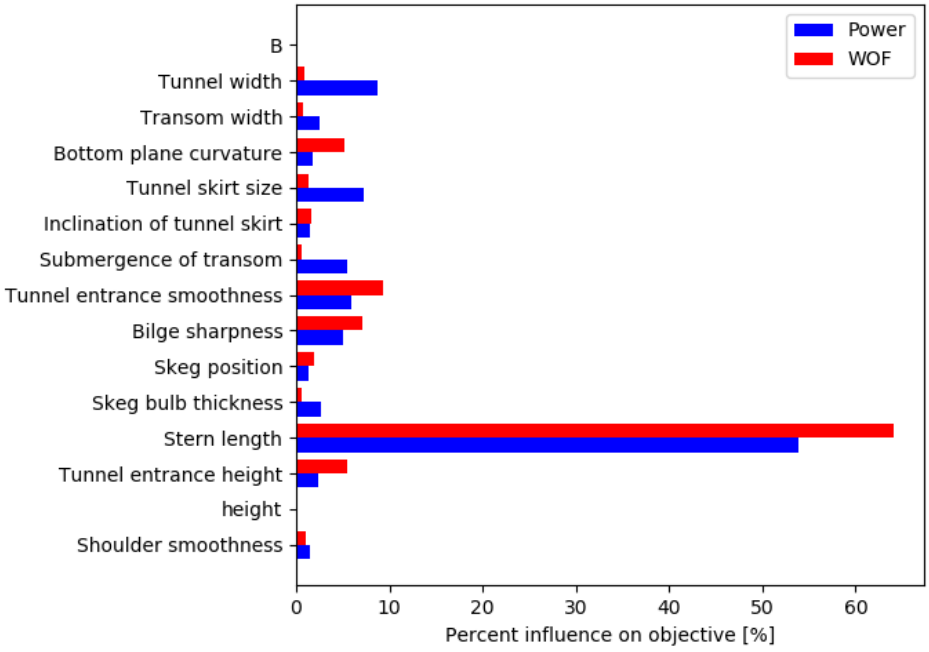

Figure 8.1: Influence of hull form aspects on the error between prediction models and power estimates or wake field quality obtained from CFD, at $h/T = 3.0$. On the horizontal axis, the influence on the error (in the same units as the objective itself) are given.

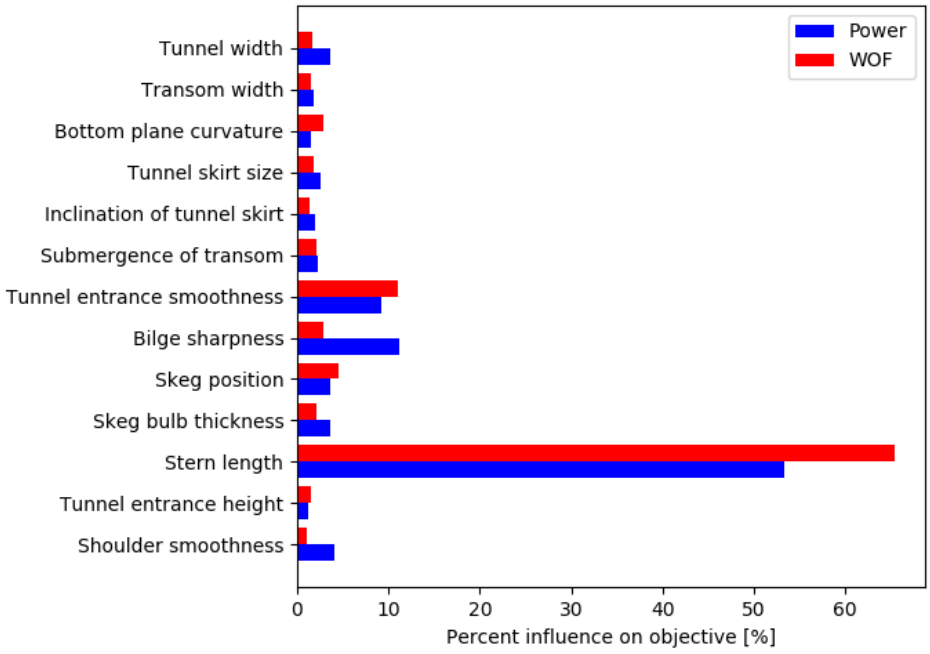

Figure 8.2: Influence of hull form aspects on the error between prediction models and power estimates or wake field quality obtained from CFD, in shallower water ($h/T = 1.5$). The horizontal axis represents the influence on the objectives in percent. Compared to $h/T = 3.0$ water (see Figure 8.1), the diagrams show that stern length and the athwartships propeller position, relatively have a larger influence on both objectives.

propulsion power is reduced and better propeller inflow is obtained. Finally, the bilge radius should be addressed: a small radius leads to higher resistance and therefore a larger propulsion power.

The next sections discuss design guidelines for the Class Va inland ship in two water depths. Design guidelines are given through the change of parameter settings for increasing displacement. Based on the sensitivity of propulsive performance to hull form parameters, these guidelines are given for the following parameters:

- Stern length
- Tunnel width
- Tunnel skirt size
- Transom submergence
- Tunnel entrance smoothness
- Bilge radius
- Curvature of the bottom plane

In chapter 7, twin-propeller ships have been discussed, in which the athwartships propeller position was found to be very important as well. Also the diameter of the propeller is important, but is not mentioned in Figures 8.1 and 8.2. This is because the propeller diameter is not being specifically varied through the choice of experimental design. However, propeller theory also shows (Van Lammeren *et al.* [88], Oosterveld [17]) that propeller diameter affects propulsive efficiency significantly, as is also observed in chapter 7. Propeller diameter is therefore assumed to still have a significant influence on propulsion power.

8.1.2. Overview of important parameters

Before discussing the optimized settings of hull form parameters for multiple displacement values, it is valuable to have a view on the impact that each of the parameters discussed has on the hull form. Figure 8.3 shows the hull form variations due to change of specific parameters. Stern length varies from 13.5 meters to 25.0 meters, measured from the transom to the point where $A_X/A_M = 0.995$. In the optimization procedures, each setting varies from 0.0 to 1.0. In the following Figures, the black frames correspond to 0.0, while red frames correspond to a setting of 1.0.

8.1.3. Design guidelines for h/T = 3.0

Figure 8.4 presents the parameter value trajectory for displacement ranging from 3810 to 3950 tonnes. Additionally, Figure 8.5 presents the corresponding body plans for six extracted points with the parameter settings obtained from Figure 8.4.

For deep water ($h/T = 3.0$), the height of the tunnel entrance decreased after optimization for deep water. This is not observed for the present test case of single propeller ships. This specific parameter is not included in Figure 8.4, because it

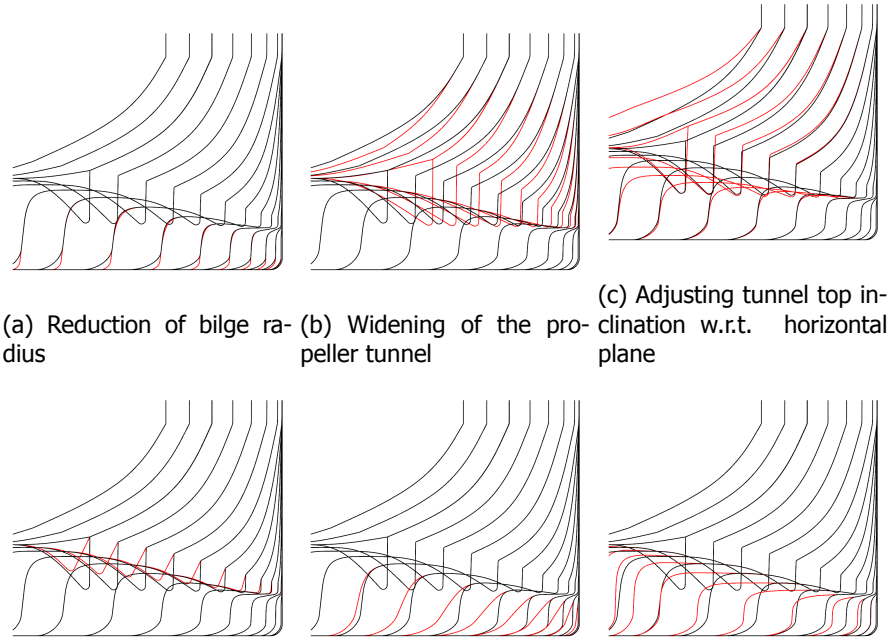

(a) Reduction of bilge radius

(b) Widening of the propeller tunnel

(c) Adjusting tunnel top inclination w.r.t. horizontal plane

(d) Reduction of tunnel skirt size

(e) Smoothening the tunnel entrance

(f) Adjustment of the bottom plane

Figure 8.3: Overview of hull form variations for the parameters used in the graphs in Figures 8.4 and 8.6.

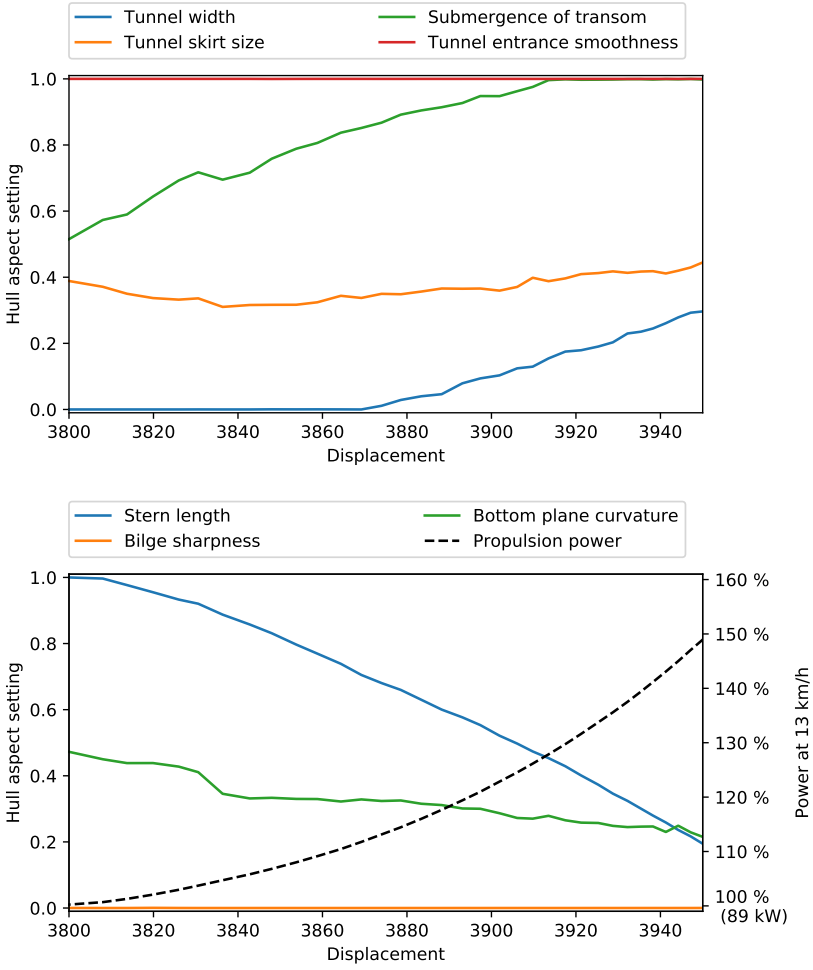

Figure 8.4: Change of hull form aspect settings depending on ship displacement, extracted from Pareto fronts created by multi-objective optimization for propulsion power and certain level of displacement, while the wake object function is constrained to a maximum value. The figures show that stern length is decreased to accommodate for more displacement. The bottom plane becomes a bit more v-shaped, and the submergence of the transom is increased as well. The smoothness of the tunnel entrance is maximized at any displacement, as is the bilge radius. Six combinations of parameter settings are extracted from these graphs to generate hull forms from, of which the body plans are presented in Figure 8.5.

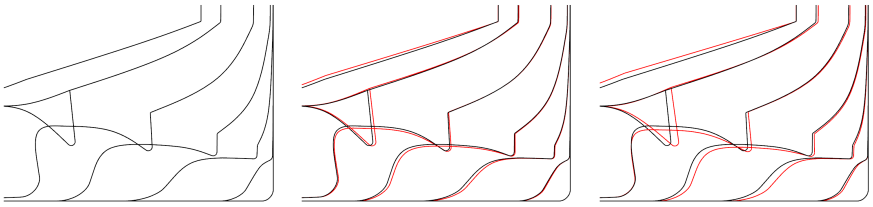

(a) $\nabla = 3810$ ton (b) $\nabla = 3838$ ton (c) $\nabla = 3866$ ton

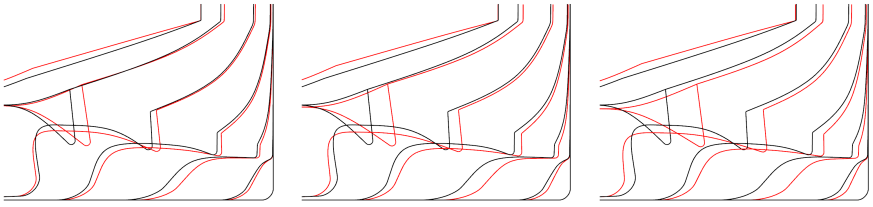

(d) $\nabla = 3894$ ton (e) $\nabla = 3922$ ton (f) $\nabla = 3950$ ton

Figure 8.5: Frames of the stern design (with tunnel) for single-propeller inland ships. The shapes are generated using the parametric model as discussed in chapter 3, with parameter settings taken from the Pareto front obtained after optimization for (maximal) displacement and (minimal) propulsion power at $h/T = 3.0$. From (a) to (f), the length of the stern decreases while the inclination of the tunnel top curve increases (and thereby lowers the tunnel top, while reducing transom draft). Furthermore, the tunnel width is increased since this parameter also affects ship displacement.

does not have a significant effect on either of the objectives, but the optimization process kept these parameters at minimal values indicating that the tunnel entrance height was kept at the maximum. Another observation for double propeller ships was that the tunnel was smoothened, by reducing the curvature of the tunnel top curve. This does not occur for the present single-propeller test case either.

Two important observations, similar to those that have been made for double-propeller ships, are that tunnel entrance smoothness is maximized for all displacement values, while bilge sharpness is minimized in all cases. In order to increase displacement, the stern region is made shorter. Also, bottom plane curvature is reduced, meaning that the bottom plane becomes v-shaped rather than s-shaped. Meanwhile, submergence of the transom is reduced. This does decrease displacement but also reduces resistance to compensate for increased resistance that follows from shortening the stern region. This indicates that if the stern region is short, the importance of the aft end of the ship increases. Designers should ensure to have the aft end of the ship rising up rather than remaining flat.

The tunnel width parameter increases with increasing displacement. The explanation is that for larger displacement, the stern region is made shorter. This also effects the orientation of the tunnel skirt with respect to the longitudinal axis: the inclination increases. Due to increased inclination, the amount of flow passing over the skirt and thereby generating vortices increases as well. These vortices contain energy and thus lead to increased resistance. To compensate for this, the tunnel width is increased.

8.1.4. Design guidelines for h/T = 1.5

Figure 8.6 shows the optimized parameter settings for varying displacement at $h/T = 1.5$. The parameter values chosen by the optimization algorithm are very similar to those for deeper water. The change of tunnel top curvature observed with twin-propeller ships when comparing optimized ships for $h/T = 1.5$ and $h/T = 3.0$ is not observed here. One important difference is that bottom plane curvature is further reduced in shallow water. Reducing this parameter results in additional displacement, which can now be used to maintain a larger stern length. This effect has also been observed for double propeller ships.

Another difference observed in chapter 7 for double-propeller ships is that stern length increases quicker in shallow water in order to maintain an as-large-as-possible propeller diameter. In the present test-case, no specific parameter to set propeller diameter was included. It may be expected though, given the commonly applicable trend that a larger diameter results in less power, this same effect applies to single-propeller ships as well. Namely, the size of the wake increases in shallow water (Rotteveel *et al.* [22]). The wake is larger, which favors the choice of a larger propeller diameter since this propeller can then take advantage of the reduced velocities in the wake (Dyne [89]), and thereby increase hull efficiency.

8.1.5. Observations

In the previous sections, the importance of hull form aspects for a Class Va single-propeller inland ship has been presented, as well as the trends of hull form pa-

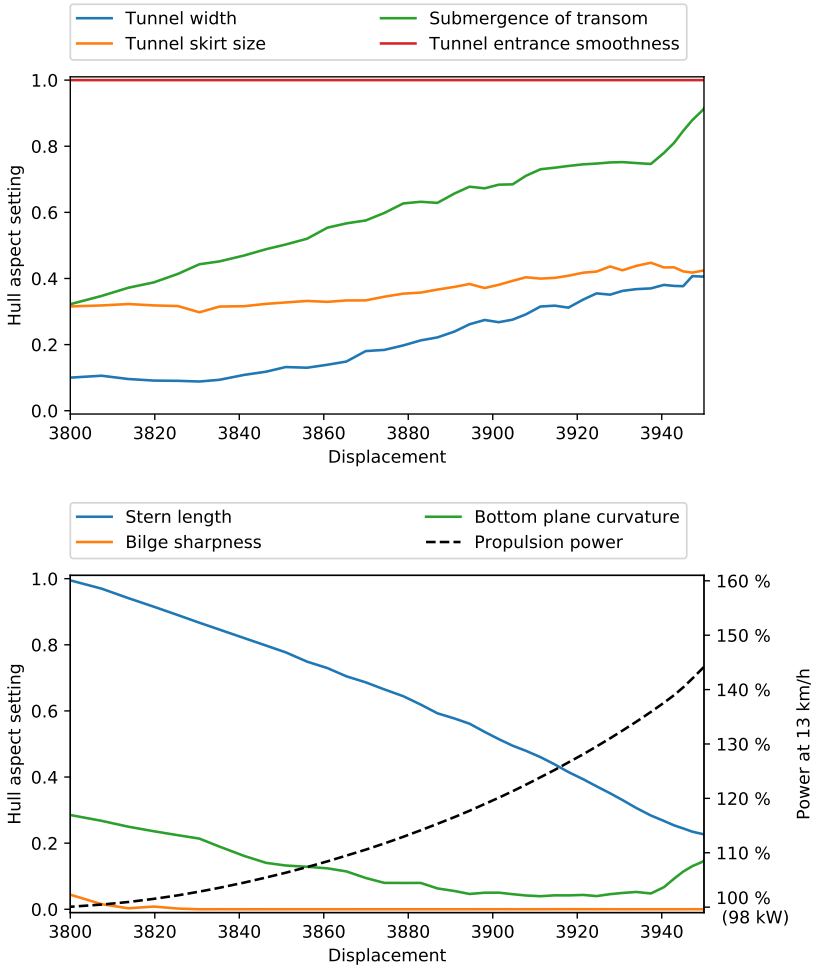

Figure 8.6: Change of hull form aspect settings depending on ship displacement, extracted from Pareto fronts created by multi-objective optimization for propulsion power and certain level of displacement, while the wake object function is constrained to a maximum value. The figures show that both stern length and the propeller diameter are decreased to accommodate for more displacement. The sharpness of the tunnel entrance is kept at a minimum. Furthermore, the bilge radius is decreased and the tunnel skirt is made larger.

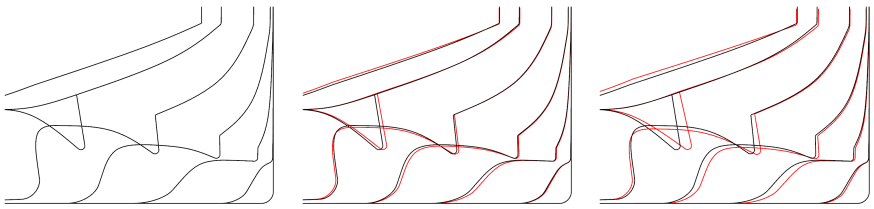

(a) $\nabla = 3810$ ton (b) $\nabla = 3838$ ton (c) $\nabla = 3866$ ton

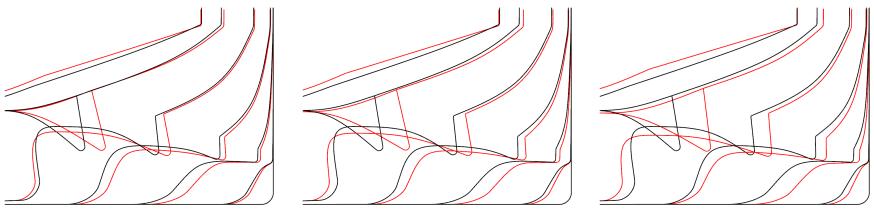

(d) $\nabla = 3894$ ton (e) $\nabla = 3922$ ton (f) $\nabla = 3950$ ton

Figure 8.7: Frames of the stern design (with tunnel) for single-propeller inland ships. The shapes are generated using the parametric model as discussed in chapter 3, with parameter settings taken from the Pareto front obtained after optimization for (maximal) displacement and (minimal) propulsion power at $h/T = 1.5$. From (a) to (f), the length of the stern decreases while the inclination of the tunnel top curve increases. Compared to $h/T = 3.0$, the bottom plane curvature is further reduced. This provides additional displacement such that a longer stern region can be maintained.

rameters depending on ship displacement at two different water depths. The most important observations are summarized in this section.

Similar to a case of twin-propeller inland ships, designers of a single-propeller inland ship should ensure that the tunnel entrance is smooth and thus has limited curvature. A sharp tunnel entrance (with a narrow bilge and vertical frames from the bottom plane up to the tunnel skirt) results in high resistance and a decrease of the quality of the propeller inflow. An explanation for this is presented in Figure 7.7. Optimization shows that before the tunnel skirt emerges from the hull, the bilge line should already bend inward to prevent a great portion of the flow having to change direction at a single time instant. Slightly smoothening this tunnel entrance helps already, at limited cost (of displacement).

Secondly, again similar to the double-propeller case, designers should attempt to enlarge the bilge radius. The optimization procedure favors maximized bilge radius, even for the maximum amount of displacement considered. The bilge radius should thus be maximized up to the limits of interior space and structural design.

Next, an important parameter to address is the length of the stern region. It is the most influential parameter for propulsive performance, both in shallow and deep water. It also significantly affects ship displacement. Using Figures 8.4 and 8.6, designers can investigate the impact of changing stern length on propulsion power.

Another important parameter is transom size. Reducing the size of the transom leads to reduced resistance, but a designer should be careful in shallow water: a smaller transom increases the inclination of the very aft end of the stern, which in shallow water can lead to separation due to the pressure gradients becoming too large. In deep water, however, an inclined aft end is clearly favored over one for which the hull above the propeller outflow is almost horizontal.

Finally, additional parameters that should be addressed are tunnel width and the shape of the bottom plane. In shallow water, this bottom plane should be entirely v-shaped. In deep water, a slightly s-shaped hull form is a good solution. However, the bottom plane should become more v-shaped for a shorter stern to prevent significant increase of resistance.

8.2. Pram-shaped sterns

As discussed in chapter 1, pram-shaped sterns are also included in this study. The hull form aspects investigated have been presented in chapter 3. The ships have been tested at three different water depths: $h = 10.50$, $h = 7.00$ and $h = 5.25$. Also, main dimensions have been varied to extend the results towards ships of classes other than those of class V of the CEMT-classification system.

The pram-shaped stern includes a non-continuous parameter that determines whether there is a skeg added to the design or not. The thickness or width of the skeg is controlled by the *Skeg width* parameter, while the sides can be inclined as well.

In this section, the focus is on the class Va ships, with main dimensions length, width and draft being 110.0, 11.40 and 3.50. This is similar to the previous discussions about double-propeller and single-propeller ships which also focused on

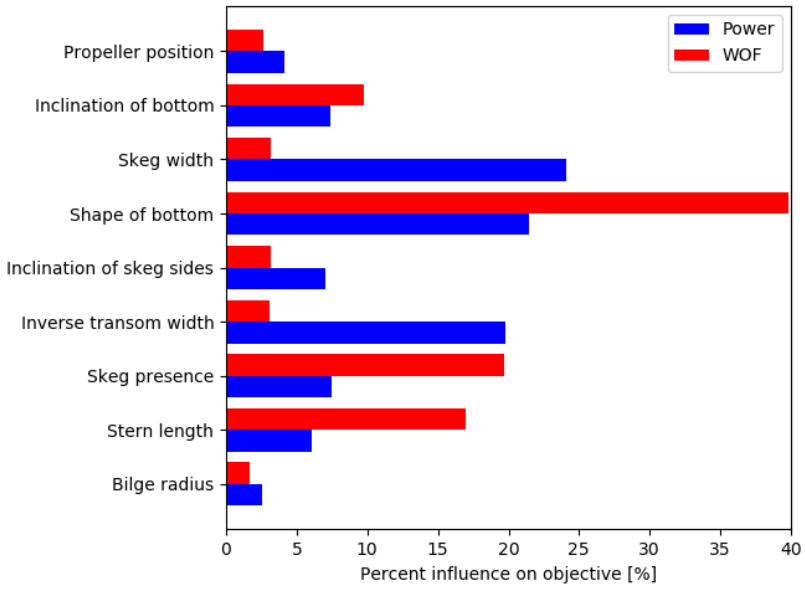

Figure 8.8: Influence of hull form aspects of a pram-shaped stern on the predictions of propulsion power and the wake object function (that is used as a measure for propeller inflow quality) at $h/T = 3.0$.

ships with main dimensions corresponding to class Va ships. Firstly, the influence of different parameters on propulsive performance is presented. These influences have been determined using the feature masking methods described in chapter 6. Next, design guidelines are presented for water depths corresponding to $h/T = 3.0$ and $h/T = 1.5$.

8.2.1. Hull form aspect sensitivity

Figure 8.8 presents the influence of hull form aspects on propulsion power and wake field quality (WOF) for a class Va inland ship with a pram-shaped stern, at a water depth of $h = 10.5$ meters ($h/T = 3.0$). The graph shows that for propulsion power, the bottom shape (determined by its curvature and inclination) as well as the transom width affect propulsion power significantly. Additionally, propeller position (which is the athwart ships propeller position) affects power as well.

Stern length affects propulsion power significantly as well. However, it is not the most influential parameter as it is for ships with a tunnel stern (see section 8.1). This is due to the smaller amount of curvature present for a pram-shaped stern: there is no tunnel entrance (which affected performance significantly for tunnel stern ships), no sharp bilge along which the flow has to pass and no tunnel skirts. The resistance produced by these elements depends on their orientation and the sharpness of their curvature (which is affected by the length of the stern region). As these features are absent for a pram-shaped stern, the influence of stern length

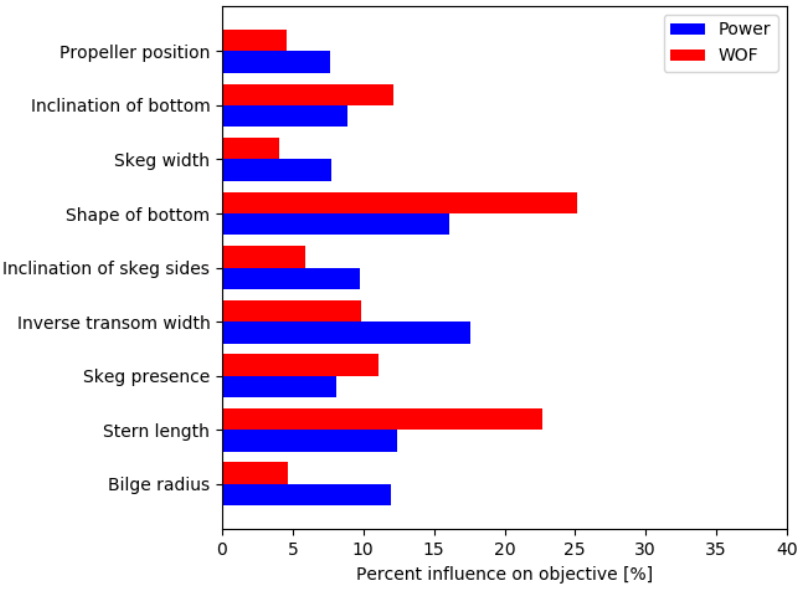

Figure 8.9: Influence of hull form aspects of a pram-shaped stern on the predictions of propulsion power and the wake object function (that is used as a measure for propeller inflow quality), at $h/T = 1.5$. In comparison with the influence analysis performed for $h/T = 3.0$, the influences of skeg presence and bottom shape have been reduced. Stern length remains equally important, while the influence of other details has increased.

is smaller.

For the determination of wake field quality, stern length is more important. Namely, although less curvature is present, stern length affects the growth of the boundary layer and the wake around the stern. It influences the rise of the bottom plane and the curvature at the point where the midship section ends and the stern region starts, two features that have an important effect on boundary layer growth. A thicker boundary layer leads to a less uniform flow at the propeller, hence the influence of stern length on wake field quality.

Apart from stern length, the shape of the bottom and the presence of the skeg have a significant influence on wake field quality. The former is explained by its effect on the growth of the boundary layer in the flow coming from the midship region and moving towards the transom. Namely, an S-shaped bottom comprises more curvature than a single-curved bottom plane, leading to stronger growth of the boundary layer. As for the presence of the skeg, the bilges of the skeg produce vortices that can pass through the propeller disk, lowering the quality of the wake field. Moreover, the presence of the skeg physically pushes the wake at the ship center plane outward, towards the propeller disk, in which the velocity gradients will then increase.

In shallow water, the importance of the shape of the bottom plane for propul-

sion power increases, as does the influence of the inclination of the bottom plane. Furthermore, the width of the transom becomes the most important parameter for propulsion performance. Also, similarly to cases for tunnel sterns, the stern length becomes more important in shallow water, although other parameters remain significantly more important for pram-shaped ships. For wake field quality, the same three parameters as for deep water remain important in shallow water, although the presence of the skeg becomes more important than the shape of the bottom.

For a Pram-shaped stern, Figures 8.8 and 8.9 show that propulsion power depends on almost all hull form aspects. At a water depth corresponding to $h/T = 3.0$, three parameters are responsible for most of the variations in propulsion power: the size of the skeg, the transom size and the shape of the bottom plane (which is either s-shaped or single curved). In shallower water, at $h/T = 1.5$, the influence on propulsion power is more spread across the hull form aspects. For the quality of the propeller inflow, three parameters account for most of the variance.

Since power is affected by all parameters involved, there is no additional choice made as is done for the single-propeller ships, in order to leave out parameters from the parameter trajectory graphs. In the following section, however, the effects that all parameters have on the hull form are presented again.

8.2.2. Overview of important parameters

Similar to section 8.1, the hull form aspects are presented again. Stern length varies from 12.5 meters to 20.0 meters, measured from the transom to the point where $A_X/A_M = 0.995$. In the optimization procedures, each setting varies from 0.0 to 1.0. In Figures 8.10 and 8.11 , the black frames correspond to 0.0, while red frames corresponds to a setting of 1.0.

8.2.3. Design guidelines for h/T = 3.0

The former section presented which hull form aspects for a pram-shaped stern are of importance for the required amount of propulsion power or the quality of the propeller inflow. In this section, the optimal settings for these parameters are searched for using optimization. The optimization problem under consideration is the minimization of propulsion power while ship displacement is being maximized.

In Figure 8.12, parameter settings trajectories for a class Va ship with a pram-shaped are presented. Comparing these images to those made for a tunnel stern, the most significant difference is that the stern length parameter does not change as much as it did for tunnel stern ships. This corresponds to the parameter sensitivity presented in Figure 8.8, where stern length is not among the most influential parameters.

Instead, a significantly changing parameter is transom size. In order to accommodate sufficient displacement, the size of the transom is increased. Furthermore, the amount of v-shape in the bottom plane is maximized throughout the entire displacement range. The high value of the bottom shape (which is between s-curved and single curve) shows that a single-curved bottom plane is preferred over a double-curved bottom. This provides more displacement while the amount of curvature is smaller. The optimization algorithm does not remove the skeg, indicating

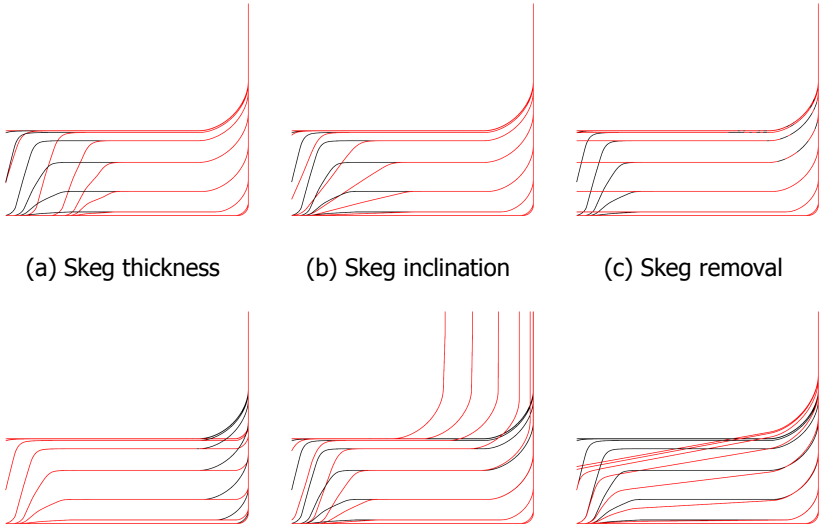

(a) Skeg thickness (b) Skeg inclination (c) Skeg removal

(d) Bilge radius at stern (e) Transom size (f) V-Shaped bottom

Figure 8.10: Overview of included hull form aspects for pram-shaped sterns. A value of 0.0 corresponds to the black lines, a value of 1.0 corresponds to the red lines.

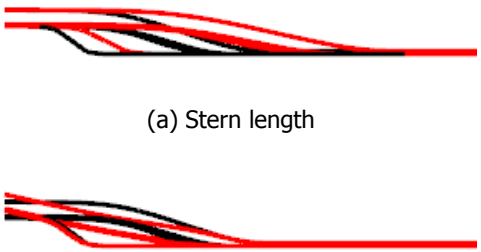

(a) Stern length

(b) Stern bottom curvature

Figure 8.11: Stern length and bottom shape for pram-shaped sterns. A value of 0.0 corresponds to the black lines, a value of 1.0 corresponds to the red lines.

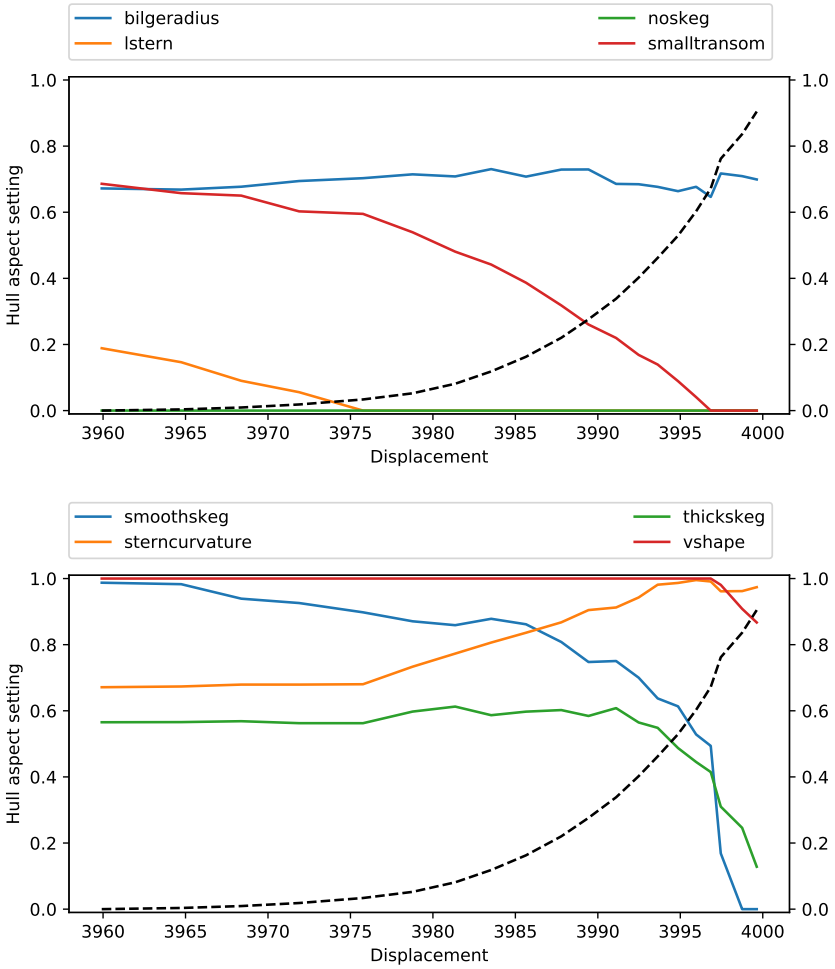

Figure 8.12: Change of hull form aspect settings depending on ship displacement, extracted from Pareto fronts created by multi-objective optimization for propulsion power and certain level of displacement, while the wake object function is constrained to a maximum value.

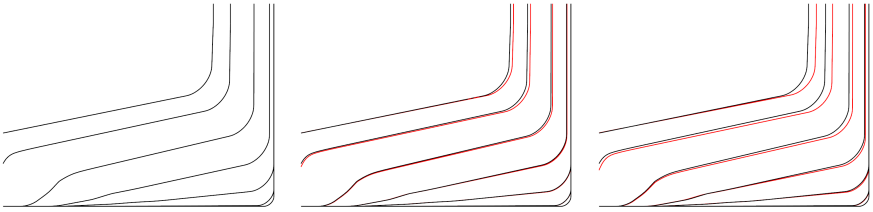

(a) $\nabla = 3960$ ton (b) $\nabla = 3968$ ton (c) $\nabla = 3976$ ton

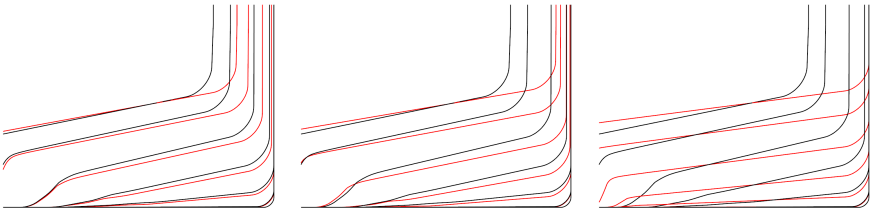

(d) $\nabla = 3984$ ton (e) $\nabla = 3992$ ton (f) $\nabla = 4000$ ton

Figure 8.13: Frames of pram-shape stern designs for varying displacement, each one being an optimal shape (at $h/T = 3.0$) for the mentioned amount of displacement. For increasing displacement, the amount of v-shape in the frames is slightly reduced. The main adjustment to the stern in order to accommodate more displacement is the increased width of the transom.

that the skeg is profitable for the displacement-to-power ratio.

Figure 8.12 also shows that for the design of the skeg, it should be relatively wide and its sides should be inclined. To finally maximize displacement, the algorithm removes the inclination of the sides and reduces the width of the skeg. This is due to the way the parameters affect the hull form: both skeg design parameters slightly affect the bottom plane frames, leading to increased displacement.

An important remark should be made regarding the range of displacement, which can be seen at the bottom of the graphs in Figure 8.12. The parametric model allows a variation of displacement by approximately 200 tons. However, the range of displacement in Figure 8.12 is only 40 tons wide. One main parameter responsible for the amount of displacement is stern length. Naturally, one would expect that increasing stern length (and thereby decreasing displacement) leads to a decrease of propulsion power since curvature is reduced and the stern has a smoother shape. However, a longer stern reduces the axial inclination of the bottom plane. Due to this, the axial component of the surface normals is reduced, and the resistance-compensating effect of the high-pressure region around aft ship is limited. Therefore, further lengthening the stern region will at a certain point lead to increased resistance rather than decreased resistance.

This explanation also applies to the choice between a single-curved bottom plane or a s-curved bottom plane: in the latter case, the bottom close to the ship's aft is flat. Due to this, the high pressure region does not produce a forward force on the hull to reduce resistance, similar to the effect of a stern region that is too long.

8.2.4. Design guidelines for h/T = 1.5

Figure 8.14 shows the change of parameter settings for shallow water, at $h/T = 1.5$, which corresponds to a water depth of $h = 5.25$ meter for a class Va ship. For most parameters, the trajectory is similar to what is observed for the deep water case. One specific difference, however, is the trajectory for the bilge radius. In shallow water, the bilge radius is made larger compared to deep water. Additionally, stern length is assigned larger values compared to the deep water case.

Another important difference is that the range of variation for ship displacement is significantly larger compared to $h/T = 3.0$. At $h/T = 1.5$, the stern length parameter is allowed to be increased further. Figure 8.15 shows this. At $h/T = 3.0$, the optimization algorithm does not manage to extend the displacement range, because there is no solution with lower displacement *and* lower propulsion power. At $h/T = 1.5$, this does not occur until displacement has become as low as around 3875 tons.

The extended displacement range can be explained as follows: the flow coming from the midship region enters the stern region and will experience an increase of the area that it can pass through. At $h/T = 1.5$, the relative increase of this area is (much) stronger due to the presence of the fairway bottom. This yields larger pressure gradients and a stronger low-pressure region at the start of the stern region, which is visualized in Figure 8.17. At ship will therefore profit from a smoother stern in shallow water.

The stern shape frames in Figure 8.16 show that in general, the ship with max-

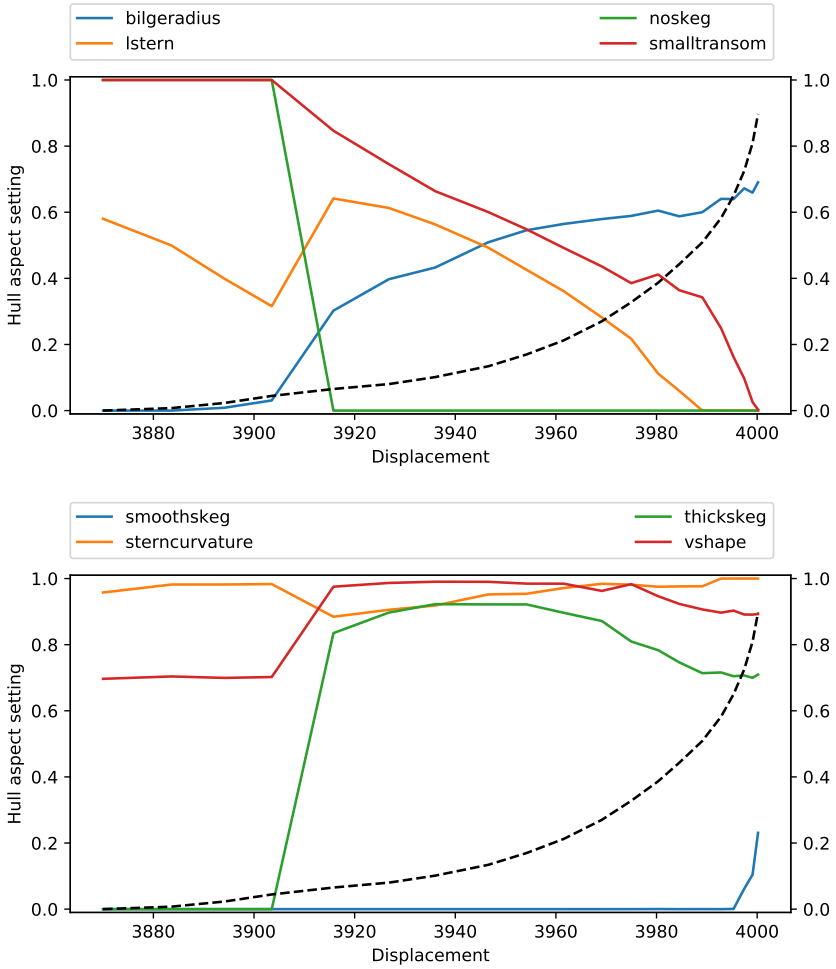

Figure 8.14: Change of hull form aspect settings depending on ship displacement, extracted from Pareto fronts created by multi-objective optimization for propulsion power and certain level of displacement, while the wake object function is constrained to a maximum value.

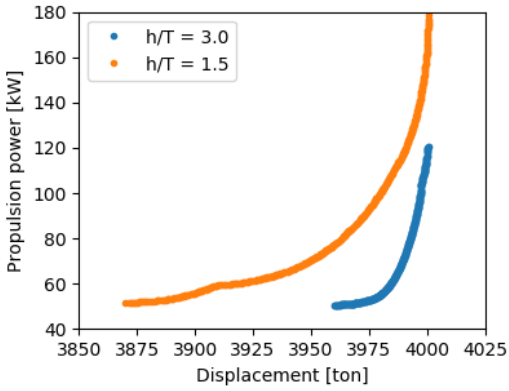

Figure 8.15: Pareto fronts for pram-shaped sterns at $h/T = 3.0$ and $h/T = 1.5$, showing that the displacement range at $h/T = 1.5$ is smaller.

imum displacement is approximately same as for deep water, presented in Figure 8.13. One difference that can be observed is that the bilge radius is larger in shallow water. The amount of transversal inclination in the bottom is the same as for the deep-water case.

8.2.5. Observations

The previous sections discussed the sensitivity of hull form parameters as well as optimal settings for these parameters for a class Va inland ship with a pram-shaped stern. In this section, the most important observations are summarized.

Propulsion power at $h/T = 3.0$ is to a large extent dependent on the shape of the bottom plane, the transom size and the design of the skeg. In shallower water, the curvature of the bottom becomes less important while the influence of using v-shaped frames increases. Furthermore, stern length is less important to the estimate of propulsion power compared to ships with a tunnel stern.

The quality of the wake field, on the other hand, does significantly depend on stern length, both in deep and in shallow water. Furthermore, the quality of the wake field also depends on the shape of the bottom and the presence of the skeg.

From the optimization procedures, it showed that the curvature of the bottom plane should be minimized, since an s-shaped bottom would reduce displacement while also leading to increased resistance and increased propulsion power. Furthermore, a v-shaped bottom plane (when viewing transverse frames) is preferable: the optimization algorithm applied the maximum amount of v-shape allowed in the parametric model. The skeg is also added to the ship, independent of displacement. The optimization algorithm applies a relatively wide skeg of which the sides are inclined.

With regard to the stern length, the observed parameter trajectory is different

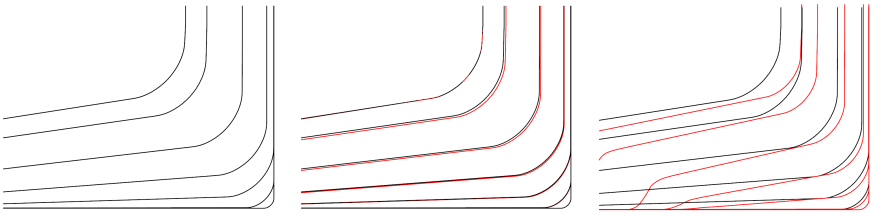

(a) $\nabla = 3870$ ton (b) $\nabla = 3896$ ton (c) $\nabla = 3922$ ton

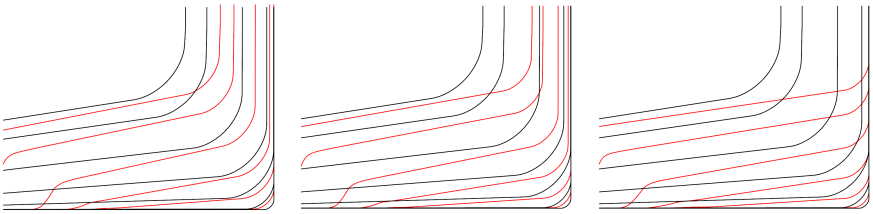

(d) $\nabla = 3948$ ton (e) $\nabla = 3974$ ton (f) $\nabla = 4000$ ton

Figure 8.16: Frames of pram-shape stern designs for varying displacement, each one being an optimal shape (at $h/T = 1.5$) for the mentioned amount of displacement. For increasing displacement, the v-shaped bottom is maintained. Main adjustments to the stern in order to accommodate more displacement are the shortening of the stern and widening the transom.

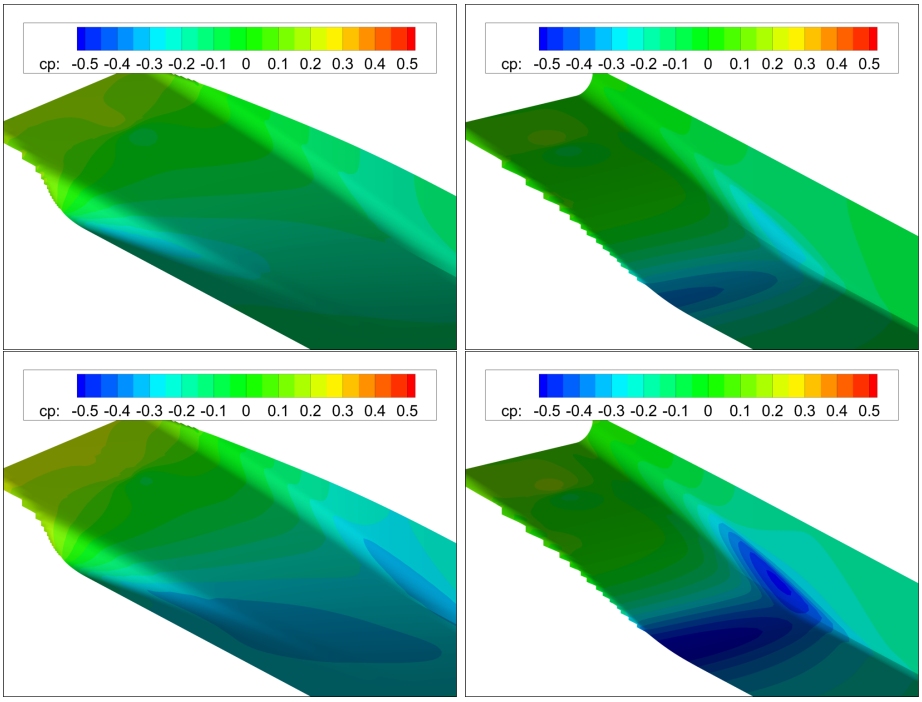

Figure 8.17: The pressure distribution around a pram-shaped stern. The top Figures correspond to $h/T = 3.0$, while the bottom Figures correspond to $h/T = 1.5$. On the left side, a long stern is used, while the right shows a short stern. The Figures show the low pressure region at the point where the midship region ends and the stern starts. Especially in shallow water, the impact of such curvature can be significant.

from that observed in ships with a tunnel stern. Whereas for a ship with a tunnel stern, propulsion power decreases with a longer stern region, this decrement is limited for pram-shaped sterns. This is explained by the reduced axial inclination of the bottom at the ship aft, which limits the resistance-reducing effect that the of the high pressure region around the stern has on the ship.

In shallow water, the stern may be made longer before resistance increases due to reduced inclination. In shallow water, the flow and pressures are affected by the increase of area that the flow passes through when entering the stern region from the midship region. At the beginning of stern region, the increase of area for the flow to pass through leads to a suction effect on the stern bottom, increasing resistance. This effect is larger in shallow water, but is reduced by a longer stern region to limit the increase of area. Therefore, the increase of resistance due to limited curvature is compensated and a longer stern can be used if displacement is not needed.

8.3. Conclusions

This chapter discussed design guidelines for single-propeller tunnel stern ships and pram-shaped stern ships. The guidelines were derived using an optimization procedure that involved two objectives: displacement and propulsion power. The resulting Pareto fronts were used to identify the changes needed to obtain a hull form with increased displacement that is still optimal in terms of propulsion power.

For single-propeller ships with a tunnel stern, one hull form aspect that designers should always pay attention to is the entrance of the tunnel. Similar to what has been observed for twin-propeller ships in chapter 7, this entrance should be smooth to achieve low resistance and to not disturb the flow towards the propellers. In order to increase displacement, the length of the stern can be reduced. Alternatively, the tunnel top curve can be lowered. This adds displacement in the stern region upstream of the propeller. However, to maintain a sufficient propeller diameter, displacement downstream of the propeller is reduced. This reduces the size of the transom as well. This option is especially favorable at deep water ($h/T >= 3.0$). In shallower water, the inclination of the tunnel top curve leads to increased pressure gradients. In shallow water, tunnel top curve inclination is restricted and the stern should be further shortened to add displacement.

Pram-shaped sterns should preferably include v-shape. This increases displacement but also reduces resistance due to a smaller portion of the flow having to bend upward after leaving the midship region. Another means to increase displacement is to increase transom width. The length of the stern region should not become too large for pram-shaped vessels, because a long stern reduces the positive impact of the high pressure occurring around the stern. Finally, the shape of the bottom plane can be single-curved for ships only sailing in relatively deep water. If keel clearance reduces to below 2.0 meters, the bottom plane can be made slightly s-shaped.

9

Conclusions and recommendations

The aim of this thesis was to gain insights in the effects of inland ship stern shape aspects on propulsive performance. Also, it was to investigate how they should be designed in order to achieve good propulsion performance. Propulsive performance was defined by two objectives: the required amount of propulsion power and the quality of the wake field. Additionally, the study did not focus on finding a single optimal design, but instead aimed to find a series of optimal designs, each with a different amount of displacement but optimal propulsion performance. Furthermore, the impact of shallow water on an optimal stern shape was investigated.

In this chapter, the main conclusions are presented first. They describe the findings regarding the effects of hull form aspects on inland ship propulsive performance. Also, the results from the optimization procedures applied are briefly discussed. Finally, recommendations with regard to further research are given.

9.1. Conclusions

In this section, this thesis' conclusions are presented. Part of the conclusions focus on findings during the process of obtaining relations between hull form parameters and propulsion performance. The other conclusions originate from observations made in chapters 7 and 8. First, conclusions regarding the process are discussed. Next, the most important hull form aspects for the included ship types (single- and double-propeller tunnel stern and a double-propeller pram-shaped stern) are discussed. Then, the observations made from the optimization procedures in chapters 7 and 8 are presented, showing which hull form aspects should, independent of displacement, be designed in the same way as well as presenting which hull form aspects should be adjusted if displacement must be made larger or smaller. Finally, the impact of shallow water on the results of the optimization procedures is discussed as well.

9.1.1. Conclusions from the process

In chapter 3, a parametric model has been developed that represents realistic stern shapes of inland ships. Multiple methods exist for parameterization of the hull form. However, it is found that distance based deformation methods have the drawback of smoothing sharp corners, which is unacceptable if the parametric model is to represent realistic inland ship sterns that do, in fact, feature certain sharp corners (as was presented in chapter 3). Therefore, a parametric model was use that performs the deformations in a series of polyline frames, before generating the smooth geometry from a coarse polygonal shape.

Chapter 5 discussed the method of estimating an effective wake fraction from the CFD calculations. From the perspective of computational efficiency, performing detailed propeller analyses for each hull considered was not feasible. Additionally, using propeller analyses requires a specific propeller geometry, thereby incorporating the efficiency of that specific propeller in the trends. Therefore, the propeller effect is modeled by a force distribution on the flow (a non-uniform actuator disk). Discretization of the propeller disk and solving two Bernoulli equations for each piece of the disk enable to subtract the propeller suction from the velocities in the propeller disk, thereby allowing to compute the effective wake fraction. Comparison with multiple detailed propeller calculations showed that this efficient method provides accurate estimates of the effective wake fraction. The proposed method can be used in optimization studies where the focus is the hull form and propeller-hull interaction, but the propeller geometry is not yet known.

The surrogate models used to perform optimization on have been discussed in chapter 6. It is concluded there that a Kriging response surface provides the most accurate estimates for a combination of hull form parameters that has not been analyzed yet. Additionally, the choice of parameters for generating the hull forms was discussed in chapter 3. The Latin Hypercube Sampling method was chosen for its design-space-filling capability while being efficient in terms of computational time. In chapter 6, it was shown that using the LHS design of experiments leads to reliable prediction models. For example, accurate estimates are obtained for a model including 18 hull shape parameters, while the model was generated from

just 300 calculations.

Finally, genetic algorithms have been applied to perform feature masking and outlier analysis. Feature masking has been performed to determine the influence of each parameter on the outcome. The algorithm would iteratively add or remove parameters from the model and test its predictive performance. The multi-objective NSGA-II algorithm allows to use predictive performance and number of features as (conflicting) objectives. For outlier analysis, point masking was applied in the same manner. Application of the NSGA-II method showed to be effective in selecting the most important parameters and to remove erroneous data points.

9.1.2. The most important hull form aspects

Figures 7.6 and 8.1 show the influence of hull form aspects for tunnel stern ships. They show that for propulsion power, stern length is the most important aspect. For double-propeller ships, this is followed by the athwartships propeller position, the curvature of the tunnel top (see Figure 9.1), the smoothness of the tunnel entrance and the propeller diameter. For single-propeller ships, propulsion power is affected by the width of the tunnel, the size of the tunnel skirt and smoothness of the tunnel entrance.

For both single-propeller and double-propeller ships with a tunnel stern, the smoothness of the tunnel entrance plays an important role in the estimated propulsion power. It is therefore important that designers pay attention to this aspect, since it does not affect displacement significantly, but designing it in an adequate way does reduce the amount of required propulsion power. In Figure 7.7, the effect of this parameter was explained. Preferably, designers should ensure that the bilge curves inward *before* the tunnel skirt starts. In this way, the amount of water that has to change direction into the tunnel is reduced. An example is given in Figure 9.2. If the bilge curves inward before the tunnel skirts starts, a resistance reduction of approximately five percent can be achieved compared to a vertical tunnel entrance (left image in Figure 9.2).

For pram-shaped ships, stern length is not the most important parameter. Instead, the shape of the bottom (which is either s-shaped or single-curved) has the largest influence. Furthermore, the width of the skeg and the width of the transom

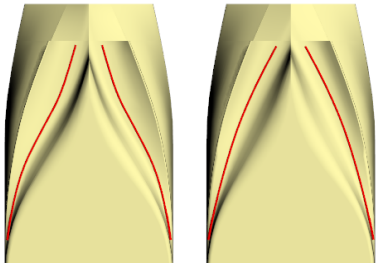

Figure 9.1: Tunnel top curve (indicated by the red line) can be s-curved or single-curved

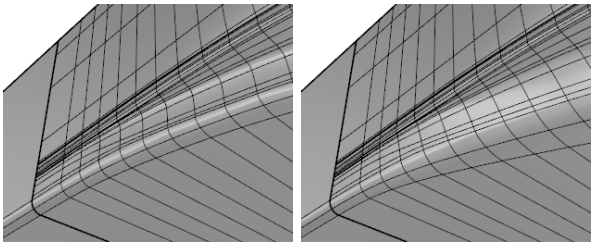

Figure 9.2: Example of the preferred design of the tunnel entrance. On the left, a tunnel entrance in which the water has to curve inward along the whole height of the tunnel. This causes additional resistance and a thicker, non uniform wake field. On the right, a smoother tunnel entrance in which the bilge curve bends inwards earlier.

affect the power estimate significantly. The large influence of the bottom shape is due to the inclination of the bottom at the aft end of the ship. As discussed in chapter 8, the high-pressure region occurring around the stern of the ship can produce a forward force (thus reducing resistance) on the ship if the orientation of the local hull surface is such that its normals point (partially) in longitudinal direction. For an s-shape bottom, however, the normals at the aft end of the ship point downward or athwartships. Therefore, an s-shape stern has higher resistance. A single-curved pram-shape is therefore preferred.

9.1.3. The design of a well-performing ship for multiple displacements

In chapter 7, the approach to obtain design guidelines was discussed. Optimization has been used, with two objectives: displacement and propulsion power. The quality of the wake field was added as a constraint. By optimizing for both power and displacement, the resulting Pareto front consists of ship designs with varying displacement, while each ship has optimal propulsive performance for the corresponding amount of displacement (Figures 7.10, 7.12). The hull form parameter values corresponding to each point on the Pareto front were plotted against displacement. This showed which hull form aspects should be changed if displacement is increased (or decreased).

Figure 9.3 shows three of the six frames plans that were presented in Figure 7.11. They represent body plans of double propeller tunnel stern designs optimized for water with a depth of $h/T = 3.0$, with displacement ranging from 3770 tons to 3945 tons. The body plans show that the tunnel entrance is made smooth (that is, the bilge curve starts curving inward before the tunnel skirt emerges, see Figure 9.2) as well as that the starting point of the tunnel skirt is lowered. Figure 7.10 presented the change of hull form parameters with changing displacement, and showed that stern length, propeller diameter and the athwartships propeller position changed the most if a ship is optimized for a different amount of displacement.

Different results were obtained when the optimization process was conducted in shallower water ($h/T = 1.5$). The tunnel entrance is still kept smooth, however the

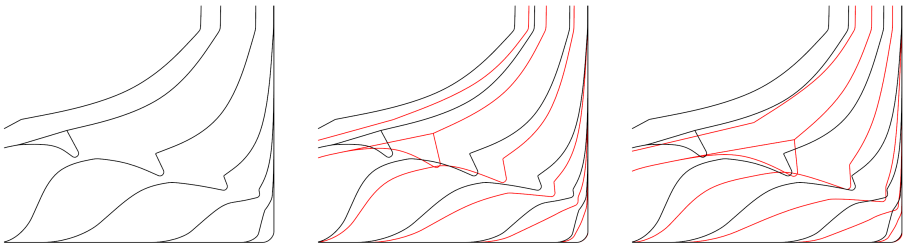

(a) $\nabla = 3770.0$ tons (b) $\nabla = 3860.0$ tons (c) $\nabla = 3950.0$ tons

Figure 9.3: A series of body plans for twin-propeller ships optimized for varying displacement, at $h/T = 3.0$. At the bottom right of each sketch, it shown that the starting point of the tunnel skirt is being lowered. Furthermore, the (the space available for) propeller diameter is being reduced and the propeller is moved further athwartships.

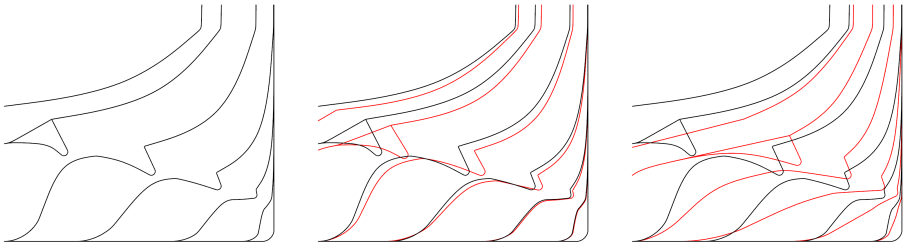

(a) $\nabla = 3770.0$ tons (b) $\nabla = 3870.0$ tons (c) $\nabla = 3970.0$ tons

Figure 9.4: A series of body plans for twin-propeller ships optimized for varying displacement, at $h/T = 1.5$. Whereas at $h/T = 3.0$, the starting point of the tunnel skirt (bottom right in each sketch) was lowered, thi does not occur to the same extent for $h/T = 1.5$. Additionally, the tunnel is more pronounced.

height of the tunnel entrance was increased. Additionally, the curvature of the tunnel top curve was adjusted. At $h/T = 1.5$, the tunnel top curve became s-shaped, providing a better axially aligned flow at the propeller plane. Also, the athwartships propeller position is reduced, while the propeller diameter is increased compared to the case where $h/T = 3.0$. The adjustments to the tunnel top curve, the propeller diameter and the propeller athwartships position all decrease displacement, which was compensated for by a shorter stern. Thus, at $h/T = 1.5$, for a displacement equal to that on $h/T = 3.0$, the optimization procedure favored a shorter stern in order to increase propeller diameter, reduce the athwartships propeller position and adjust the tunnel top curve to obtain horizontally aligned propeller inflow.

For a single-propeller tunnel stern, a different data set has been used with different parameters. This dataset did not include the athwartships propeller position

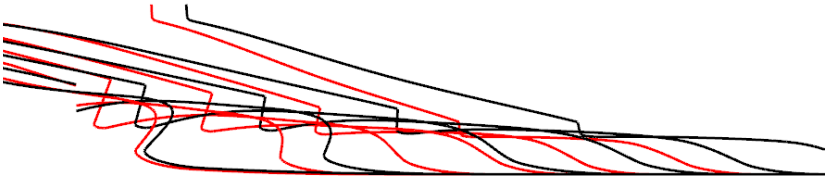

Figure 9.5: Buttocks for a single-propeller inland ship, optimized for minimum propulsion power at $h/T = 3.0$, with a displacement of 3894 ton (black lines are the parent hull with 3810 ton, the red lines are the vessel with increased displacement). Changes applied to increase displacement include increasing the length of the stern region and increasing the inclination of the tunnel top curve. The latter is indicated in the figure by the tunnel being lowered upstream (right) of the propeller position, while the inclination of the aft end is increased. In shallower water ($h/T = 1.5$), the optimization procedure favored a less inclined tunnel top curve.

and there was no parameter directly affecting the propeller diameter. Similarly with double-propeller ships, the stern length was the parameter that was adjusted primarily in order to increase displacement. Additionally, the inclination of the tunnel top curve was adjusted as shown in Figure 9.5. This reduced the submergence of the transom, but also lowered the tunnel top ahead of the propellers. Furthermore, the tunnel was made wider in order to accommodate more displacement (since the tunnel width parameter also drags the hull around the tunnel skirt outward).

For a single-propeller ship in shallower water, the length of the stern is adjusted in a similar way as it is at $h/T = 3.0$. However, the tunnel top curvature is optimized differently. Similar to the double-propeller ship, the optimization procedure at $h/T = 1.5$ preferred a more axially aligned inflow. This was obtained by decreasing the inclination of the tunnel top curve (see Figure 9.5) as presented in Figure 8.6.

Pram shapes should not have a double-curved bottom at the stern. Both in shallow and deep water, the optimization algorithm preferred a single-bent bottom plane. Additionally, the frames should be v-shaped to minimize propulsion power. Furthermore, the stern region of a pram-shaped stern should be short rather than long (within limits). Shortening the stern increases the longitudinal component of the normal vectors on the stern bottom, thereby increasing the forward force excited by the high-pressure region around the stern. In shallower water ($h/T = 1.5$), the length of the stern for a pram-shaped stern type was increased. The optimization algorithm compensated the loss displacement due to a longer stern by increasing the width of the transom. Skeg inclination is reduced in shallow water.

9.2. Recommendations

This research has shown that in shallow water, the result of a ship hull optimization process changes. Furthermore, it showed that several hull form aspects are more important to propulsion performance than others. However, the research did have its limitations. For example, wave formation was not included in the calculations. Also, the design of the bow was omitted during this research in favor of the stern, because the stern design is more complex (as discussed in chapter 1). This section

discusses multiple recommendations for further research, as well as why they are important. The section is divided in multiple subsections. First, recommendations with regard to design aspects are discussed. After that, possible changes to the set-up of the computations are discussed. Finally, several operational aspects are discussed as well.

9.2.1. Design aspects

The shape of the bow has not been included in this research, since the effects of the bow shape on ship performance are less complex than that for the stern (which involves significant interaction between the propeller and the hull). Therefore, ways to obtain a well-performing bow shape are better understood. Additionally, the bow can be optimized with tools that are less complex, cheaper, and less time-consuming compared to viscous CFD calculations required to investigate the flow around the stern. However, the bow shape may affect the trim and sinkage of the ship, both of which affect the flow around the stern. Additionally, the majority of wave resistance is due to the bow shape. Therefore, an accurate choice in regard to displacement, cargo capacity and propulsion power should also include the bow. An investigation of systematically varied bow shapes has been performed by Habben Jansen [90] and it was shown that a full bow with smooth shoulders provides decent performance (i.e. low resistance). An investigation that combines the most important aspects of this thesis and that by Habben Jansen [90] could should show how the combination of bow and stern should be designed, depending on required displacement. This combination does not just focus on finding lowest resistance, also the position of the center of buoyancy is important, since that should preferably match that of the center of gravity. Hence, it is not possible to pick the bow with lowest resistance and the stern with the best flow characteristics.

A design aspect that has not been specifically included in this thesis is the integrated tunnel. All tunnel sterns investigated in this thesis have a tunnel skirt that clearly emerges out of the hull. As it is shown that the tunnel skirt leads to higher resistance (van der Meij and Raven [19]), an investigation similar to that done for this thesis, but for integrated tunnel, may lead to ships with lower resistance. One aspect that should be accounted for, however, is that the integrated tunnel should encapsulate the propeller enough in order to prevent ventilation at limited draft. An example of an integrated tunnel is presented in Figure 9.6.

Furthermore, this thesis focused on hull form aspects. To do so, the choice was made to not include appendages such as a propeller duct or rudders. The former, however, does affect the flow around it. Therefore, local hull form variations affecting the hull close to the duct may have their impact being altered by the design of the duct. Furthermore, the performance of the duct (which accounts for up to 30 percent of the total thrust produced by the propeller and the duct together) is affected by the flow towards it. This flow is affected by the hull form. It is therefore suggested to investigate combined variations of hull form and propeller duct in order to optimize the ship. This, however, requires a more complex flow solver than the efficient one used in this thesis (PARNASSOS).

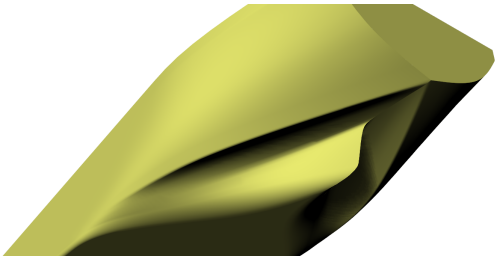

Figure 9.6: Example of a stern shape with an integrated tunnel

9.2.2. Computational aspects

In view of computational time and cost, the CFD calculations for this thesis did not include the formation of a wave pattern. This was assumed acceptable since inland ships navigate at low Froude numbers, and the major part of wave resistance is generated by the bow which is not varied in this investigation. However, there are multiple (small) impacts that the free surface can have on the ship. One is the interaction between the wave pattern formed by the bow and the shape of the stern. The aft shoulder, although not much pronounced in inland ships, produces a wave through, which may be in phase with a wave trough or a wave crest. This respectively leads to an increase or a decrease of resistance, depending on the position of the aft shoulder.

Another impact of waves occurs below the free surface. A wave trough leads to a pressure decrease up to a certain distance under water, while a wave crest leads to an increase of pressure. In case a wave crest occurs around the aft end of the skeg, the high pressure induced by the wave pattern increases the pressure gradients along the skeg. This increases the chance of flow separation. Due to this effect, the propulsive performance of the ship becomes more sensible to hull form variations, and trends may be affected for ships where separation almost occurs.

An investigation including free surface effects is therefore interesting, but comes with a high cost. Namely, multiple ship speeds have to be included as well. A suggestion is to apply a multi-fidelity method, combining data from (relatively) cheap and fast double-body calculations with data from free-surface calculations. However, the variations applied in free-surface calculations should be chosen carefully to ensure that ship designs for which wave formation clearly affects their performance, are included.

9.2.3. Operational aspects

The operation variation may be extended by including even shallower water. Chapter 8 showed that in shallow water, the difference by which a pram-shaped stern outperforms (for propulsion power per cubic meter of displacement) a tunnel stern decreases. The present thesis focused on h/T values of 1.5 and higher, but significant difference occur in the flow around the stern (and also at the bow) at a water depth corresponding to $h/T = 1.2$. This has been shown in (Rotteveel *et al.* [22]).

At such water depths, the ship design should be adapted for flow approaching the propellers from aside the ship, while the amount of flow coming from underneath the ship is very limited. A study into very low h/T values should investigate how often very low h/T values occur, but also whether a ship optimized for a higher h/T value remains operable. Namely, optimization for very low h/T could be required if heavy vibration nuisance or maneuvering problems occur otherwise, even though such low h/T values rarely occur.

Another operational aspect is limited draft. Inland ships operate at limited draft in case they are unloaded or if water depth is very low, such that larger draft is simply impossible. At limited draft, the propeller is close to the water surface or can even emerge above it. The tunnel skirts prevent propeller ventilation in such a case. In the present study, however, the tunnel skirts where included in every tunnel stern considered, and the optimization algorithm could not remove it to reduce resistance. The flow solver is not able to model a propeller (partially) emerging from the water surface. A solver that can include this is more complex and expensive, but an optimization study including limited draft could lead to a tunnel skirt that does not produce unnecessarily high resistance, while still preventing propeller ventilation at limited draft.

Acknowledgements

It took some time, more time than I initially hoped for. But it is done! I completed my thesis. It was quite the process. When I started as a PhD Candidate at Delft University, the research description was not much more than: "Something with inland ship resistance and propulsion". In hindsight, it offered great freedom on how to approach the subject. Sometimes, maybe, a bit too much freedom. I've spent quite some time deleting computational results, throwing away parts of my thesis or looking into options that I have long forgotten by now. Fortunately, my research was part of a joint industry project that involved several companies involved in inland ship design. That had me first investigating their wishes and needs, followed by regular meetings where the research' direction was kept in line. Not only did the companies give focus to the work; they also gave a great connection to reality, away from the desk and computer. This combination of amazing freedom and industry partners hoping the work fullfills their wishes made my PhD a very learnful journey with a result that I'm surely proud of.

But I wouldn't have completed (and even started) this thesis if it wasn't for my supervisor Robert. Robert, thank you for setting up the Top Ships project and asking me to do the research. Thank you for your practical view on matters during my PhD: I tended to delve deeper and deeper in small, sometimes minimal, parts of the work, even digging past the question to be answered. You managed to ask the right, practical, questions that helped me keep focus and put my effort to good use. Even after I left Delft, you motivated me to complete the work you can finally read now. Thanks for your support, advice and the discussions we had.

Significant support also came from Christian at MARIN. Christian, thank you for all the help with setting up computations. Thank you for helping to checking my calculations, results and methods used. Also, thank you for pointing me to the right person, or introducing me, when needed. It was nice having a second workplace at MARIN. It made it much easier asking the needed questions and having discussions.

The industry participants of the Top Ships project together formed a helpful, critical and nice group to have discussions and meetings with: Jan Jaap, Redmer, Jan and Guus from Conoship, Herbert and Egbert from SARC, René from Groenendijk & Soetermeer, Leo and Sjouke from Sip Marine, Chris and Bert from Concordia Shipping. Thank you for the critical remarks, for the practical insights and your advice on how to approach the topic and continue the research. The discussions we had taught me a lot about the (Dutch) inland shipping sector, although there is probably much more to learn.

Thanks to my doctoral committee to take the effort to read and review my thesis, to present at the defence and for the discussions we will have during the defence. Hans Hopman and Tom van Terwisga, my promotors, thank you for the discussions we had. Hans, your input from a different viewpoint was valuable to maintain the

link of my work to the field of (conceptual) ship design. Tom, thanks for your in-depth knowledge on ship propulsion; it helped to know which direction to look at moments I was stuck or searching for options. Also, thank you for involving me in the master course on resitance and propulsion; there is no way to better understand a topic than to explain it to others.

Thanks to all my colleagues at the M & TT department for making the time as a PhD Candidate at Delft University a good one. Maria, Teus, Jialun, Wenhua, Hamid and Javad, my office mates; thank you for the discussions and talks we had about varying topics. Your company was one of the great assets of working at the Delft University; to learn and talk about different cultures. Etienne and Austin, thanks for involving me in the Naval Ship Design course; it definitely taught me that hydromechanics are not the only complex thing about ship design. Gem, thanks for the talks about many things, both related to research and not related to work at all. Good luck finishing your research and thesis. Agnieta, Koen, Marc, Lindert and Lode; thanks for the coffee breaks, the beers at the faculty drinks or anywhere else. I hope we'll keep running into each other frequently.

The people at MARIN: Wytze, Chris, Henry, Joy, Pierre, Jesse, Maxime, Tomasz, Thomas: thanks for the discussions at the (accurately planned) hourly coffee breaks. Hoyte and Auke, thanks for your advice and helping with getting PARNASSOS to work and even applying adaptations to the software to aid my research.

Thanks to my friends back in Katwijk and around: it is great to have a place without even a remote relation to work, where you can really relax after a working week. Whether its putting up activities for the Scouts, playing Super Smash Bros at a Nintendo, skiing and snowboarding, or just having some drinks: it's all things I really value in my life.

My parents: thank you for all the support throughout the years of school, studying and working on my PhD. You made it all possible and kept on being interested, even when there was no progress at all and I was rather not asked about it. Mark, my brother, thank you for standing by my side at my defence as my paranymph. I feel honored with you standing there.

There's one person that should definitely be mentioned here: my partner in life and everything around it: Ariënne. Thank you for your amazing patience during the countless evenings I spent working on my PhD. Thank you for being honestly interested in my work and for trying (and managing) to understand the subjects. Thanks for your support during all of my PhD, especially when I had to complete it aside my work at MARIN. Thank you for everything. I love you.

There's probably more people I should have mentioned: if you belong to that group, please forgive me.

One thing remains: People often asked me if I would do it again or if they should start a PhD. Looking back, it was a great, learnful journey that just cost too much time. But I would surely recommend to do it. For those thinking about it, or those thinking about considering it, take this advice: Do not leave the university before setting a date for your defence!

Curriculum Vitæ

Erik Rotteveel was born in Leiden on December 30, 1989. Living in Rijnsburg, the Netherlands, Erik finished secondary school in 2008 at the Pieter Groen College in Katwijk. After this, Erik started his bachelor studies in Maritime Technology at the Delft University, which was completed in 2011 and followed by a Master studies in Maritime Technology, specializing in ship hydromechanics. The master studies was completed with a thesis on shallow water effects on ship manoeuvring forces. In this thesis, a potential flow method (DelKelv) was used to assess the effect of water depth on lateral hull forces and yawing moments.

After completing his master's thesis, Erik started his PhD at the Delft University of Technology. The contents of this research are described in the present work. During his time as a PhD Candidate, Erik also participated in teaching two master's courses. One was on the design of complex vessels, where students were to make a conceptual design of a naval vessel or submarine, thereby using a layout-tool consisting of a combination between Microsoft Excel and Rhinoceros 3D. The second focused on advanced topics in resistance and propulsion: cavitation, energy saving devices and optimization of ships using CFD.

In 2018, after four years of working on his PhD at the Delft University, Erik started working as a project manager in the ships department of MARIN. There, he uses CFD calculations, model tests, voyage simulations and other tools to improve the powering performance of cargo vessels, while mostly focusing on inland shipping.

List of Publications

Publications related to the research in this dissertation:

- E. Rotteveel, R. Hekkenberg, and J. Liu, Design guidelines and empirical evaluation tools for inland ships, EIWN 2014: European Inland Waterway Navigation Conference in Budapest (2014).
- E. Rotteveel and R. Hekkenberg, The influence of shallow water and hull form variations on inland ship resistance, 12th International Marine Design Conference, Tokyo (2015).
- E. Rotteveel, A. van der Ploeg, and R. Hekkenberg, Optimization of ships in shallow water with viscous flow computations and surrogate modeling, Practical design of ship and other floating structures (PRADS), Kopenhagen (2016).
- E. Rotteveel, R. Hekkenberg and A. van der Ploeg, Inland ship stern optimization in shallow water, Ocean Engineering, 141, pp. 555-569 (2017).

Publications where the author contributed:

- J. Liu, R. Hekkenberg, E. Rotteveel, A proposal for standard manoeuvres and parameters for the evaluation of inland ship manoeuvrability, EIWN 2014: European Inland Waterway Conference in Budapest (2014).
- J. Liu, R. Hekkenberg, E. Rotteveel and J.J. Hopman, Literature review on evaluation and prediction methods of inland vessel manoeuvrability, Ocean Engineering, vol. 106, pp. 458-471 (2015).
- J. Liu, R. Hekkenberg, E. Rotteveel and J.J. Hopman, Hydrodynamic characteristics of multiple-rudder configurations, Ships and Offshore Structures, vol. 12, 6th (2017).
- A.A. Kana, E. Rotteveel, Development and lessons learned of a block-based conceptual submarine design tool for graduate education, 13th International Marine Design Conference, Helsinki (2018).
- Q. Zeng, C. Thill, R. Hekkenberg and E. Rotteveel, A modification of the ITTC57 correlation line for shallow water, Journal of Marine Science and Technology, (2018).

References

[1] B. voorlichting Binnenvaart, *Waardevol Transport* (BvB, 2016).

[2] M. Beelen, *Structuring and modelling decision making in the inland navigation sector*, Ph.D. thesis, Universiteit Antwerpen (Belgium) (2011).

[3] H. Heuser and E. Müller, *Verdrangungsschiffe auf flachem Wasser,* Neue Ergebnisse hydrodynamischer Forschung und ihre Anwendung bein Entwurf, Schiffstechnik, B **33**, 3 (1986).

[4] J. Holtrop and G. Mennen, *A statistical power prediction method,* International Shipbuilding Progress **25** (1978).

[5] I. U. Hollenbach, C. Chryssostomidis, and K. Johansson, *Estimating Resistance and Propulsion for Single-Screw and Twin-Screw Ships in the Preliminary Design* (Massachusetts Institute of Technology, MIT Sea Grant College Program, 1999).

[6] H. Guldhammer and S. A. Harvald, *Ship resistance: Effect of form and principal dimensions* (Akademisk. Forlag, 1965).

[7] P.-J. Pompée, *About modelling inland vessels resistance and propulsion and interaction vessel-waterway key parameters driving restricted/shallow water effects,* in *Proceedings of SMART Rivers 2015* (2015).

[8] F. Vesting, R. Johansson, and R. E. Bensow, *Parameter influence analysis in propeller optimisation,* in *Third International Symposium on Marine Propulsors* (2013).

[9] L. Larsson and H. Raven, *The principles of naval architecture series: Ship resistance and flow,* Society of Naval Architects and Marine Engineers (SNAME) (2010).

[10] M. Hoekstra, *Numerical simulation of ship stern flows with a space-marching Navier-Stokes method* (TU Delft, Delft University of Technology, 1999).

[11] A. Van der Ploeg, L. Eça, and M. Hoekstra, *Combining accuracy and effciency with robustness in ship stern flow computation,* in *Twenty-Third Symposium on Naval Hydrodynamics* (2001).

[12] H. C. Raven, A. Van der Ploeg, and A. Starke, *Computation of free-surface viscous flows at model and full scale by a steady iterative approach,* .

[13] dr.ir J.U. Brolsma and ir. K. Roelse, *Richtlijnen Vaarwegen 2011*, Tech. Rep. (Rijkswaterstaat, 2011).

[14] R. G. Hekkenberg, *Inland ships for efficient transport chains* (TU Delft, Delft University of Technology, 2013).

[15] Q. Wald, *Performance of a propeller in a wake and the interaction of propeller and hull,* Journal of Ship Research **9** (1965).

[16] T. van Terwisga, *On the working principles of energy saving devices,* in *3rd International Symposium on Marine Propulsors, May* (2013) pp. 5–8.

[17] M. W. C. Oosterveld, *Wake adapted ducted propellers*, Ph.D. thesis, TU Delft, Delft University of Technology (1970).

[18] H. Ghassemi, S. Majdfar, and H. Forouzan, *Calculations of the hydrodynamic characteristics of a ducted propeller operating in oblique flow,* Ship Science & Technology **10**, 31 (2017).

[19] K. van der Meij and H. C. Raven, *Promising hydrodynamic improvements for inland vessels,* in *European Inland Waterway Navigation Conference* (Budapest, Hungary, 2014).

[20] E. Rotteveel and R. Hekkenberg, *The influence of shallow water and hull form variations on inland ship resistance,* in *International Marine Design Conference. Tokyo* (2015).

[21] E. Rotteveel, R. Hekkenberg, and J. Liu, *Design guidelines and empirical evaluation tools for inland ships,* in *EIWN 2014: European Inland Waterway Navigation Conference, Budapest, Hungary, 10-12 September 2014* (Budapest University of Technology and Economics, 2014).

[22] E. Rotteveel, A. van der Ploeg, and R. Hekkenberg, *Optimization of ships in shallow water with viscous flow computa-tions and surrogate modeling,* Proceedings of PRADS2016 **4**, 8th (2016).

[23] N. von der Stein, *Weitere Schritten in der Optimierung der Hinterschiffsform für schiebende Großmotorschiffe,* Binnenschiffahrt-ZfB , 341 (1991).

[24] J. Liu, R. Hekkenberg, E. Rotteveel, and H. Hopman, *Literature review on evaluation and prediction methods of inland vessel manoeuvrability,* Ocean Engineering **106**, 458 (2015).

[25] J. Liu, *Impacts of rudder configurations on inland vessel manoeuvrability*, Ph.D. thesis, Delft University of Technology (2017).

[26] R. Hekkenberg and C. Thill, *Retrofit solution for inland ships: the moveit! approach,* in *European Inland Waterway Navigation Conference* (2014).

[27] T. J. C. Terwisga, *Weerstand en voortstuwing van bakken: een literatuurstudie* (Maritiem Research Instituut Nederland, 1989).

[28] R. Latorre and F. Ashcroft, *Recent developments in barge design, towing and pushing*, Tech. Rep. (1980).

[29] J. Holtrop and G. Mennen, *An approximate power prediction method,* International Shipbuilding Progress **29**, 166 (1982).

[30] J. Holtrop, *A statistical re-analysis of resistance and propulsion data,* International Shipbuilding Progress **31**, 272 (1984).

[31] J. Holtrop, *De weerstand van bakvormige vaartuigen,* Schip en Werf de Zee **3**, 149 (1991).

[32] N. von der Stein, *Beitrag zur Formgebung und deren systematischer Bewertung bei hochbelasteten Mehrschrauben-Tunnelschiffen*, Ph.D. thesis, Aachen, Technische Hochschule (1986).

[33] H. H. Heuser, *Optimized hull form and propulsion for inland cargo ships,* Ships for coastal and inland waters–design, building, operation., Duisburg, Germany (1994).

[34] H. Raven, *A computational study of shallow-water effects on ship viscous resistance,* in *29th symposium on naval hydrodynamics, Gothenburg* (2012).

[35] H. Lackenby, *The effect of shallow water on ship speed,* The Shipbuilder and Marine Engine-Builer **70**, 446 (1963).

[36] O. Schlichting, *Schiffswiderstand auf beschränkter Wassertiefe,* Jahrbuch Schiffbautechnischen Gesellschaft **35**, 127 (1934).

[37] T. Jiang, *A new method for resistance and propulsion prediction of ship performance in shallow water,* in *Practical Design of Ships and Other Floating Structures. Proceedings of the Eighth International Symposium on Practical Design of Ships and Other Floating Structures*, Vol. 1 (2001).

[38] A. Millward, *The effect of water depth on hull form factor,* International shipbuilding progress **36**, 283 (1989).

[39] H. Raven, *A new correction procedure for shallow-water effects in ship speed trials,* in *Proceedings of the 2016 PRADS Conference, Copenhagen* (2016).

[40] N. von der Stein, *Praktische Fortschritte in der Hinterschiffsgestaltung durch neue Einblicke in die Strömungsverhältnisse,* Zeitschrift für Binnenschiffahrt und Wasserstraßen **3**, 106 (1989).

[41] S. A. Harvald, *Wake and thrust deduction at extreme propeller loadings for a ship running in shallow water,* RINA Supplementary Papers **119** (1977).

[42] J. Kulczyk, *Propeller-hull interaction in inland navigation vessel,* WIT Transactions on The Built Environment **12** (1970).

[43] J. Kulczyk, M. Zawislak, and A. Zielinski, *Prediction of the ship wake on a restricted waterway. in: Marine technology v,* Publication of: WIT Press (2003).

[44] S. Geerts, B. Verwerft, M. Vantorre, and F. Van Rompuy, *Improving the efficinecy of small inland vessels,* in *European Inland Waterway Navigation Conference. Baja, Hungary* (2010).

[45] D. Radojčić, *Environmentally friendly inland waterway ship design for the danube river,* World Wide Fund for Nature International Danube-Carpathian Programme (WWF-DCP), Ime projekta: Danube Navigation, Republika Srbija (2009).

[46] J. Zöllner, *Strömungstechnische Möglichkeiten zur Reduzierung des Kraftstoffverbrauchs und der CO2-Emissionen von Binnenschiffen,* in *ZKR Kongress Rheinschifffahrt und Klimawandel, Bonn* (2009).

[47] K. van der Meij, *MoVeIT! Report D2.1 CFD Calculations*, Tech. Rep. (Maritime Research Institute Netherlands, 2013).

[48] J. Maisonneuve, S. Harries, J. Marzi, H. Raven, U. Viviani, and H. Piippo, *Towards optimal design of ship hull shapes,* in *Proceedings of the 8th International Marine Design Conference* (2003) pp. 31–42.

[49] F. A. Viana, *Things you wanted to know about the latin hypercube design and were afraid to ask,* in *10th World Congress on Structural and Multidisciplinary Optimization* (sn, 2013) pp. 1–9.

[50] F. A. Viana, G. Venter, and V. Balabanov, *An algorithm for fast optimal latin hypercube design of experiments,* International journal for numerical methods in engineering **82**, 135 (2010).

[51] L. Larsson, F. Stern, and M. Visonneau, *Cfd in ship hydrodynamics - results of the gothenburg 2010 workshop,* in *MARINE 2011, IV International Conference on Computational Methods in Marine Engineering* (Springer, 2013) pp. 237–259.

[52] M. Hoekstra and L. Eça, *Parnassos: An efficient method for ship stern flow calculation,* in *Osaka Colloquium* (1998).

[53] A. Starke, A. v. d. Ploeg, and H. Raven, *Viscous free surface flow computations for self-propulsion conditions using parnassos,* in *Gothenborg Workshop on CFD in Ship Hydrodynamics* (2010).

[54] M. Hoekstra, L. Eca, J. Windt, and H. Raven, *Viscous flow calculations for kvlcc2 and kcs models using the parnassos code,* in *Proceedings of the Gothenburg Workshop* (2000).

[55] B. Starke, *A validation study of wake-field predictions at model and full scale Reynolds numbers,* in *Proceeding of the 4th Numerical Towing Tank Symposium* (2001).

[56] B. Starke, J. Windt, and H. Raven, *Validation of viscous flow and wake field predictions for ships at full scale,* in *Proceedings of the 26th Symposium on Naval Hydrodynamics* (2006).

[57] H. Raven, *Computation of shallow-water effects on ship viscous flow and resistance*, Tech. Rep. (Maritime Research Institute Netherlands (MARIN), 2012).

[58] ITTC, *Practical guidelines for ship cfd applications,* in *Recommended Procedures and Guidelines* (2014).

[59] L. Eça and M. Hoekstra, *On the influence of the iterative error in the numerical uncertainty of ship viscous flow calculations,* in *26th Symposium on Naval Hydrodynamics* (2006) pp. 17–22.

[60] L. Eça and M. Hoekstra, *A procedure for the estimation of the numerical uncertainty of cfd calculations based on grid refinement studies,* Journal of Computational Physics **262**, 104 (2014).

[61] D. Rijpkema, B. Starke, and J. Bosschers, *Numerical simulation of propeller-hull interaction and determination of the effective wake field using a hybrid rans-bem approach,* in *Third International Symposium on Marin Propulsors, SMP2013.(submitted)* (2013).

[62] J. Baltazar, D. Rijpkema, J. Falcão de Campos, and J. Bosschers, *A comparison of panel method and rans calculations for a ducted propeller system in open-water,* in *Third International Symposium on Marine Propulsors (SMP2013), Launceston, Tasmania, Australia* (2013).

[63] J. N. Newman, *Marine hydrodynamics* (MIT press, 1977).

[64] J. E. Kerwin and J. B. Hadler, *Principles of naval architecture series: Propulsion,* The Society of Naval Architects and Marine Engineers (SNAME) (2010).

[65] J. Carlton, *Marine propellers and propulsion* (Butterworth-Heinemann, 2011).

[66] J. W. Lewis, F. W. DeBord, and V. A. Bulat, *Resistance and propulsion of ice-worthy ships* (Society of Naval Architects and Marine Engineers, 1982).

[67] J. E. Kerwin, *Marine propellers,* Annual review of fluid mechanics **18**, 367 (1986).

[68] A. Jonk and J. v. d. Beek, *Some aspects of propeller-hull interaction,* in *Fifth LIPS Propeller Symposium, Drunen* (1983).

[69] A. van der Ploeg, *Object functions for optimizing a ship's aft body,* in *11th International Conference on Computer and IT Applications in the Maritime Industries (COMPIT), Liège, Belgium* (2012).

[70] M. B. Wilson, *Selected elementary criteria for evaluating propeller-induced surface force excitation,* Philosophical Transactions of the Royal Society of London, Series A: Physical and Engineering Sciences. **334**, 319 (1991).

[71] R. Tibshirani, *Regression shrinkage and selection via the lasso,* Journal of the Royal Statistical Society. Series B (Methodological) , 267 (1996).

[72] H. Zou and T. Hastie, *Regularization and variable selection via the elastic net,* Journal of the Royal Statistical Society: Series B (Statistical Methodology) **67**, 301 (2005).

[73] E. A. Nadaraya, *On estimating regression,* Theory of Probability & Its Applications **9**, 141 (1964).

[74] H. Kim, C. Yang, S. Jeong, F. Noblesse, *et al.*, *Hull form design exploration based on response surface method,* in *The Twenty-first International Offshore and Polar Engineering Conference* (International Society of Offshore and Polar Engineers, 2011).

[75] F. Vesting and R. E. Bensow, *On surrogate methods in propeller optimisation,* Ocean Engineering **88**, 214 (2014).

[76] A. J. Smola and B. Schölkopf, *A tutorial on support vector regression,* Statistics and computing **14**, 199 (2004).

[77] V. Vovk, *Kernel ridge regression,* in *Empirical inference* (Springer, 2013) pp. 105–116.

[78] S. An, W. Liu, and S. Venkatesh, *Face recognition using kernel ridge regression,* in *Computer Vision and Pattern Recognition, 2007. CVPR'07. IEEE Conference on* (IEEE, 2007) pp. 1–7.

[79] I. Guyon and A. Elisseeff, *An introduction to variable and feature selection,* Journal of machine learning research **3**, 1157 (2003).

[80] M. Karagiannopoulos, D. Anyfantis, S. Kotsiantis, and P. Pintelas, *Feature selection for regression problems,* Proceedings of the 8th Hellenic European Research on Computer Mathematics & its Applications, Athens, Greece **2022** (2007).

[81] M. L. Raymer, W. F. Punch, E. D. Goodman, P. C. Sanschagrin, and L. A. Kuhn, *Simultaneous feature extraction and selection using a masking genetic algorithm,* in *Proceedings of the 7th International Conference on Genetic Algorithms, San Francisco, CA* (1997) pp. 561–567.

[82] J. Yang and V. Honavar, *Feature subset selection using a genetic algorithm,* IEEE Intelligent Systems and their Applications **13**, 44 (1998).

[83] H. Frohlich, O. Chapelle, and B. Scholkopf, *Feature selection for support vector machines by means of genetic algorithm,* in *Tools with artificial intelligence, 2003. proceedings. 15th ieee international conference on* (IEEE, 2003) pp. 142–148.

[84] K. Deb, A. Pratap, S. Agarwal, and T. Meyarivan, *A fast and elitist multiobjective genetic algorithm: Nsga-ii,* IEEE transactions on evolutionary computation **6**, 182 (2002).

[85] W. F. Punch III, E. D. Goodman, M. Pei, L. Chia-Shun, P. D. Hovland, and R. J. Enbody, *Further research on feature selection and classification using genetic algorithms.* in *ICGA* (1993) pp. 557–564.

[86] J. Weston, S. Mukherjee, O. Chapelle, M. Pontil, T. Poggio, and V. Vapnik, *Feature selection for svms,* in *Advances in neural information processing systems* (2001) pp. 668–674.

[87] K. Deb and H. Jain, *An evolutionary many-objective optimization algorithm using reference-point-based nondominated sorting approach, part i: Solving problems with box constraints.* IEEE Trans. Evolutionary Computation **18**, 577 (2014).

[88] W. Van Lammeren, J. Van Manen, and M. Oosterveld, *The wageningen b-screw series,* (1969).

[89] G. Dyne, *The principles of propulsion optimization,* (1995).

[90] A. Habben Jansen, *The influence of the bow shape of inland ships on the resistance*, Master's thesis, Delft University of Technology (2016).